

**Development and Pharmacological Evaluation of
Positron Emitted-Ligands for Imaging of
Benzodiazepine Receptors at *In Vivo***

2005

Jun Maeda

A dissertation submitted in partial fulfillment of the requirements leading to the
degree of Doctor (Pharmacy) presented to the Department of Toxicology,
Hoshi University, Tokyo, Japan

This dissertation is dedicated to my parents and brother.

Table Contents

Abbreviations	1
Chemical structure of PET ligands used in present study	2
Chemical structure of benzodiazepine ligands used in present study	3
General Introduction	4

Chapter 1

Imaging of $\alpha 5$ subunit of GABA_A/BZ receptor by [¹¹C]Ro15-4513

Introduction	10
<u>Experiment 1-1</u>	
<i>In vitro</i> [¹¹ C]Ro15-4513 binding in the rat brain	11
<u>Experiment 1-2</u>	
<i>In vivo</i> [¹¹ C]Ro15-4513 binding in the monkey brain	17
Discussion	33

Chapter 2

Imaging of peripheral benzodiazepine receptor by [¹¹C]DAA1106

Introduction	36
<u>Experiment 2-1</u>	
Synthesis, distribution and metabolite of [¹¹ C]DAA1106	38
<u>Experiment 2-2</u>	
<i>In vivo</i> binding property of [¹¹ C]DAA1106 in the rat and monkey	50
Discussion	63

Chapter 3

Imaging of peripheral benzodiazepine receptor by ^{18}F -labeled DAA1106

Introduction	66
<u>Experiment 3</u>	
Synthesis, distribution and metabolite of [^{18}F]fluoro-methyl-DAA1106 and [^{18}F]fluoro-ethyl-DAA1106	67
Discussion	82
General Conclusion	87
List of publication	89
Acknowledgments	90
References	91

Abbreviations

Data analysis

ANOVA	analysis of variance
AUC	area under curve
B_{max}	maximum specific binding
K_d	dissociation constant
K_i	inhibition constant
IC₅₀	50% inhibition concentration
ID₅₀	50% inhibition dose
logD	distribution coefficient
logP	partition coefficient
PSL	photo-stimulated luminescence

Drugs and pharmacological terms

BBB	blood-brain barrier
BZ	benzodiazepine
CBR	central benzodiazepine receptor
CNS	central nervous system
GABA	γ-amino butyric acid
Tris	2-amino-2-hydroxymethyl-1,3-propanediol
PBR	peripheral benzodiazepine receptor

Injection routes

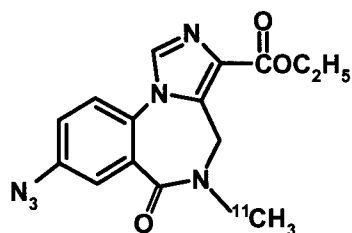
<i>i.m.</i>	intramuscular
<i>i.v.</i>	intravenous

Instruments

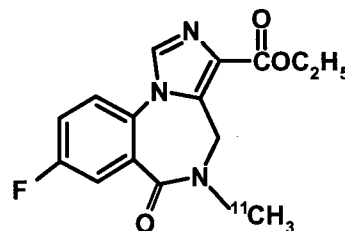
HPLC	high performance liquid chromatography
MRI	magnetic resonance image
PET	positron emission tomography
SPECT	single photon emission computed tomography
UV	ultraviolet

Chemical structure of PET ligands used in present study

Central benzodiazepine receptor PET ligands

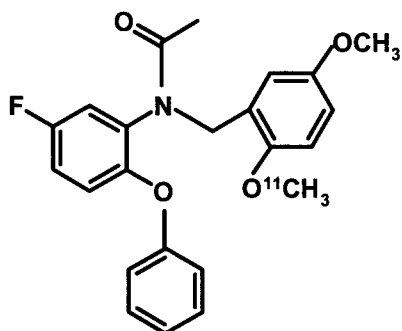


8-Azido-5,6-dihydro-5-^[11C]-methyl-6-oxo-4H-imidazo[1,5-a][1,4]benzodiazepine-3-carboxylic acid ethyl ester;
^[11C]Ro15-4513

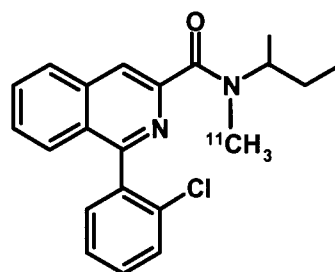


8-Fluoro-5,6-dihydro-5-^[11C]-methyl-6-oxo-4H-imidazo[1,5-a][1,4]benzodiazepine-3-carboxylic acid ethyl ester;
^[11C]Ro15-1788 (flumazenil)

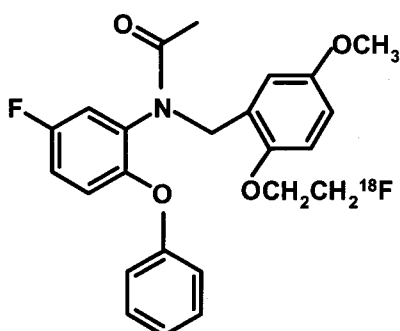
Peripheral benzodiazepine receptor PET ligands



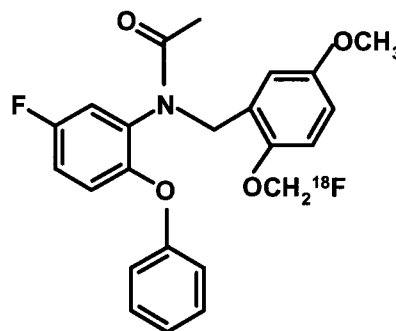
N-(5-fluoro-2-phenoxyphenyl)-N-(2-^[11C]methoxy-5-methoxybenzyl)acetamide;
^[11C]DAA1106



1-(2-Chlorophenyl)-N-^[11C]methyl-N-(1-methylpropyl)-3-isoquinolinecarboxamide;
^[11C]PK11195



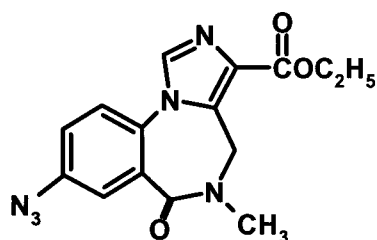
N-(5-fluoro-2-phenoxyphenyl)-N-(2-(2-^[18F]fluoroethoxy)-5-methoxybenzyl)acetamide;
^[18F]Fluoro-ethyl-DAA1106



N-(5-fluoro-2-phenoxyphenyl)-N-(2-^[18F]fluoromethoxy-5-methoxybenzyl)acetamide;
^[18F]Fluoro-methyl-DAA1106

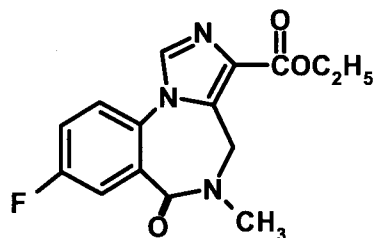
**Chemical structure of benzodiazepine receptor ligands used
in present study**

Central benzodiazepine receptor ligands



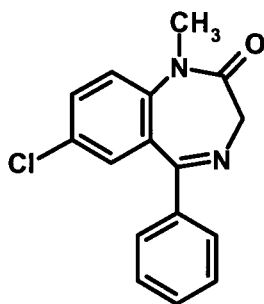
Ro15-4513

α 5 subunit selective partial inverse agonist



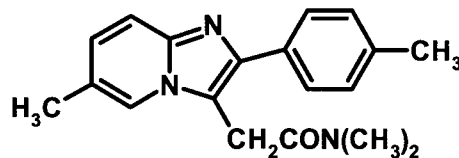
Ro15-1788 (flumazenil)

nonselective antagonist



Diazepam

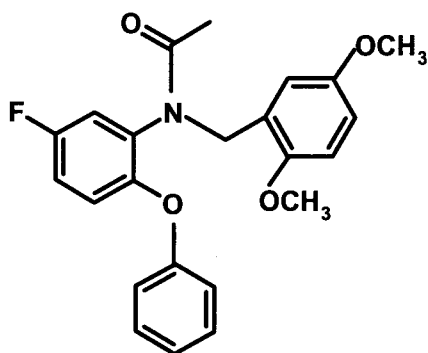
α 1,2,3 and 5 subunit agonist



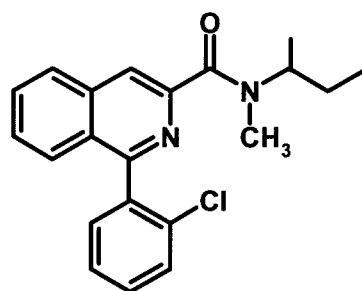
Zolpidem

α 1, 2 and 3 subunit agonist

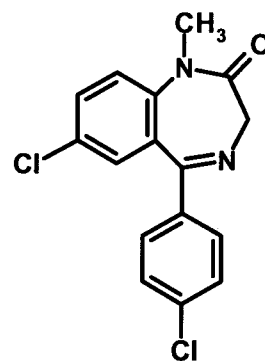
Peripheral benzodiazepine receptor ligands



DAA1106



PK11195



**Ro5-4864
(4'-Chloro-diazepam)**

General Introduction

Positron emission tomography (PET) is a method to detect the injected positron-emitting tracer *in vivo* using a γ -scintillation camera with coincidence counter. PET enables the measurement of biochemical parameters such as blood flow, glucose metabolism, and neurotransmission in humans and animals^{1,2}. Carbon-11 (^{11}C), nitrogen-13 (^{13}N), oxygen-15 (^{15}O), and fluorine-18 (^{18}F) are often used in PET studies²⁻⁴. Since a positron nuclide generally has a short half-life, like for example, 20.4 min for ^{11}C , 9.99 min for ^{13}N , 2.04 min for ^{15}O , and 109.8 min for ^{18}F respectively, the radiation produced by the positron tracer is relatively lower than that produced by other radiographies²⁻⁴. In addition, these elements are widely distributed in several bioactive substances or chemical compounds. Therefore, the positron nuclides can be introduced into various compounds without modifying their biochemical properties, such as pharmacokinetics and affinity for receptor or enzyme. Currently, glucose uptake is most frequently measured by 2- ^{18}F fluoro-2-deoxy-D-glucose. In April 2002, the National Health Insurance permitted the use of 2- ^{18}F fluoro-2-deoxy-D-glucose PET in several diagnostic procedures such as, determination of the foci in refractory epilepsy, diagnosis of several tumors, and the viability test in myocardial infarction⁵. PET has gained popularity as a diagnostic tool not only in specialized institutes but also in many general hospitals.

Positron is a complementary electron particle; it was discovered as a positively charged electron in 1932⁶. In 1933, Joliot and Curie⁷ succeeded in synthesizing the positron-emitted nuclide, ^{13}N , by irradiating boron with α -rays. Research on artificial isotopes gained momentum after the invention of the cyclotron by Lawrence; the cyclotron accelerates several elementary particles using a magnetic field⁸⁻¹⁰. For their achievements in radiochemistry, Joliot and Curie were awarded the Nobel Prize in Chemistry in 1935, and Lawrence was awarded the Nobel Prize in Physics in 1939. *In vivo* noninvasive imaging using radiotracers for the diagnosis of various diseases has been in use since the 1950s^{11,12}. The two drawbacks of using β -rays produced by ^{14}C and ^3H in this process are—impermeability of the body and intense radiation due to a long half life. Therefore, γ -rays emitted by isotopes are utilized for investigations. The positron-emitting nuclides

possess an advantage over single photon-emitting nuclides in terms of spatial resolution, because the two photons produced by a positron extend in symmetrical directions¹³⁾.

PET is a method by which positrons are detected *in vivo* by coincidence imaging using a γ -scintillation camera. In 1975, Ter-Pogossian et al.¹⁴⁾ succeeded in producing the prototype of the γ -scintillation camera for positron coincidence imaging and named the procedure as “positron emission transaxial tomography.” The principles of PET scanning are related to the unique properties of the positrons emitted by isotopes. After a subject is *i.v.* administered the positron-labeled tracer, the labeled tracer gets distributed in several tissues. The positron emitted from an atom, encounters a nearby free electron in the tissues. The positron annihilates the electron, and as a result, two 511 keV gamma-ray photons are emitted in opposite directions. The collision of the photons with the scintillator, such as Bi₄Ge₃O₁₂ (BGO) crystal, produces faint luminescence, which is amplified by a photomultiplier and then transduced to electronic signals¹³⁾ (see Fig. A). The two photons are detected using two coincidence scintillation counters placed outside the body^{1,13)}. The midpoint of the scintillation counters that detect the two photons corresponds to the point of positron decay. Thus, PET has an advantage over single photon emission computed tomography (SPECT) in terms of spatial resolution.

PET is recognized as the best method for the *in vivo* measurement of neurotransmitter receptors and enzymes in the brain¹⁶⁾. In the past century, numerous receptor ligands of the central nervous system (CNS) have been synthesized for use in medicines and pharmacological research. Concomitantly, several ligands have been labeled with positron nuclides, and their availability for diagnosis has been investigated using PET⁴⁾. In 1983, Wagner first reported the imaging of dopamine D2 receptor in the human brain using [¹¹C]N-methylspiperone¹⁷⁾. Subsequently, Farde et al. reported that [¹¹C]raclopride could be used to visualize the dopamine D2 receptor in the brain of normal and schizophrenic humans^{18,19)}. [¹¹C]Raclopride has excellent selectivity, low non-specific binding, and rapid brain kinetics. Therefore, it is considered to be an ideal PET tracer for imaging and the quantification of neuroreceptors in the brain.

It is difficult to develop PET ligands for receptors and enzymes in the brain because despite their high affinity and good selectivity *in vitro*, the receptor ligands do not always

recognize their receptors *in vivo*. Apart from the manner in which *in vitro* binding occurs, the *in vivo* binding of a PET tracer is characterized by lipophilicity and metabolism⁴⁾. In order to examine the neurotransmitter receptor or enzyme in the CNS, a PET tracer must penetrate into the blood-brain barrier BBB. In case of passive diffusion, the speed of permeability of the compounds through the BBB correlates to $\frac{\log P}{\sqrt{\text{Mol. Weight}}}$ ²⁰⁾. The

partition coefficient, log P, which is the logarithmic ratio of distribution between octanol and water (pH 7.0), represents the lipophilicity of the compound. Chemical compounds that possess either a charge or a large molecular weight are prevented by the BBB from accessing to the CNS, whereas high-lipophilic (log P > 4) PET tracers are eliminated slowly and have a greater non-specific binding in the brain²¹⁻²³⁾. Thus, PET tracers with log P = 2.0 display optimal lipophilicity because of the rapid kinetics and the low non-specific binding²¹⁻²³⁾. Furthermore, PET tracers are often catabolized to several labeled or unlabeled metabolites *in vivo*. In case a labeled metabolite having no affinity for a receptor is distributed in the brain, differentiating the specific binding from the total radioactivity is difficult^{24,25)}. Therefore, the generation of obstructive metabolites from PET tracers must be avoided.

BZs are important drugs used in the treatment of several CNS disorders such as epilepsy, anxiety disorders, and insomnia²⁶⁾. The BZ receptor (or binding site) was classically categorized into three types, namely, ω_1 , ω_2 , and ω_3 ²⁷⁾. At present, it is generally distinguished into two types—the central type and the peripheral type²⁸⁾. The CBR is located in the GABA_A/BZ receptor chloride channel complex (GABA_A/BZ receptor), whereas the PBR is independent of one. Several institutes have reported the synthesis of a positron-labeled ligand with both types of benzodiazepine receptor.

The GABA_A/BZ receptor is a pentameric assembly derived from a combination of various subunits such as α_1 – α_6 , β_1 – β_3 , γ_1 – γ_3 , δ , ϵ , π , and θ , indicating the diversity of subunit combinations. This is reflected in the various functional properties and ligand selectivity of the GABA_A receptors^{26, 29-31)}. Previous reports indicated that most of the native GABA_A receptor types contained at least one each of the α , β , and γ subunits. Among these subunits, the α and γ_2 subunits play an essential role in benzodiazepine

binding^{29,30}). The diversity of the α subunit is necessary not only for the ability of BZ binding but also for ligand selectivity^{26,31}). Labeling of various benzodiazepine ligands with positron nuclides has been attempted for use in brain PET. Initially, flunitrazepam with ^{11}C was evaluated; however, its specific binding is indistinguishable from the non-specific binding due to high lipophilicity and slow kinetics³²). On the other hand, a CBR antagonist, [^{11}C]Ro15-1788 (flumazenil), developed by the Frederic Joliot Hospital can recognize CBR by PET. This compound exhibits rapid kinetics in the brain and is displaced by a high dose of benzodiazepines³³). It is now believed that among several BZ PET ligands, [^{11}C]flumazenil is the most useful tracer for CBR imaging by PET. In clinical studies, the *in vivo* [^{11}C]flumazenil binding is variable in only a few disorders such as epilepsy^{34,35}) and Huntington's disease³⁶). Current studies conducted on GABA_A α -subunit transgenic mice have revealed that each of the different pharmacological effects, such as anti-anxiety, anti-convulsion, muscle relaxation, sedation, and hypnosis, produced by BZs are mediated through the six discrete α subunits³⁷⁻⁴¹). It is regarded that flumazenil binds to a total BZ-binding site, because it has homogeneous affinity for all the six α subunits⁴²). Thus, the development of a subunit-specific ligand is necessary to understand the detailed role of GABA_A/BZ receptor³¹).

PBR was found to be a BZ-binding site in peripheral tissue by Braestrup and Squires⁴³). Tissues with high or moderate densities of PBR, such as adrenal cortex, cardiac muscle, and skin, derive a large part of their metabolic energy from active oxidative phosphorylation⁴⁴). In contrast, tissues containing low levels of PBR, such as brain, skeletal muscle, and smooth muscle, are primarily dependent on glycolysis⁴⁴). PBR density is lower in the brain than in other tissues, whereas it is exclusively expressed in glial cells⁴⁵). Therefore, it is assumed that glial cells can be recognized by the PBR ligand. The availability of the BZ derivative [^{11}C]Ro5-4864 (4'-chlorodiazepam) was evaluated at the Karolinska Institute, but it was found that [^{11}C]Ro5-4864 failed to accumulate in a glioma in the human brain⁴⁶). These results indicate that [^{11}C]Ro5-4864 is not suitable for imaging of PBR. In contrast, the glioma could be visualized by PET⁴⁷) using an isoquinoline derivative [^{11}C]PK11195. However, the use of [^{11}C]PK11195 presents the serious problem of its very low accumulation in the human brain despite its high lipophilicity. It is difficult

to quantify the density of [¹¹C]PK11195 binding *in vivo* by PET.

The specific aims of the proposed research are described as follows:

- 1) The extent of [¹¹C]Ro15-4513-binding *in vivo* is higher in the frontal cortex and limbic areas than in other brain regions. This localization of the Ro15-4513-binding is evidently different from that of the typical benzodiazepine PET tracer, [¹¹C]flumazenil. In order to confirm the subunit-selectivity of the *in vivo* [¹¹C]Ro15-4513 binding, the influence of diazepam (insensitive to α_4 and α_6 subunits) and zolpidem (sensitive to α_1 , α_2 , and α_3 subunits) was investigated.
- 2) Glial cells play an important role in brain dysfunction such as in Alzheimer's disease, and it is hoped that an imaging tool for glial cells is developed. In order to visualize the function of glial cells, novel PBR PET ligands [¹¹C]DAA1106, [¹⁸F]Fluoro-methyl-DAA1106 and [¹⁸F]fluoro-ethyl-DAA1106 were developed and investigated in this study.

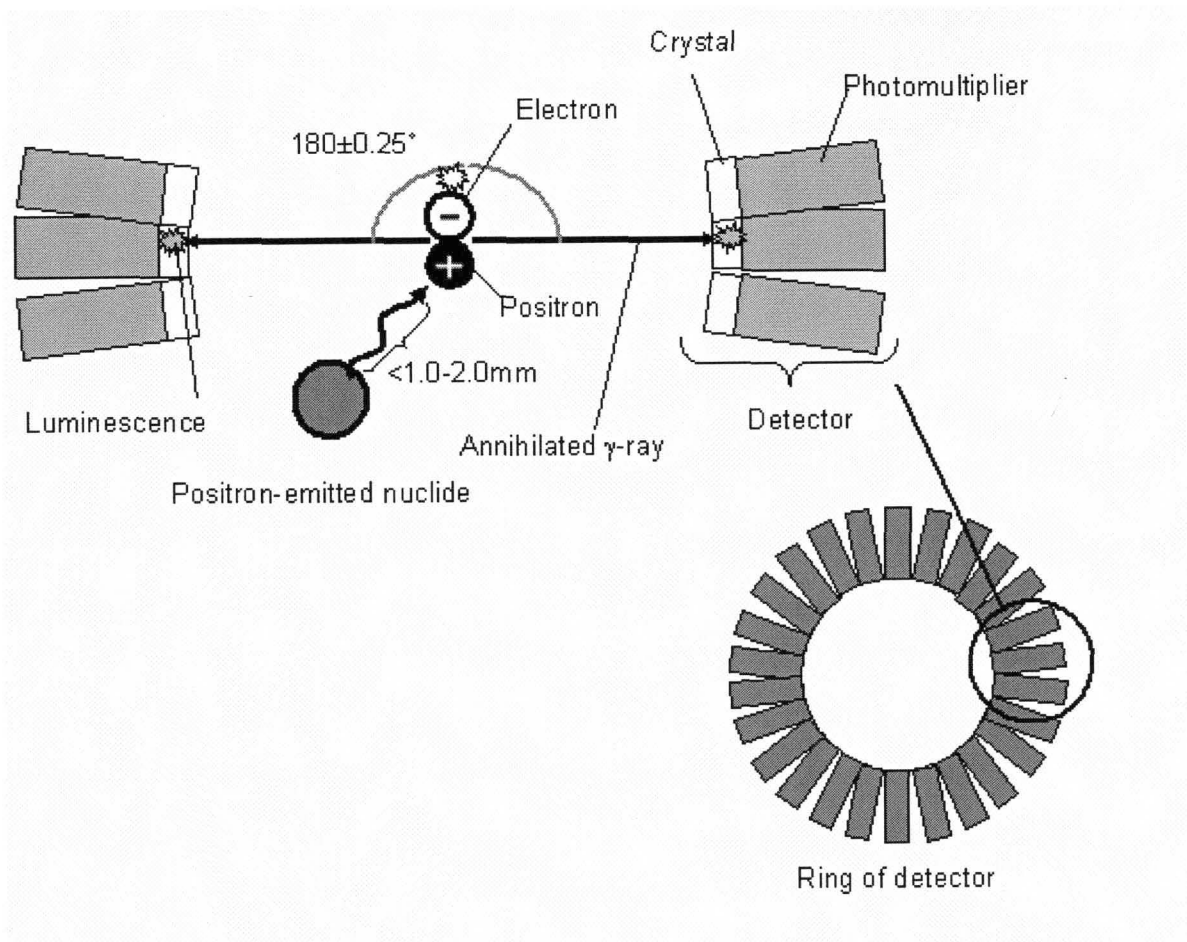


Fig. A

Illustration of the annihilation of positrons and its detection for the radiation by coincidence method.

Chapter 1

Imaging of $\alpha 5$ subunit of GABA_A/BZ receptor by [¹¹C]Ro15-4513

INTRODUCTION

The CBR is located in the GABA_A/BZ receptor and plays an important role in several disorders such as epilepsy, anxiety disorder and insomnia^{26,48}). Several ligands have been developed to visualize BZ receptors *in vivo*⁴⁹⁻⁵⁵), and [¹¹C]flumazenil and [¹²³I]iomazenil have been commonly used at several institutions. The *in vivo* distributions of flumazenil and iomazenil have been reported to be similar in the monkey brain⁵⁶). However, a different distribution pattern has been reported for the [¹¹C]Ro15-4513 binding compared to that of [¹¹C]flumazenil⁵²). [¹¹C]Flumazenil accumulates widely in the cerebral cortex, but accumulation in the occipital cortex is relatively higher compared to other cortical regions^{49-52,57}). On the other hand, [¹¹C]Ro15-4513 accumulates to relatively higher levels in the anterior cingulate cortex, hippocampus and insular cortex than in other cortical regions^{52,53,58}). The mechanism involved in these different distribution patterns has not been fully examined, but the role of BZ receptor subtypes has been suggested^{58,59}).

The GABA_A/BZ receptor is composed of several subunits, and the diversity of subunit combinations can result in various functional differences^{26,29,31}). It has been reported that the typical GABA_A receptor complex contains two α subunits, two β subunits and one γ subunit^{26,29,31}). The α subunits are reported to be essential for BZ binding, and their diversity (6 subtypes) can present different affinities for several BZ ligands^{26,31}). Furthermore, each subunit has different distribution patterns^{60,61}). The BZ receptor partial inverse agonist Ro15-4513 is reported to have relatively higher affinity for the $\alpha 5$ subunit-containing GABA_A/BZ receptor than the other types of α subunits *in vitro*^{42,62,63}).

In this chapter, I investigated the pharmacological properties of [¹¹C]Ro15-4513 binding in the monkey brain to clarify the mechanisms involved in the regional differences of distribution using PET.

Experiment 1-1

***In vitro* [¹¹C]Ro15-4513 binding in the rat brain**

Materials and Methods

Synthesis of radiotracers

Detail production system of [¹¹C]methyl iodide was described in previous reports^{64,65}. [¹¹C]Ro15-4513 was synthesized by N-methylation of N-desmethyl precursor Ro44-3492. Briefly, [¹¹C]CH₃I was allowed to react with Ro44-3492 (0.5mg) in presence of NaH (1 mg) in anhydrous dimethylformamide (500 μl) at 40 °C for 1 min. After the reaction, H₂O/CH₃CN (6:4, 0.5 mL) added in reactive production, and then [¹¹C]Ro15-4513 was separated by reverse phase HPLC column (YMC-Pack Pro C-18, 250 mm length × 10mm inside diameter, YMC, Kyoto) with mobile phase as H₂O/CH₃CN (6 : 4, flow rate 4 mL/min). The elution was evaporated, and re-dissolved in sterile saline with 1% polysorbate and 2% ethanol. The specific radioactivity of [¹¹C]Ro15-4513 solution was greater than 74 Ci/μmol, and chemical purity was greater than 95 %.

Competition of [¹¹C]Ro15-4513 binding by BZ compounds

[¹¹C]Ro15-4513 binding was evaluated by *in vitro* autoradiography in the frozen rat brain section. The rat brains were rapidly removed, and then frozen by powdered dry ice. The frozen brain was cut into 20 μm thick sagittal sections using cryotome (HM560; Carl Zeiss Co. LTD., Germany) at -15 °C. The sliced brains were mounted silan-coated slide glass (Matsunami glass Ind., Ltd., Japan) and were stored in deep-freezer (80 °C). The brain sections were pre-incubated in 50 mM Tris-HCl buffer (pH 7.4, room temperature) for 15 min, and then incubated in 50 mM Tris-HCl buffer (pH 7.4, 4 °C) with 120 mM sodium chloride and [¹¹C]Ro15-4513 (185 MBq/L, about 5 nM) for 60 min. After the incubation they were rinsed by ice-cold Tris-HCl buffer for 2 min at twice, and finally dipped into ice-cold water for 10 sec. In competition study, diazepam (1 nM–100 μM) or zolpidem (10 nM–100 μM) was added in incubation buffer. Non-specific binding was

estimated in the presence of 10 μ M of flumazenil.

The brain sections were dried by warm blow and immediately were contacted to imaging plate (Fuji Film Co. LTD, Japan) for 2 hr. The radioactivity in the brain sections was measured by BAS1800 II system (Fuji Film Co. LTD, Japan). Regions of interest were placed on the hippocampus, frontal cortex and cerebellum and the photo-stimulated luminescence (PSL)/mm² values were measured.

Data analysis

Data were expressed as percent of control binding (% control). Competition curve was fitted by graphical soft Prism[®], and 50 percent of inhibitory concentration (IC₅₀) was determined.

RESULTS

Fig. 1-1 shows autoradiogram of [¹¹C]Ro15-4513 binding in the rat brain. Ten μM of flumazenil completely inhibit the [¹¹C]Ro15-4513 binding all brain regions. On the other hands, cerebellar [¹¹C]Ro15-4513 binding remained despite presence of diazepam (100 μM). Similarly, zolpidem could not inhibit the [¹¹C]Ro15-4513 binding in the hippocampus, frontal cortex and cerebellum.

Fig. 1-2 shows competition curves of diazepam (1nM – 100 μM) and zolpidem (10nM – 100 μM) to the [¹¹C]Ro15-4513 specific binding. Remain of cerebellar [¹¹C]Ro15-4513 binding in presence of diazepam (100 μM) was estimated to 25 percent of control binding, which corresponds to diazepam-insensitive binding. Competition of [¹¹C]Ro15-4513 binding by zolpidem exhibits to two-site binding model. Twenty percent of [¹¹C]Ro15-4513 binding in the frontal cortex hippocampus and cerebellum remained in presence of 100 μM of zolpidem, while thalamic binding was completely inhibited by zolpidem. Respective IC₅₀ values were represented in Table 1-1.

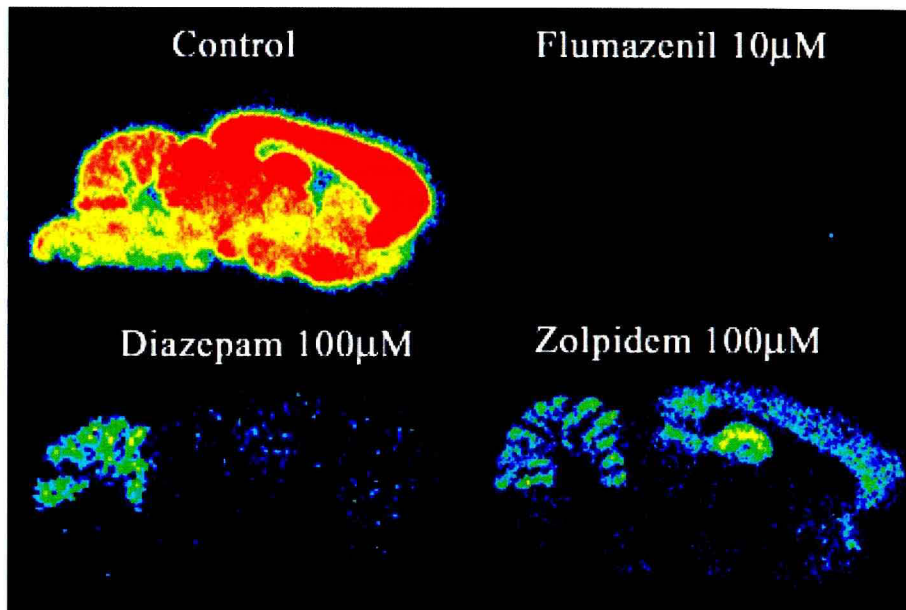


Fig. 1-1

In vitro autoradiogram of $[^{11}\text{C}]\text{Ro15-4513}$ binding in the sagittal brain section.

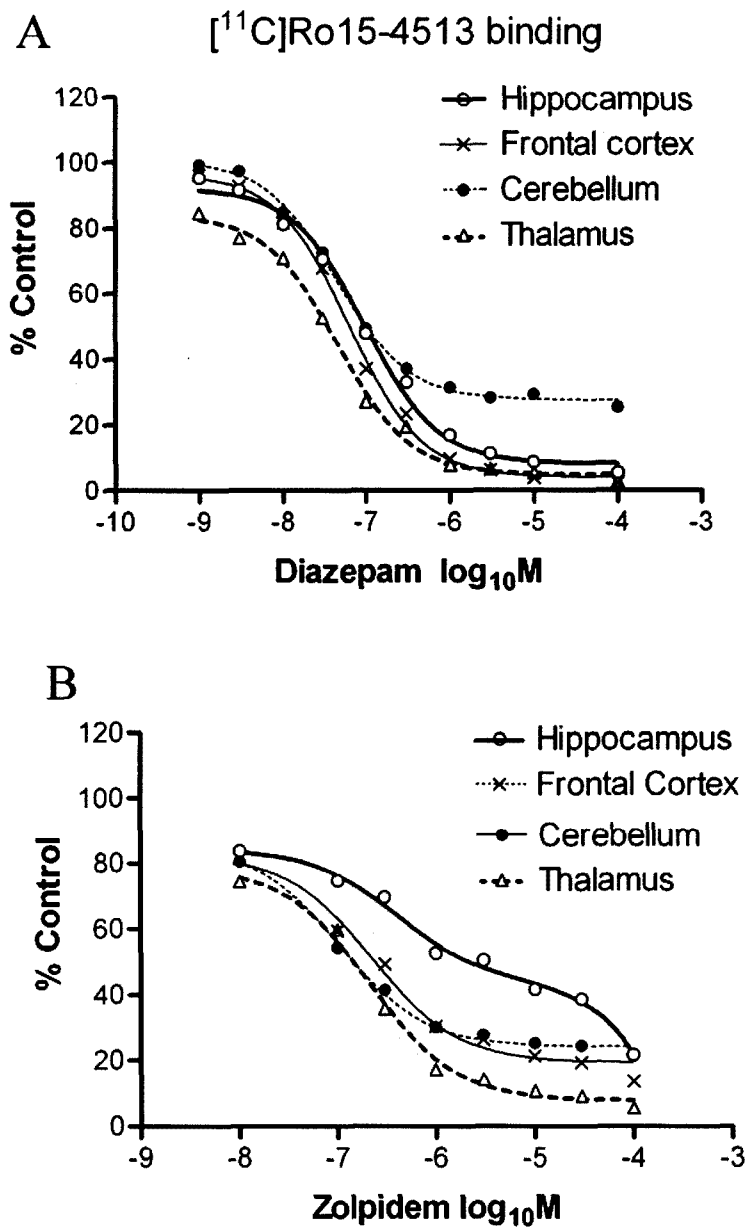


Fig. 1-2

Competition curve of $[^{11}\text{C}]\text{Ro15-4513}$ binding in 4 brain regions. **A:** Inhibition of $[^{11}\text{C}]\text{Ro15-4513}$ binding produced by diazepam (1nM-100 μM). **B:** Inhibition of $[^{11}\text{C}]\text{Ro15-4513}$ binding produced by zolpidem (10nM-100 μM)

Table 1-1 IC₅₀ value of diazepam and zolpidem to [¹¹C]Ro15-4513 binding *in vitro*.

Drug	IC ₅₀ (nM)			
	Hippocampus	Frontal cortex	Cerebellum	Thalamus
Diazepam	93	62	44	45
Zolpidem	High 40* Low 1620	242	107	215

* Competition of [¹¹C]Ro15-4513 binding by zolpidem in the hippocampus was separated to two binding site.

Experiment 1-2

***In vivo* [¹¹C]Ro15-4513 binding in the monkey brain**

MATERIALS AND METHODS

Synthesis of radiotracers

Detail method about synthesis of [¹¹C]Ro15-4513 was described in the Experiment 1-1. Method about synthesis of [¹¹C]Ro15-1788 was reported in previous reports⁶⁴). Specific radioactivity of [¹¹C]Ro15-4513 in the control and drug displacement scans ranged from 16 to 202 GBq/μmol (67.8 ± 10.3 GBq/μmol, mean ± S.E.M.) at the time of injection.

Animals

Three young male rhesus monkeys (*Macaca mulatta* purchased from SLC, Japan) weighing 5.0-6.0 kg were used. The monkeys were maintained and handled in accordance with recommendations by the US National Institutes of Health and our guidelines (National Institute of Radiological Sciences, Japan). A head fixation system for the monkey chair was developed based on the surgical procedure described by Obayashi et al.⁶⁶). A magnetic resonance image (MRI) of each monkey's brain was obtained with a Philips Gyroscan S15 / ACS II (1.5T) with three-dimensional T1-weighted axial MRI sequence^{66,67}). The studies were approved by the Animal Ethics Committee of the National Institute of Radiological Sciences, Chiba, Japan.

PET scan

All PET scans were performed using a high-resolution SHR-7700 PET camera (Hamamatsu Photonics, Shizuoka, Japan) designed for laboratory animals, which provides 31 transaxial slices 3.6 mm (center-to-center) apart, a 33.1-cm field of view, and spatial resolution of 2.6 mm full-width at half-maximum⁶⁸). The monkeys were repeatedly anesthetized with ketamine at 10 mg/kg/hr *i.m.* (Ketalar[®], Sankyo Co. LTD, Tokyo, Japan)

every hour throughout the session and immobilized with the head fixation device to ensure accuracy on re-positioning⁶⁶). The drug-treatment scans were separated by at least 2-week intervals.

After transmission scans for attenuation correction using a ⁶⁸Ge-⁶⁸Ga source for 30 min, dynamic emission scan in 3-dimensional acquisition mode was performed for 90 min (2 min x 5 scans, 4 min x 10 scans, 10 min x 4 scans). The tracer was injected via the cephalic vein by a single bolus at the start of the emission scan. Injected doses of [¹¹C]Ro15-4513 were 33.2–164.0 MBq (130.0 ± 5.6 MBq, mean ± SEM). For the determination of densities and affinities, the tracer containing various amounts of cold mass (34 pmol – 1.0 μmol) for 10 different PET scans was used.

PET data analysis

All emission scan images were reconstructed with a 4.0-mm Colsher filter, and circular regions of interest of 3-mm diameter were placed on the anterior cingulate cortex, frontal cortex, insular cortex, parietal cortex, temporal cortex, occipital cortex, striatum, thalamus, hippocampus, cerebellum and pons using an image analysis software with reference to each monkey MRI (in-house software PET Analyzer for Windows[®] 67,69). The region of interest values were expressed in kBq/mL, normalized to the injected radioactivity of 37 MBq (1.0 mCi), and plotted against time.

In vivo Scatchard analysis

The data were obtained at systematically varied ligand concentrations and analyzed by means of saturation curves or Scatchard plots^{58,70,71}). The binding parameters for [¹¹C]Ro15-4513 were obtained by performing 10 separate scans and various specific radioactivities on one animal. For the low specific-radioactivity conditions, 30-1000 nmol of cold Ro15-4513 was added to the tracer. The hyperbolic saturation curve of tracer binding was defined as:

$$B = B_{\max} \times \frac{F}{K_d + F} \quad (1)$$

In case of two-site binding, the hyperbolic equation (1) is modified to the following

equation:

$$B = B_{\max 1} \times \frac{F}{K_{d1} + F} + B_{\max 2} \times \frac{F}{K_{d2} + F} \quad (2)$$

where B is the concentration of bound ligand (pmol/mL), F the concentration of free ligand (pmol/mL), B_{\max} the total receptor density (pmol/mL), and K_d the dissociation constant (nM). B was defined as the difference in radioactivity between region of interest values of specific binding regions and the pons (F), since the density of GABA_A/BZ receptors is negligible^{51,53,58,72} and transient equilibrium is established when the specific binding (B) radioactivity is maximal^{70,71}. The B_{\max} and K_d values were calculated by non-linear hyperbolic analysis with the equation one-site model (1) or two-site model (2) using the fitting software Prism[®] (GraphPad Software Inc., USA). Also, the regressed hyperbolic curve (x is F and y is B) was transformed to create the Scatchard plot graph (x is B and y is B/F). Fitting was evaluated by F-test on the variance of plotted points. Binding potential is defined as:

$$\text{Binding potential} = B_{\max} / K_d$$

When specific radioactivity of [¹¹C]Ro15-4513 is very high, the B/F value at the equilibrium condition approximates binding potential⁶⁷.

Effect of BZ drugs on [¹¹C]Ro15-4513 binding

Flumazenil (Anexate[®], Yamanouchi Pharmaceutical Co. Ltd., Tokyo, Japan), diazepam (Horizon[®], Yamanouchi Pharmaceutical Co. Ltd.) and zolpidem (Tocris Cookson Ltd., Bristol, UK) were purchased. Zolpidem was dissolved in propylene glycol with 20% ethanol.

Diazepam has affinity for GABA_A/BZ receptors with $\alpha 1$, $\alpha 2$, $\alpha 3$ and $\alpha 5$ subunits but not $\alpha 4$ and $\alpha 6$ subunits, while the imidazobenzodiazepine compounds flumazenil and Ro15-4513 have affinity for both diazepam-insensitive subunits^{37,48,73-75}. Zolpidem has higher affinity for the $\alpha 1$ subunit than for the $\alpha 2$ and $\alpha 3$ subunits and is insensitive to the $\alpha 5$ subunit^{42,62,76}.

Each drug was *i.v.* injected slowly for 2 min, 15-20 min prior to injection of the tracers. Drug-induced inhibition was calculated by the following equation⁷⁷:

$$\% \text{ Inhibition} = 100 \times \left(1 - \frac{\int_2^{60} C_D(t) dt}{\int_2^{60} C_F(t) dt} \right)$$

where C_D and C_F are radioligand concentrations in the presence and absence of drug treatment, respectively. The integrals of radioligand concentrations (AUC) were calculated for the period from 2 to 60 min after tracer injection. Data of the drug effect from one monkey was plotted against drug-injection doses (mg/kg, *i.v.*) with logarithmic conversion. The plotted data were regressed to a one-site competition curve using Prism[®] (GraphPad Software Inc., USA), and then 50% inhibition dose (ID_{50}) values were calculated.

Data analysis

The time-activity curve of [¹¹C]Ro15-4513 was normalized to the injected dose of 37 MBq. The effects of BZs were evaluated based on the time-activity curves of each region by two-way ANOVA with repeated measures.

RESULTS

After *i.v.* injection of [¹¹C]Ro15-4513 with high specific radioactivity, the radioactivity rapidly increased in all regions, reaching a maximum at around 15 min post injection. The uptake of [¹¹C]Ro15-4513 was highest in the anterior cingulate cortex, followed by the hippocampus, occipital cortex and thalamus; it was lowest in the pons (Fig. 1-3). The distribution of [¹¹C]Ro15-4513 was obviously different from [¹¹C]flumazenil (Fig. 1-4). High accumulation was also observed in the insular and temporal cortices. Fig. 1-5 shows that flumazenil at 0.1 mg/kg, *i.v.* inhibited the accumulation of [¹¹C]Ro15-4513 in the anterior cingulate cortex and occipital cortex but not in the pons [$F_{18,72} = 1.45$ ($p=0.14$)] according to repeated two-factor ANOVA.

Fig. 1-6A shows the saturation curves of specific binding in the anterior cingulate cortex. The data were evaluated by hyperbolic analysis with a one- or two-site saturation model. Specific binding was fitted by the one-site binding model ($r^2 = 0.982$) and two-site binding model ($r^2 = 0.977$) (Fig. 1-6A). Statistical analysis by F-test between the one- and two-site models revealed no significant difference [$F_{9,9} = 1.25$ ($p=0.75$)]. The Scatchard plot of [¹¹C]Ro15-4513 (Fig. 1-6B) showed that the data fitted by the one-site binding model ($r^2 = 0.919$) deviated from the data points at low concentrations of the ligand compared to the two-site binding model ($r^2 = 0.984$). The F-test between the two site models indicated that the two-site binding model fitted better to the data than the one-site binding model [$F_{9,9} = 5.13$ ($p=0.023$)]. In the two-site binding model, binding potential of [¹¹C]Ro15-4513 in the anterior cingulate cortex was calculated as 1.80 for the high-affinity site and 1.06 for the low-affinity site. The high-affinity site shared 63% in total binding potential of [¹¹C]Ro15-4513 in the anterior cingulate cortex. Similar results were also observed in the insular cortex and striatum, while a different affinity site could not be detected in the occipital cortex and cerebellum (Fig. 1-7 and Table 1-2). The *in vivo* B_{max} and K_d values of [¹¹C]Ro15-4513 binding are summarized in Table 1-2.

Fig. 1-8 shows the MRI and summation images of [¹¹C]Ro15-4513. Flumazenil and diazepam inhibited the accumulation of [¹¹C]Ro15-4513 in all cortical regions (Fig. 1-8F and 1-8G). The images of [¹¹C]Ro15-4513 with medium-specific radioactivity show that

the binding in the occipital cortex was relatively retained (Fig. 1-8C). On the contrary, zolpidem preferentially inhibited binding in the occipital cortex and cerebellum compared to other regions (Fig. 1-8E).

Fig. 1-9 shows that both diazepam and zolpidem inhibited the specific binding of [¹¹C]Ro15-4513 in the anterior cingulate cortex and occipital cortex. The magnitude of the effect was not significantly different in the occipital cortex [$F_{18,72} = 1.17$, ($p=0.31$)], but in the anterior cingulate cortex the binding was only partly inhibited by zolpidem compared to the inhibition by diazepam [$F_{18,72} = 14.75$, ($p<0.001$)]. The drug-induced effects are summarized in Table 1-3. The effects of diazepam at 5.0 mg/kg and flumazenil at 0.1 mg/kg did not differ significantly among the 10 brain regions studied [diazepam: $F_{9,20} = 0.81$, ($p=0.61$); flumazenil: $F_{9,20} = 1.04$, ($p = 0.45$)], while there were significant regional differences in the effect of zolpidem at 10 mg/kg [zolpidem ($F_{9,20} = 3.52$, $p = 0.009$)].

Fig. 1-10 shows the dose-displacement curves of specific binding by diazepam (Fig. 1-10A) and zolpidem (Fig. 1-10B). The inhibition by diazepam was dose-dependent (Fig. 1-10A). On the other hand, about 70% of the specific binding remained after pretreatment with 10-20 mg/kg of zolpidem, and dose-dependent inhibition was observed only in the occipital cortex and cerebellum (Fig. 1-10B).

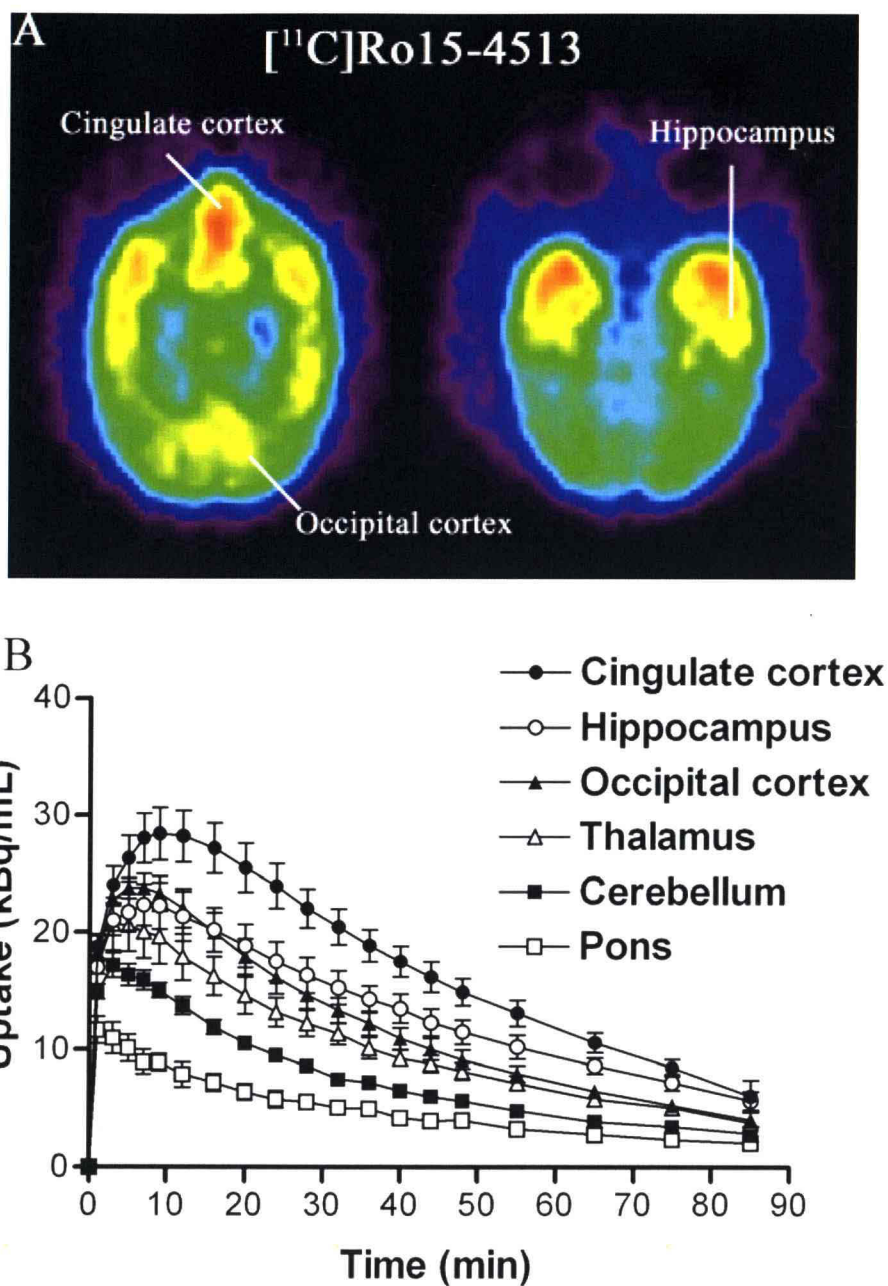


Fig. 1-3

A: Summation image of $[^{11}\text{C}]\text{Ro15-4513}$ in the monkey brain from 2 min to 60 min. B: Time-activity curves of $[^{11}\text{C}]\text{Ro15-4513}$ in 6 brain regions for 90 min in rhesus monkeys (n=3). Injected radioactivity was normalized to 37 MBq. $[^{11}\text{C}]\text{Ro15-4513}$ was highly accumulated in the anterior cingulate cortex and hippocampus but lowest in the pons. Data are presented as mean \pm S.E.M.

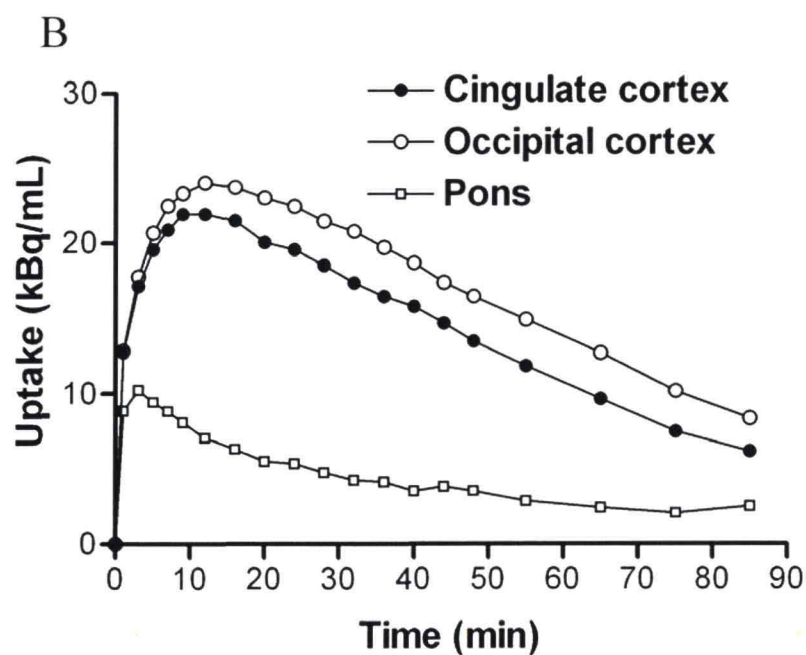
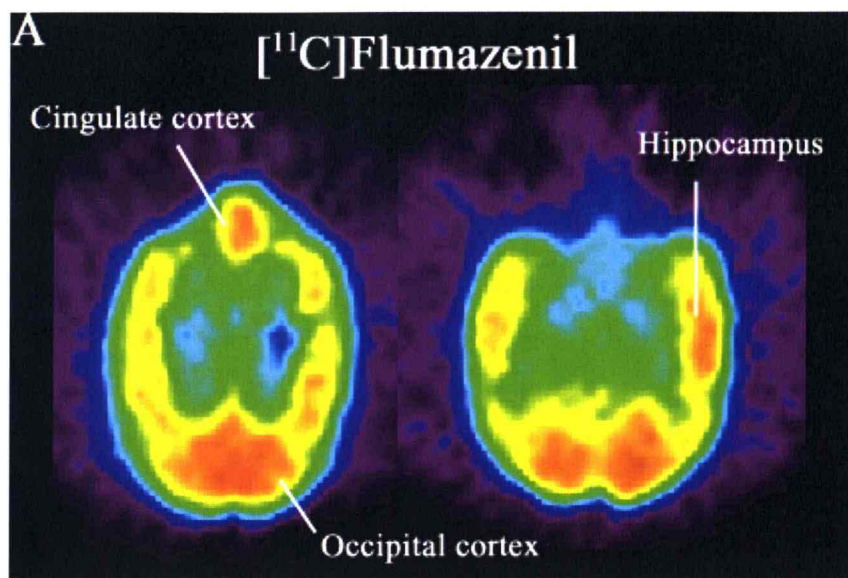


Fig. 1-4

A: Summation image of $[^{11}\text{C}]\text{flumazenil}$ in the monkey brain from 2 min to 60 min. B: Time-activity curves of $[^{11}\text{C}]\text{flumazenil}$ in 3 brain regions for 90 min in one rhesus monkey. Injected radioactivity was normalized to 37 MBq.

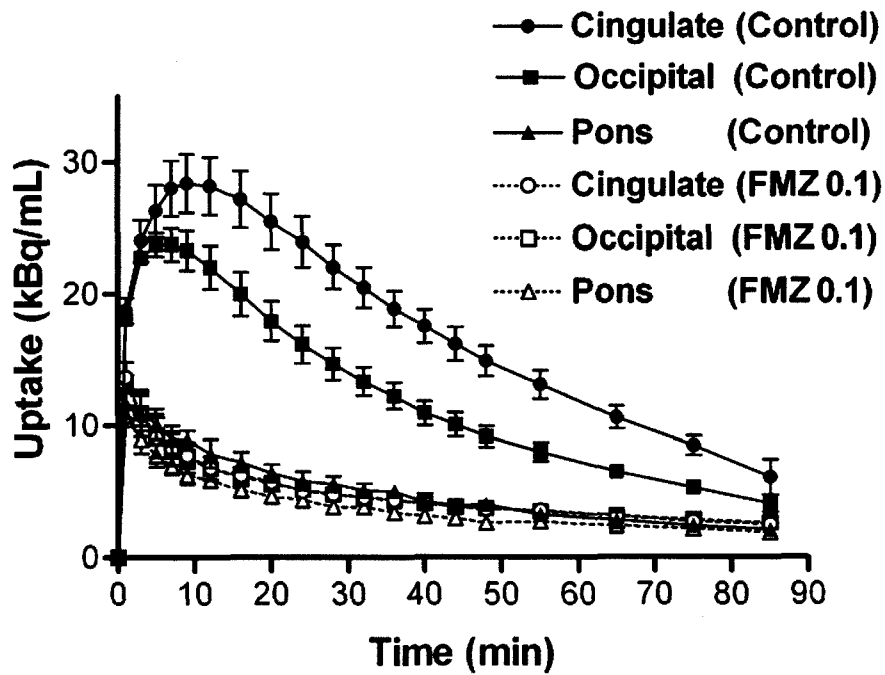


Fig. 1-5

Effect of pretreatment with flumazenil on [¹¹C]Ro15-4513 binding in three brain regions (n=3). The injected radioactivity was normalized to 37 MBq. Flumazenil diminished the radioactivity in the anterior cingulate cortex and occipital cortex markedly but did not significantly affect the binding in the pons. Data are presented as mean ± S.E.M.

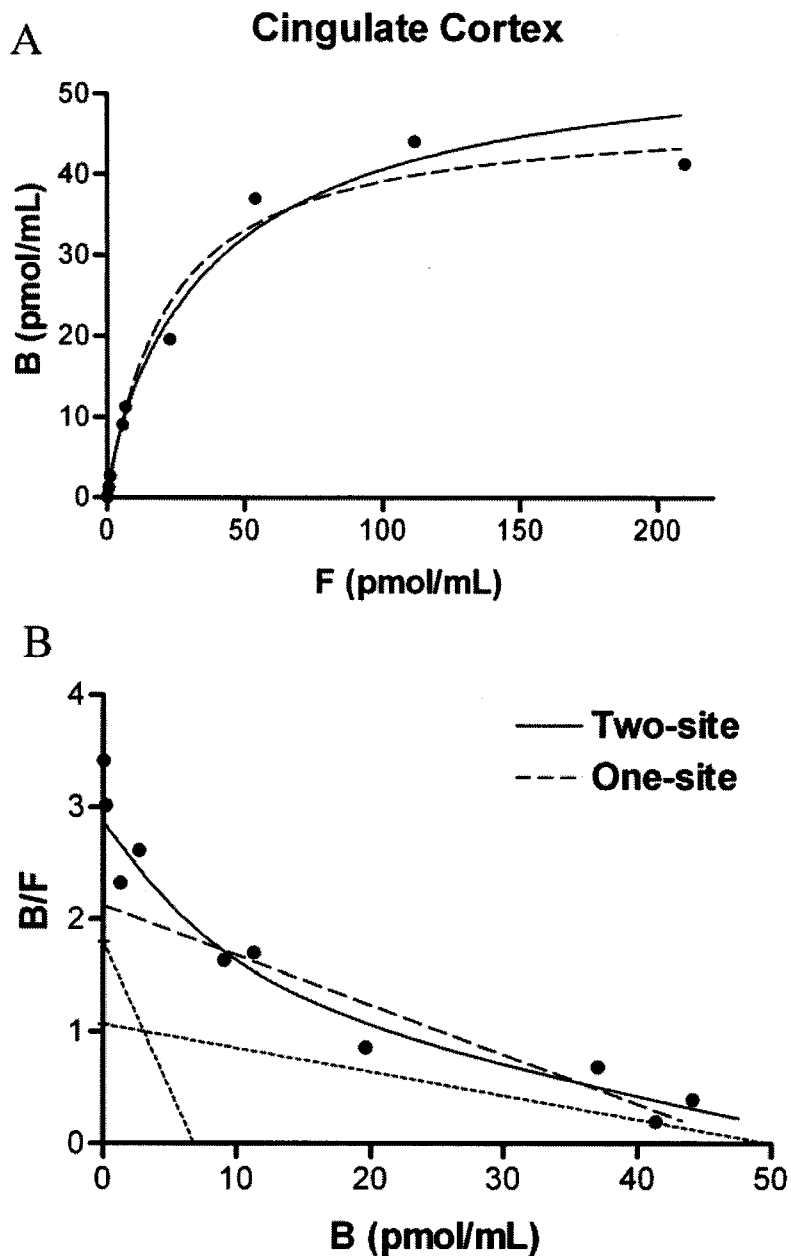


Fig. 1-6

A: Hyperbolic saturation curve of [¹¹C]Ro15-4513 specific binding in the anterior cingulate cortex. The plotted data was fitted by one- (broken line) and two-site models (continuous line). **B:** Scatchard plot of [¹¹C]Ro15-4513 specific binding. The plot was obtained by transforming the hyperbolic saturation curve (A). The broken and continuous lines show one- and two-site models, respectively. The dotted lines represent the regression curve by two-site model separated into two lines with different affinities. The data were obtained from one monkey.

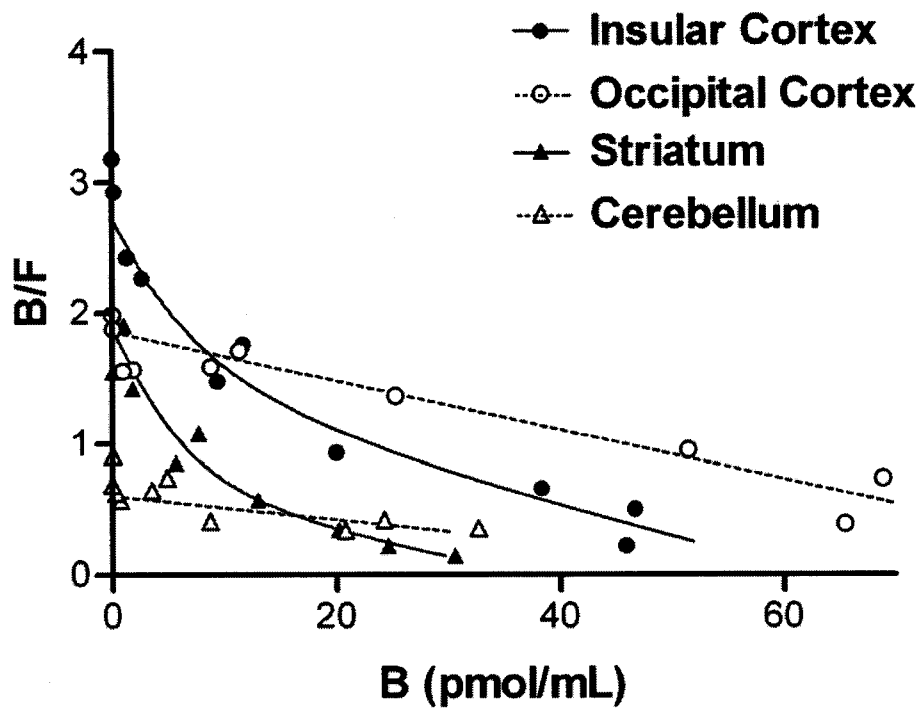


Fig. 1-7

Scatchard plot of the insular cortex, striatum, occipital cortex and cerebellum. The continuous and broken lines (insular cortex and striatum) showed regression to two- and one-site models, respectively.

Table 1-2 B_{max} (pmol/mL) and Kd (nM) values of [¹¹C]Ro15-4513 binding in 10 regions

Region	One site binding model		Two site binding model			
	B _{max}	Kd	High affinity		Low affinity	
			B _{max}	Kd	B _{max}	Kd
Amygdala	29.38	14.91	1.11	0.67	30.79	20.46
Cerebellum	51.35	78.10			n.d. ^a	
Cingulate cortex	47.98	22.59	6.82	3.79	49.99	46.80
Frontal cortex	38.80	22.42	1.96	2.10	39.86	30.49
Hippocampus	34.58	22.85	0.62	0.88	35.37	26.60
Insular cortex	54.38	27.50	5.42	3.50	57.65	49.37
Occipital cortex	98.67	53.21			n.d. ^b	
Striatum	28.32	21.46	6.09	4.31	31.35	67.62
Temporal cortex	41.42	21.69	7.88	5.30	40.60	46.14
Thalamus	51.60	48.41	5.40	6.86	57.90	95.14

^an.d. : not detected

^bn.d.: No difference in affinity between high and low.

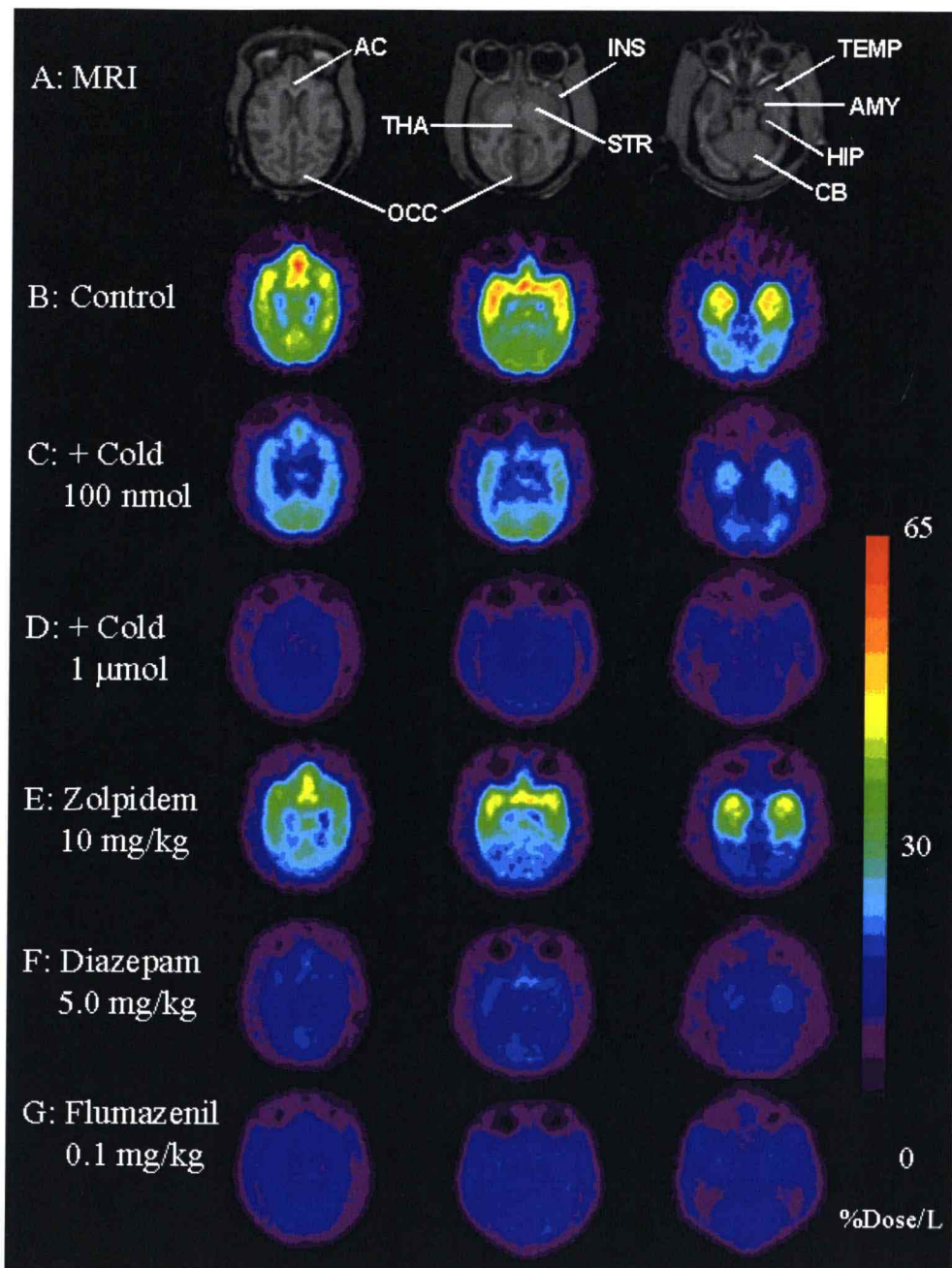


Fig. 1-8

Summation images of [^{11}C]Ro15-4513 accumulation in the monkey brain from 2 min to 60 min after tracer injection. The images were adjusted to 65% injection dose per liter. **A**, MRI; **B**, control ([^{11}C]Ro15-4513); **C**, plus 100 nmol of Ro15-4513/body; **D**, 1.0 μmol of Ro15-4513/ body; **E**, zolpidem 10 mg/kg; **F**, diazepam 5.0 mg/kg; **G**, flumazenil 0.1 mg/kg. AC, anterior cingulate cortex; AMY, amygdala; CB, cerebellum; HIP, hippocampus; INS, insular cortex; OCC, occipital cortex; STR, striatum; TEMP, temporal cortex; THA, thalamus

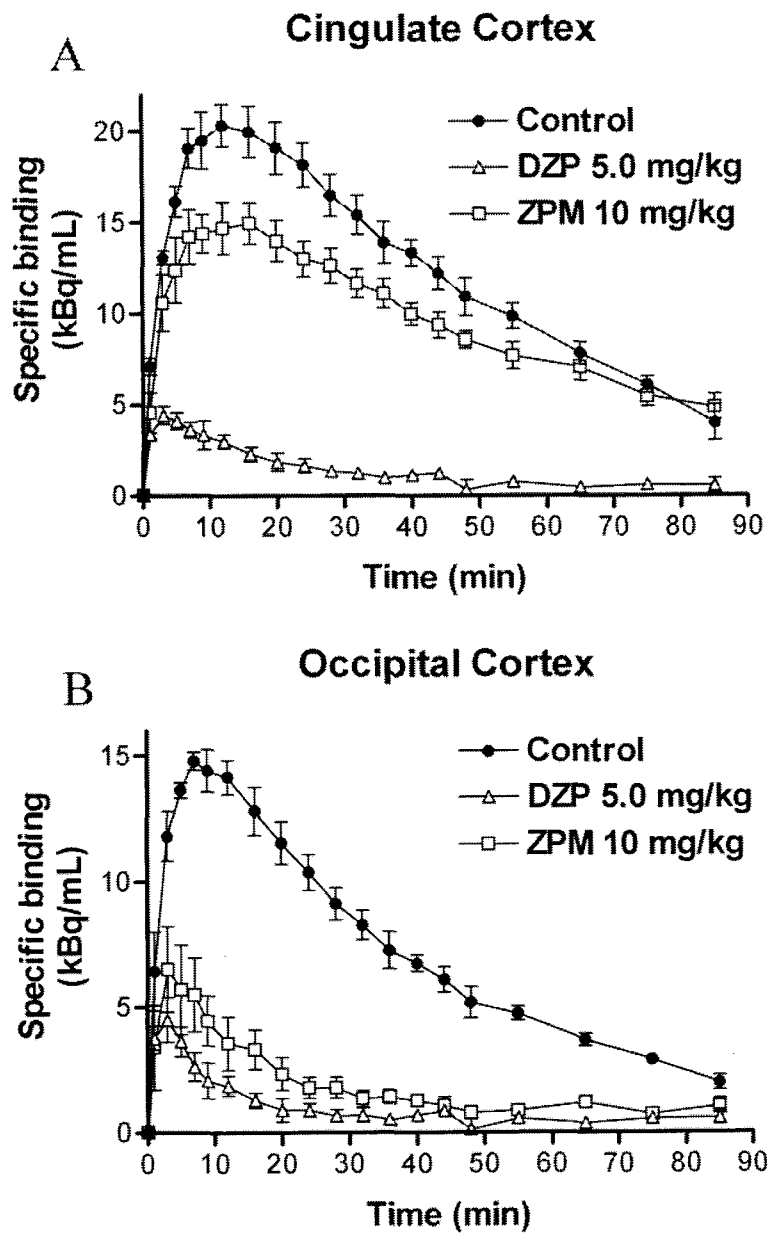


Fig. 1-9

Time-activity curves of [^{11}C]Ro15-4513 specific binding in the anterior cingulate cortex (A) and occipital cortex (B) from three monkeys. The concentration of radioactivity (kBq/mL) was normalized to 37 MBq dose injection. The circles, open triangles and open squares represent control, diazepam treatment and zolpidem treatment, respectively. Data are presented as mean \pm S.E.M.

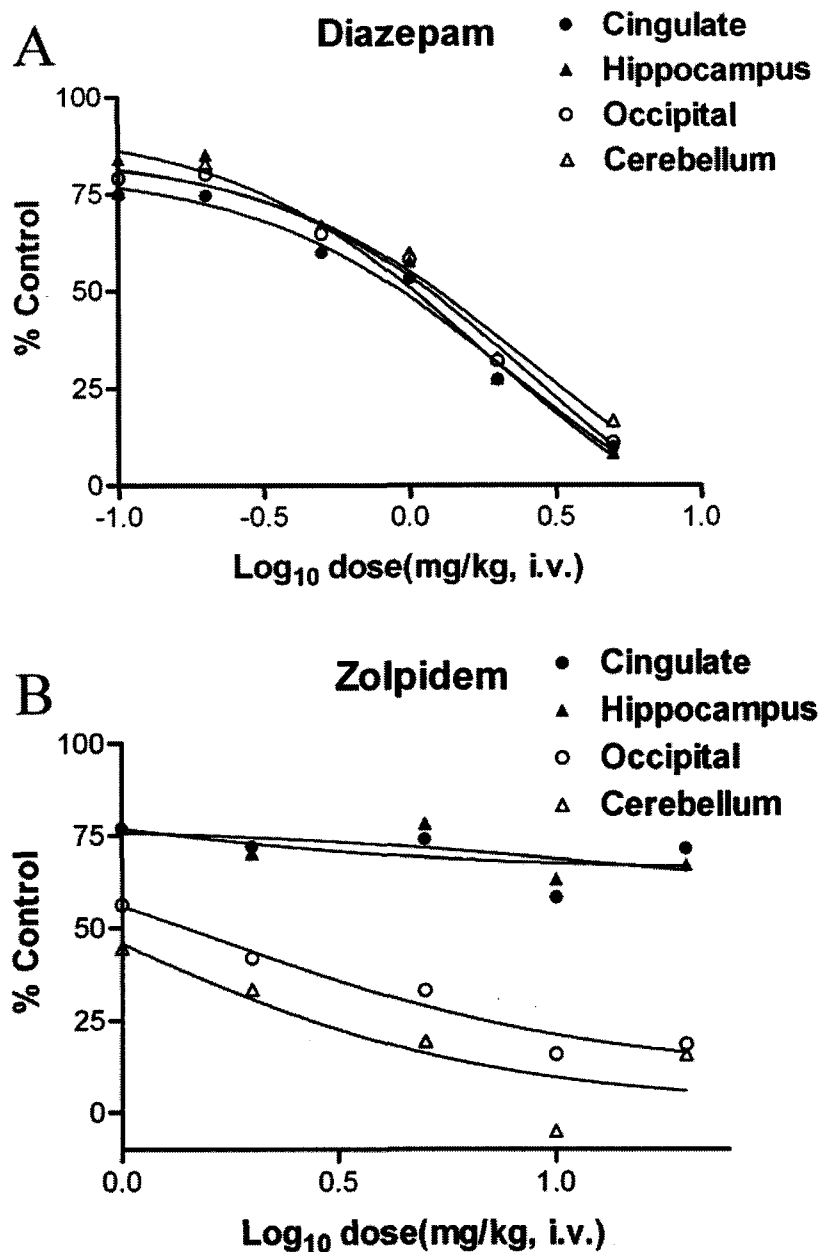


Fig. 1-10

A: Displacement curves of [¹¹C]Ro15-4513 binding by diazepam. The manner of inhibition corresponded to one-site competition in each brain region, and there was no significant regional difference. The IC₅₀ value was 1.8-2.6 (mg/kg, *i.v.*). **B:** Displacement curves of [¹¹C]Ro15-4513 binding by zolpidem. The IC₅₀ values in the occipital cortex and cerebellum were 1.7 and 0.9 (mg/kg, *i.v.*), respectively. The inhibition by zolpidem in the anterior cingulate cortex and hippocampus did not reach 50% of control binding. The data were obtained from one monkey. The doses are presented as a logarithm of injection dose (mg/kg).

Table 1-3 Inhibition of [¹¹C]Ro15-4513 binding by BZ ligands

Region	% Inhibition ± S.E.M.								
	Diazepam 5.0 (mg/kg, i.v.)			Zolpidem 10 (mg/kg, i.v.)			Flumazenil 0.1 (mg/kg, i.v.)		
Amygdala	89.2	±	2.1	26.5	±	10.2	92.6	±	1.1
Cerebellum	82.6	±	5.4	83.0	±	11.8	90.4	±	2.5
Anterior cingulate cortex	88.8	±	2.3	23.4	±	9.9	93.6	±	1.0
Frontal cortex	94.3	±	3.9	44.9	±	12.6	96.6	±	2.6
Hippocampus	90.0	±	3.3	33.2	±	12.3	91.3	±	2.2
Insular cortex	89.6	±	2.5	29.1	±	10.9	92.9	±	1.4
Occipital cortex	88.4	±	3.1	75.6	±	6.1	89.6	±	2.1
Striatum	90.7	±	3.2	27.2	±	14.3	94.7	±	1.4
Temporal cortex	87.9	±	1.6	20.8	±	9.5	92.8	±	1.5
Thalamus	91.2	±	3.8	29.2	±	13.1	93.8	±	3.0

DISCUSSION

[¹¹C]Ro15-4513 was highly accumulated in the anterior cingulate cortex, insular cortex and lower temporal cortex, and was lowest in the pons. This was consistent with previous monkey^{58,78)} and human data^{52,53)}. The present results indicated that there were two different types of [¹¹C]Ro15-4513 binding in the brain regions, one being a mixture of high- and low-affinity binding sites, the other a low-affinity binding site (Fig. 1-7 and Table 1-2). Analyses were carried out using the pons as reference region, where the density of BZ receptors is negligible according to previous monkey PET studies^{51,58)}. Further, the present study also showed that the radioactivity of [¹¹C]Ro15-4513 in the pons was not significantly affected by a 0.1 mg/kg (*i.v.*) dose of flumazenil (Fig. 1-5).

The high-affinity binding site is distributed over the frontal cortex, temporal cortex and limbic areas, while the low-affinity site is located in the occipital cortex and cerebellum. Previous reports of *in vivo* and *in vitro* binding studies have indicated that Ro15-4513 binding possesses two different affinities in the fronto-temporal cortex and limbic regions^{58,79)}, while cerebellar Ro15-4513 binding exhibits a homogeneous affinity site⁷⁹⁾. However, only homogenous affinity has been reported for [¹¹C]flumazenil binding in the frontal and occipital cortices⁵⁷⁾. The existence of a high-affinity site can result in a higher binding potential in the fronto-temporal limbic regions (Fig. 1-6 and 1-7). The high-affinity site of [¹¹C]Ro15-4513 (K_d ; 3.79 nM) showed about 14-fold higher affinity than that of the low affinity site (K_d ; 50.0 nM). This difference is consistent with the report that Ro15-4513 has 10-20-fold higher affinity for $\alpha 5$ subunit-containing GABA_A/BZ receptor ($K_i = 0.7$ nM) compared to $\alpha 1$, $\alpha 2$ and $\alpha 3$ subunits ($K_i = 7-10$ nM) *in vitro*⁶²⁾. However, agonist binding sites are known to show a heterogeneous affinity state⁸⁰⁾. Mehta and Shank⁷⁹⁾ have reported that both [³H]Ro15-4513 and [³H]flunitrazepam have two-affinity binding sites *in vitro*, but the high-affinity binding site of [³H]flunitrazepam did not overlap with that of [³H]Ro15-4513. Moreover, the non-selective BZ agonists [¹¹C]triazolam and [¹¹C]NNC13-8199 showed higher accumulations in the occipital cortex in primate PET studies^{54,81)}. This distribution of both BZ agonists in the brain is similar to that of the antagonist binding with [¹¹C]flumazenil. Thus, the high-affinity binding site of

[¹¹C]Ro15-4513 can not be explained by the agonist selective high-affinity binding site observed *in vitro*. On the other hand, zolpidem (10 mg/kg, *i.v.*) fully blocked [¹¹C]Ro15-4513 binding in the occipital cortex and cerebellum, which contain a low-affinity binding site (Fig. 1-10 and Table 1-3), while 60 to 80% of the binding was not blocked in other brain regions. Zolpidem has been reported to have a 10-fold higher affinity for the $\alpha 1$ subunit-containing GABA_A/BZ receptor than for the $\alpha 2$ and $\alpha 3$ subunits, and almost no affinity for the $\alpha 5$ subunit^{42,62,76,77}). Diazepam and flumazenil showed no obvious regional differences in the inhibition of [¹¹C]Ro15-4513 binding (Table 1-3). Both compounds have no selectivity among the $\alpha 1-3, 5$ subunits^{42,63,76}). Moreover, a loss of zolpidem-insensitive binding in [³H]flumazenil has been reported in chromosome-disrupted mouse at the $\alpha 5\gamma 3$ subunits⁸²). Thus, the zolpidem-insensitive binding could reflect mainly the binding to the $\alpha 5$ subunit-containing GABA_A/BZ receptor complex. These data indicate that the high-affinity binding site of [¹¹C]Ro15-4513 represents the $\alpha 5$ subunit-containing GABA_A/BZ receptor.

It has been reported that Ro15-4513 also has an affinity for the diazepam-insensitive site that consists of $\alpha 4$ or $\alpha 6$ subunit^{37,48,73-75}), which are located in the thalamus and cerebellum, respectively^{60,61}). In the present PET study, diazepam (5.0 mg/kg, *i.v.*) blocked [¹¹C]Ro15-4513 binding in the cerebellum as well as in other brain regions (Fig. 1-9, Table 1-3). This suggests that Ro15-4513 binding for the $\alpha 6$ subunit in the cerebellum is negligible *in vivo*. We consider that the negligible binding to $\alpha 4$ and $\alpha 6$ subunits of [¹¹C]Ro15-4513 *in vivo* may be explained by influence of GABA_A receptor δ subunit. The δ subunit is exclusively expressed in the cerebellum and thalamus, and prefers to combine with the $\alpha 6$ subunit^{61,83}). The δ subunit replaces the $\gamma 2$ subunit, resulting in less sensitivity to Ro15-4513^{83,84}). In fact, the disruption of δ subunits markedly increased the cerebellar binding of Ro15-4513 *in vitro*⁸⁵).

The present results indicate that the binding potential of [¹¹C]Ro15-4513 with high specific radioactivity can reflect a relatively high signal of the $\alpha 5$ subunit. For quantification of the high-affinity site of [¹¹C]Ro15-4513 binding, its specific radioactivity needs to be controlled at a high level, because the high-affinity site of [¹¹C]Ro15-4513 was easily blocked by its radio-inactive Ro15-4513 due to low density. Although the role of the

$\alpha 5$ subunit is still not clear compared with other α subunits, [^{11}C]Ro15-4513 binding is abundant in the anterior cingulate and insular cortices, and these distributions suggest a possible role in emotion and memory^{86,87}). From my study, I can conclude that the application of the ligand [^{11}C]Ro15-4513 should prove to be useful for studying the function of the $\alpha 5$ subunit in the GABA_A/BZ receptor complex.

Chapter 2

Imaging of peripheral benzodiazepine receptor by [¹¹C]DAA1106

INTRODUCTION

Binding sites for BZ were initially identified by the binding of [³H]diazepam not only in the brain but also in peripheral organs like kidney, liver and lung^{43,88}). BZ derivative Ro5-4864 binds only to PBR with nanomolar affinity⁴³) and binding sites different from BZ binding sites on GABA_A/BZ receptor were named PBR. PBR is primarily found on mitochondrial membranes in various peripheral tissues^{44,89-91}). Although the term “peripheral” was widely used in the literature, specific ligands for PBR such as [³H]Ro5-4864 and [³H]PK11195 revealed that PBR was also expressed in the brain⁹²⁻⁹⁵). The PK11195 binding in cultured microglia and astrocytes was at 8-fold higher density than in cultured neurons⁹⁶), suggesting that PBRs localize in glial cells in the brain. The expression of PBR *in vivo* is reported to be increased in microglia activated by brain injury⁹⁷⁻¹⁰⁰). PBR binding in the brain is highest in the olfactory bulb^{93,95,101,102}) an area of dense microglia population¹⁰³).

PBR is composed of at least three subunits, isoquinoline binding protein¹⁰⁴⁻¹⁰⁶), a voltage-dependent anion channel and an adenine nucleotide carrier¹⁰⁷). The trimeric complex is a critical component of the mitochondrial permeability transitional pore, which plays an important role in passage of various biogenic compounds between the cytoplasm and mitochondrial intermembrane or matrix¹⁰⁸). A cholesterol-binding site was observed in the carboxyl terminus of isoquinoline binding protein, and the activation of PBR is suggested to be involved in the regulation of cholesterol transport into mitochondria and in steroidogenesis¹⁰⁹).

[¹¹C]PK11195 is currently being used to visualize PBR in the brain, and especially for the evaluation of lesions, by positron emission tomography (PET)¹¹⁰⁻¹¹²). [¹¹C]PK11195 binding was reported to be increased in the stroke region¹¹³), plaque of multiple

sclerosis^{110,112}), the cortex of Alzheimer disease¹¹¹) and epileptic foci¹¹⁴). The mechanism of the increase in [¹¹C]PK11195 binding has been suggested as representing a reflection of activated microglia^{45,110,111,115}). These reports suggested the diagnostic values of PBR in many disorders.

DAA1106 (see page 3) was originally developed as an anxiolytic with a different structure from other PBR compounds such as PK11195 and Ro5-4864¹¹⁶⁻¹¹⁸). The inhibition constant (K_i) of DAA1106 to [³H]DAA1106 (0.043 nM) is one order smaller than that of PK11195 (0.77 nM), and it also has good selectivity for PBRs¹¹⁶). DAA1106 does not promote steroidogenesis in mitochondrial fraction, suggesting that DAA1106 has an antagonistic property for PBRs¹¹⁹). The aim of this chapter is to characterize and evaluate [¹¹C]DAA1106 as a PET ligand for PBRs in the brains of rodent and monkey.

Experiment 2-1

Synthesis, distribution and metabolite of [¹¹C]DAA1106

MATERIALS AND METHODS

Radiochemistry and synthesis of [¹¹C]DAA1106

Carbon-11 was produced by $^{14}\text{N}(\text{p}, \alpha)^{11}\text{C}$ nuclear reaction using a CYPRIS HM-18 cyclotron (Sumitomo Heavy Industry Co. Ltd., Tokyo, Japan). A dose calibrator (IGC-3R Curiometer; Aloka, Tokyo, Japan) was used for all radioactivity measurements if not otherwise stated. Reverse phase high performance liquid chromatography (HPLC) was performed using a JASCO HPLC system: effluent radioactivity was determined using a NaI (Tl) scintillation detector system.

[¹¹C]CH₃I for radiosynthesis was synthesized from cyclotron-produced [¹¹C]CO₂ as described previously⁶⁴). Briefly, the [¹¹C]CO₂ was bubbled into 50 mM LiAlH₄ in anhydrous tetrahydrofuran (500 μL). After evaporation of the tetrahydrofuran, the remaining complexes were treated with 57% hydrogen iodide (HI; 300 μL). [¹¹C]CH₃I was transferred under a helium gas flow with heating into a reaction vessel containing anhydrous dimethylformamide (300 μL), DAA1123 (0.3–0.5 mg) and NaH (3–5 μL, 0.5 g/20 mL dimethylformamide) cooled to -15 – -20°C. After radioactivity reached a plateau, the reaction vessel was warmed to 30°C and kept for 3 min. After adding CH₃CN/H₂O (6/4, 500 μL), the radioactive mixture was applied to a semi-preparative HPLC column. HPLC semi-preparative purification was completed on a YMC J'sphere ODS-H80 column (10 mm inside diameter × 250 mm length) using a mobile phase of CH₃CN/H₂O (60/40) at a flow rate of 6.0 mL/min. The retention time for [¹¹C]DAA1106 was 9.5 min, whereas that for DAA1123 was 6.7 min. The radioactive fraction corresponding [¹¹C]DAA1106 was collected in a sterile flask containing polysorbate (80) (75 μL) and ethanol (150 μL), evaporated to dryness under vacuum, re-dissolved in 7 mL of sterile normal saline and passed through a 0.22 μm Millipore filter for analysis and the animal experiments.

Radiochemical purity and specific activity determinations

Radiochemical purity was assayed by analytical HPLC (column: CAPCELL PAK C₁₈, 4.6 mm inside diameter × 250 mm length, UV at 254 nm; mobile phase: CH₃CN/H₂O = 6/4). The retention time for [¹¹C]DAA1106 was 5.8 min at a flow rate of 2.0 mL/min. Confirmation of [¹¹C]DAA1106's identity was achieved by co-injection with the authentic non-radioactive DAA1106. Specific activity of [¹¹C]DAA1106 was determined by comparison of the assayed radioactivity to the mass associated with the carrier UV peak at 254 nm.

Biodistribution study in the mouse

A saline solution of [¹¹C]DAA1106 (average of 8 MBq/200 μL, specific activity: 120 GBq/μmol) was injected into ddY mice (30–40 g, 9 weeks, male) through the tail vein. Five mice for each time point were sacrificed by cervical dislocation at 1, 5, 15, 30 or 60 min postinjection. The whole brain, liver, lung, heart, kidney, adrenal and blood samples were quickly removed. As for the brain, the cerebellum, olfactory bulb, striatum, hippocampus, thalamus, hypothalamus and cerebral cortex were further dissected and weighed. The radioactivity present in the various tissues were measured in a Packard autogamma scintillation counter, and expressed as a percentage of the injected dose per gram of wet tissue (% injection dose/g). All radioactivity measurements were corrected for decay.

To determine *in vivo* specificity and selectivity of [¹¹C]DAA1106 binding to PBR, DAA1106, PK11195 or Ro15-1788 at a dose of 1 mg/kg each, was mixed with [¹¹C]DAA1106 (8 MBq/200 μL; specific activity: 95 GBq/μmol) and injected into ddY mice (n=5), respectively. At designated time points (1, 5, 15, 30 or 60 min), these mice were sacrificed and the whole brains were removed quickly. The brain tissue samples (cerebellum, olfactory bulb, striatum, hippocampus, thalamus, hypothalamus and cerebral cortex) were dissected and treated as described above.

Metabolite assay in plasma and brain tissue

After *i.v.* administration of [¹¹C]DAA1106 (70–90 MBq/200 μL) into ddY mice (n=3), these mice were sacrificed by cervical dislocation at 1, 5, 15, 30 or 60 min after

[¹¹C]DAA1106 injection. Blood (0.7–1.0 mL) and whole brain samples were removed quickly. The blood sample was centrifuged at 15,000 rpm for 1 min at 4°C to separate plasma, which (250 µL) was collected in a test tube containing CH₃CN (500 µL) and a solution of the authentic unlabeled DAA1106 (1.1 mg/5.0 mL of CH₃CN, 10 µL). After the tube was stirred for 15 sec and centrifuged at 15,000 rpm for 1 min for deproteinization, the supernatant was collected. The extraction efficiency of radioactivity into the CH₃CN supernatant ranged from 78% to 91% of the total radioactivity in the plasma. On the other hand, the cerebellum and forebrain including the olfactory bulb were dissected from the mouse brain and homogenized together in an ice-cooled CH₃CN/H₂O (1/1, 1.0 mL) solution containing DAA1106. The homogenate was centrifuged at 15,000 rpm for 1 min at 4°C and supernatant was collected. The recovery of radioactivity into the supernatant was 68–87% based on the total radioactivity in the brain homogenate.

An aliquot of the supernatant (100–500 µL) obtained from the plasma or brain homogenate was injected into the HPLC with a highly sensitive positron detector¹²⁰⁾ for radioactivity, and analyzed under the same HPLC conditions described above except the mobile phase of CH₃CN/H₂O with a ratio of 1/1. The percent ratio of [¹¹C]DAA1106 (retention time=10.6 min) to the total radioactivity (corrected for decay) on the HPLC chromatogram was calculated as % = (peak area for [¹¹C]DAA1106 /total peak area) ×100.

Drugs

DAA1106 and its desmethyl precursor DAA1123 (*N*-5-fluoro-2-phenoxyphenyl)-*N*-(2-hydroxy -5-methoxybenzyl)acetamide) were provided by Taisho Pharmaceutical Co. Ltd. (Tokyo; Japan). PK11195 and Ro15-1788 were purchased from Sigma Co. Ltd. (Milwaukee, WI). DAA1106, PK11195 and Ro15-1788 were dissolved in distilled water and ethanol (1 mg/1.8 mL/0.2 mL) and used for *in vivo* studies. If not otherwise stated, chemicals were purchased from Wako Pure Industries Co. Ltd. (Japan) and Aldrich Co. Ltd. (Milwaukee, WI) with the highest grade commercially available.

RESULTS

[¹¹C]DAA1106 was synthesized by *O*-[¹¹C]methylation of the corresponding phenol precursor DAA1123 with [¹¹C]CH₃I in the presence of NaH at 30°C for 3 min (Fig. 2-1). The radiochemical yield of [¹¹C]DAA1106 was largely dependent on the amount of NaH used for this reaction. When more than two equivalents of NaH relative to DAA1123 were used, the desired product [¹¹C]DAA1106 was observed in the purification HPLC chromatogram (retention time= 7 min, Fig2-2). Limiting the amount of NaH could restrain the formation of the unknown radioactive product. When one equivalent of NaH was used, only [¹¹C]DAA1106 was formed as a reaction product. Using the optimized reaction condition, [¹¹C]DAA1106 was successfully obtained with radioactivity incorporation yields of 72±16% (based on the HPLC chromatogram, n=8). The radiosynthesis, semi-preparative HPLC, and formulation were completed in an average synthesis time of 22 min (n=8). At the end of synthesis, 970–1580 GBq of [¹¹C]DAA1106 was obtained as an injection solution of sterile normal saline after 10–15 min proton (14.2 MeV on target) bombardment at a beam current of 15 μA. The final formulated solution was chemically and radiochemically pure (>98%) as determined by analytic HPLC. The specific activity of [¹¹C]DAA1106 was 90–156 GBq/μmol at end of synthesis.

The radioactivity time course was determined for six specific regions of the mouse after injection of [¹¹C]DAA1106. Table 2-1 shows the decay corrected percent dose per gram data for all regions. As shown in Table 2-1, a high initial concentration of radioactivity (>5% injection dose/g) was found in the heart, kidney, adrenal and lung. The distribution pattern of uptake was in agreement with the previous *in vitro* findings on the distribution of PBR in the peripheral systems^{43,44}). The highest radioactivity of [¹¹C]DAA1106 was found in the lung and this level was higher than that of [¹¹C]PK11195¹²¹). The high uptakes in the lung and heart may be related to the mitochondrial contents containing PBR. On the other hand, a high concentration of radioactivity (2.1–3.5% injection dose/g) was also found in the brain, the target tissue in this study. The values were about 1.5-2 fold higher than those of [³H]PK11195 in the mouse brain at the corresponding times¹²¹).

The radioactivity distribution of [¹¹C]DAA1106 in the mouse brain is shown in Table

2-2. As can be seen, [¹¹C]DAA1106 showed a rapid penetration across BBB into all brain regions at 1 min after *i.v.* administration. The uptakes of [¹¹C]DAA1106 in the olfactory bulb and cerebellum were higher than 2.8% injection dose/g at 5 min post-injection. The radioactivity accumulated with time in all regions examined, and the concentrations in these regions reached a peak during 15–30 min, and then declined until 60 min postinjection. Among the brain regions examined, the highest uptake of radioactivity (4.2% injection dose/g at 30 min) was observed in the olfactory bulb, the highest PBR density area in the mouse brain. Following by the olfactory bulb, a high radioactivity level of [¹¹C]DAA1106 (3.5% injection dose/g at 30 min) was also detected in the cerebellum, whereas a moderate or low uptake was observed in the cerebral cortex, hypothalamus, striatum and hippocampus. The radioactivity of [¹¹C]DAA1106 in the thalamus was the lowest among the brain regions examined.

The *in vivo* selectivity and specificity of [¹¹C]DAA1106 was tested by co-injecting the unlabeled DAA1106, PBR-selective PK11195 and CBR-selective Ro15-1788 at a dose of 1 mg/kg, with [¹¹C]DAA1106, respectively. The results of these blocking studies at 30 min postinjection are presented in Fig. 2-3. Co-injection with the unlabeled DAA1106 exhibited a statistically significant reduction of radioactivity in the brain regions compared with the control group. The most significant reduced uptake was found in the olfactory bulb (14% of control) and cerebellum (16% of control). Other brain regions (striatum, hippocampus, thalamus, hypothalamus and cerebral cortex) showed a moderate decrease (20–54%) in the percent uptake of [¹¹C]DAA1106. These results revealed a high specific binding of [¹¹C]DAA1106 in all brain regions examined, especially in the olfactory bulb and cerebellum. PBR-selective PK11195 (1 mg/kg) also produced a significant reduction of radioactivity in all brain regions, to an extent similar to that obtained using of the same amount of the non-radioactive DAA1106. The largest decrease in binding occurred in the olfactory bulb (10%) and in the cerebellum (13%) compared with the saline group. In contrast, CBR-selective Ro15-1788 co-injection did not show a clear inhibitory effect on the uptake of [¹¹C]DAA1106 (Fig. 2-3). In the cerebellum, hypothalamus and thalamus, Ro15-1788 showed a modest (less than 20%) increase in bindings.

Metabolites of a radiotracer in the plasma which enter the brain can confound PET

imaging studies of neuroreceptors, whether or not the labeled metabolites bind to the target receptor. The plasma and extract of homogenized brain tissues of mice were examined by HPLC for radioactivity after *i.v.* administration of [¹¹C]DAA1106 (70–90 MBq). The percentages of the unchanged [¹¹C]DAA1106 (retention time=10.2 min) in the total radioactivity of the plasma and brain tissues are shown in Fig. 2-4. As can be seen, in the plasma, the amount of [¹¹C]DAA1106 continued to decrease during the entire experiment and a labeled metabolite was observed as early as 2 min after injection. The fraction corresponding to the unchanged [¹¹C]DAA1106 in the plasma was 65% at 5 min, 17% at 30 min, and 6% of the total radioactivity at 60 min postinjection (Fig. 2-4). The radiolabeled metabolite was more polar than [¹¹C]DAA1106 as estimated by the retention order (retention time=1.8 min) on a reversed phase HPLC column. In contrast, in the brain homogenate, only [¹¹C]DAA1106 was detected with no evidence (<5%) of any radioactive metabolites even at 60 min postinjection (Fig. 2-4).

The metabolism of DAA1106 in the rat liver fraction was previously examined and debenzoylation of DAA1106 was found to be a major metabolite route¹¹⁷). The debenzoylated compound (*N*-(5-fluoro-2-phenoxyphenyl)acetamide) was inactive up to 10,000 nM concentration in displacing both [³H]PK11195 from PBR and [³H]flunitrazepam from CBR. Therefore, the presence of this non-radioactive debenzoylated metabolite could not affect the specific binding of [¹¹C]DAA1106 in the brain, even if it passed the BBB and entered the brain. On the other hand, no radiolabeled metabolite except the unchanged [¹¹C]DAA1106 was detected in the brain homogenates. Thus, while extensively metabolized in the plasma, the radiolabeled metabolite of [¹¹C]DAA1106 did not appear to cross the BBB in this species. These findings can reveal that all of the specific binding determined in the mouse brain was due to [¹¹C]DAA1106 itself and not influenced by the radiolabeled metabolite.

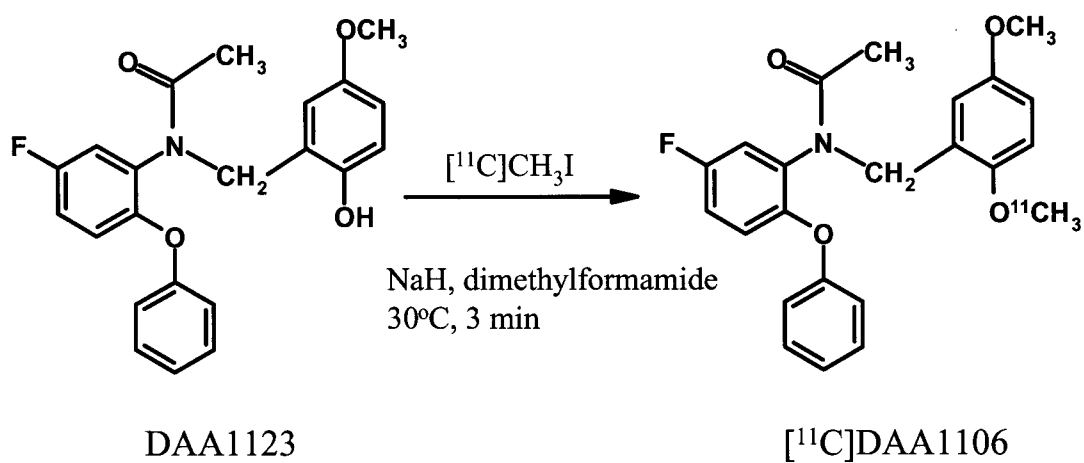


Fig. 2-1

Scheme of radiosynthesis of $[^{11}\text{C}]\text{DAA1106}$.

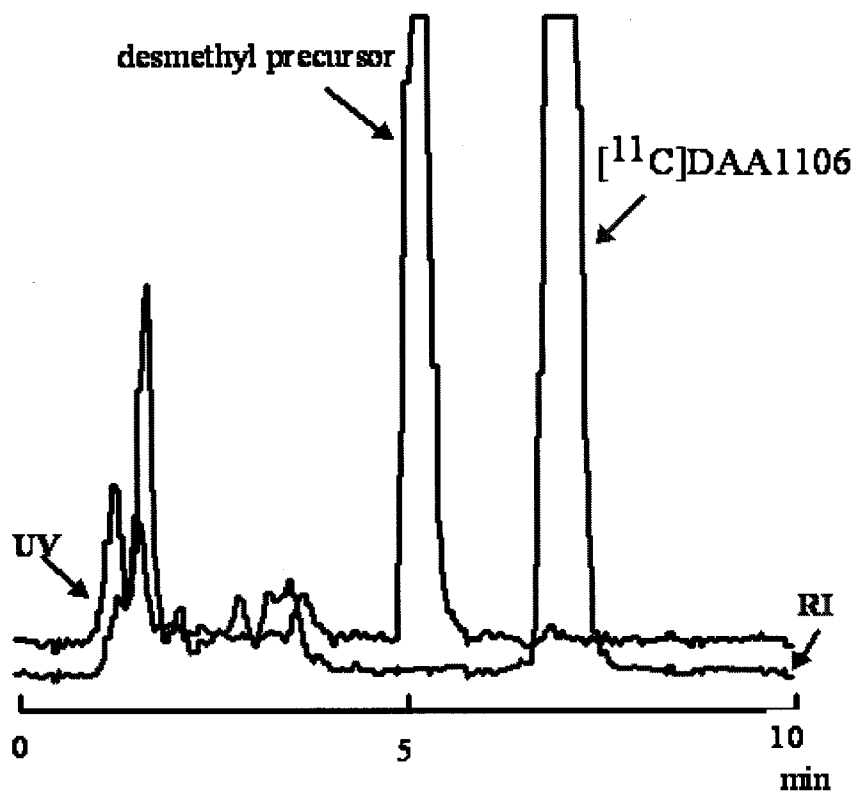


Fig. 2-2

Chromatogram of [¹¹C]DAA1106 and its precursor.

Table 2-1 Distribution of [¹¹C]DAA1106 in mice at 1, 5, 15, 30, 60 min postinjection

Tissue	1 min	5 min	15 min	30 min	60 min
Blood	2.53 ± 0.28	1.65 ± 0.34	2.41 ± 0.42	2.13 ± 0.53	1.43 ± 0.3
Heart	10.45 ± 1.94	11.59 ± 2.36	16.52 ± 3.41	11.54 ± 1.85	7.49 ± 2.01
Liver	1.35 ± 0.41	1.75 ± 0.41	2.1 ± 0.58	1.81 ± 0.67	1.81 ± 0.54
Kidney	12.4 ± 2.35	12.55 ± 2.43	10.01 ± 1.85	9.55 ± 2.81	7.48 ± 1.58
Adrenal	8.15 ± 1.31	7.41 ± 1.28	6.58 ± 1.45	5.31 ± 0.82	5.1 ± 0.98
Lung	90.15 ± 8.15	80.32 ± 9.14	70.84 ± 8.52	48.15 ± 5.1	28.35 ± 2.1
Brain	2.53 ± 0.94	2.81 ± 1.05	3.54 ± 0.98	2.79 ± 0.68	2.12 ± 0.88

Table 2-2 Brain regional distribution of [¹¹C]DAA1106 in mice at 1, 5, 15, 30, 60 min postinjection

Region	1 min	5 min	15 min	30 min	60 min
Cerebellum	2.61 ± 0.89	2.78 ± 0.38	3.42 ± 0.28	3.52 ± 0.21	1.86 ± 0.19
Olfactory bulb	2.79 ± 0.61	2.88 ± 0.34	3.56 ± 0.55	4.21 ± 0.45	1.97 ± 0.71
Hippocampus	0.53 ± 0.21	0.82 ± 0.3	1.52 ± 0.31	1.7 ± 0.23	0.80 ± 0.25
Striatum	0.81 ± 0.15	1.28 ± 0.39	1.82 ± 0.35	1.81 ± 0.36	1.12 ± 0.25
Cerebral cortex	1.42 ± 0.26	1.34 ± 0.1	2.35 ± 0.39	2.3 ± 0.68	1.56 ± 0.69
Hypothalamus	1.28 ± 0.18	1.35 ± 0.18	1.45 ± 0.16	1.41 ± 0.31	1.16 ± 0.38
Thalamus	1.03 ± 0.2	1.51 ± 0.35	1.42 ± 0.21	1.23 ± 0.34	1.19 ± 0.29

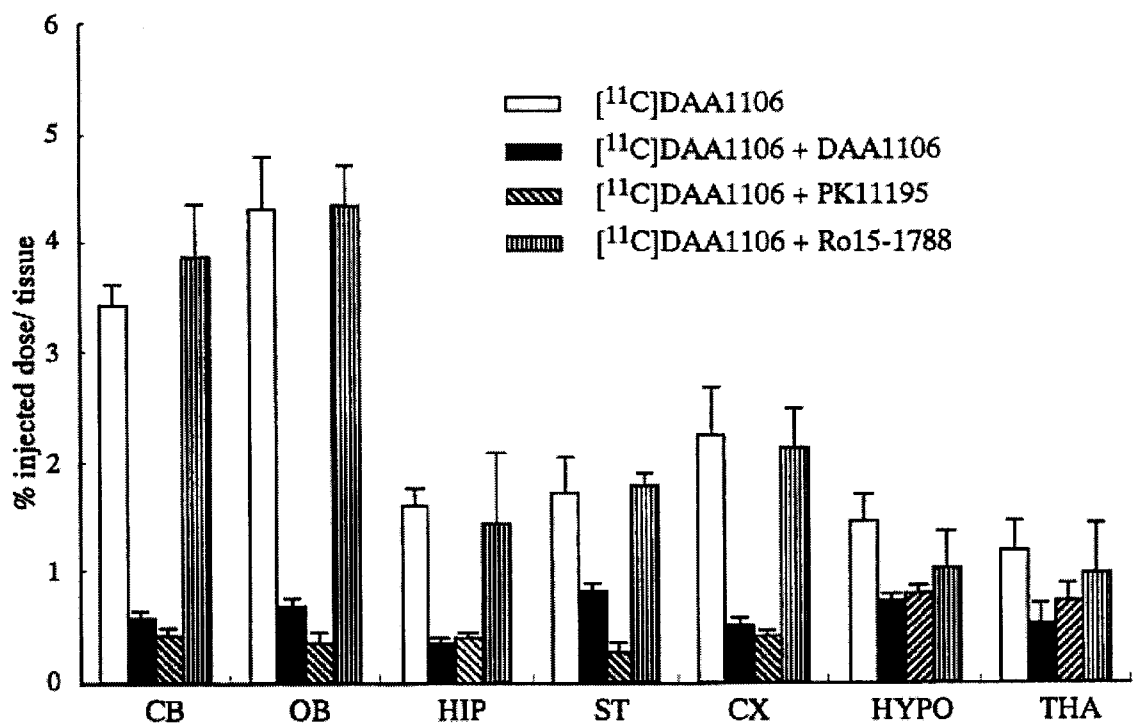


Fig. 2-3

Effect of unlabeled DAA1106 (1 mg/kg), PBR-selective PK11195 (1 mg/kg) and CBR-selective Ro 15-1788 (1 mg/kg) on [¹¹C]DAA1106 concentrations (mean ± SEM., n=5) in selected regions of mouse brains at 30 min postinjection of [¹¹C]DAA1106 (8 MBq). Abbreviations: CB = cerebellum; OB = olfactory bulb; HIP = hippocampus; ST = striatum; CX = cerebral cortex; HYPO = hypothalamus; THA = thalamus.

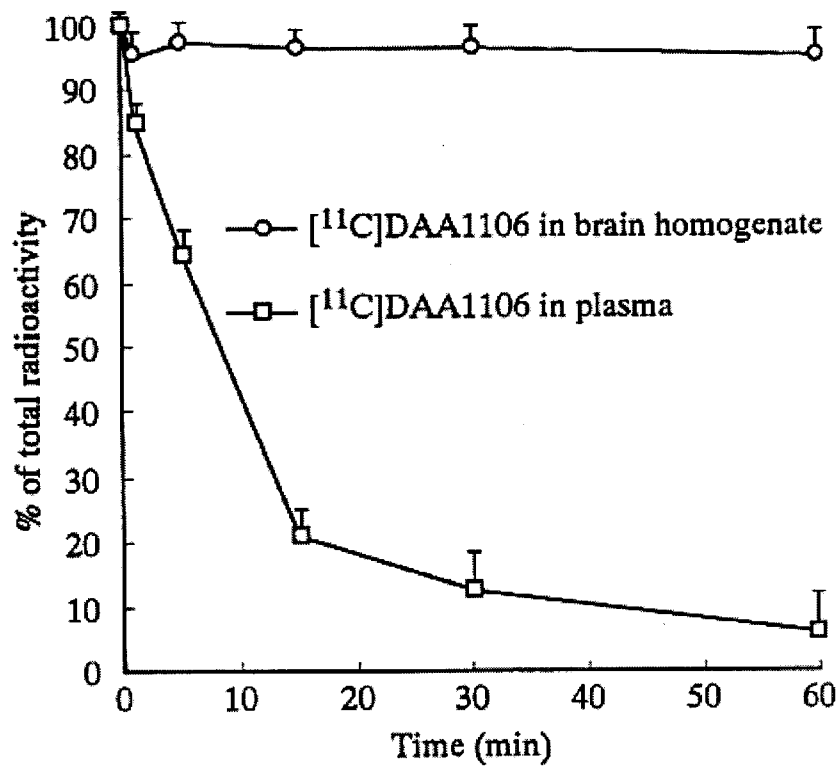


Fig. 2-4

Percent (mean \pm SEM, $n=3$) of the unchanged $[^{11}\text{C}]\text{DAA1106}$ in the plasma and brain homogenate of mouse at several time points after the injection of $[^{11}\text{C}]\text{DAA1106}$ (70–90 MBq).

Experiment 2-2

***In vivo* binding property of [¹¹C]DAA1106 in the rat and monkey**

MATERIALS AND METHODS

Synthesis of radiotracers

Synthesis of [¹¹C]DAA1106 was carried out as experiment 2-1. The log*D* value of [¹¹C]PK11195 between octanol/phosphate buffer (pH7.4) was determined by shaken flask method as described in detail previously¹²²⁾. Specific radioactivity of [¹¹C]DAA1106 was 175 ± 78 GBq/μmol (mean ± SD; >60 GBq/μmol), and that of [¹¹C]PK11195 was >74 GBq/μmol at the end of synthesis. The tracer was injected to animals within 20 min following synthesis.

[¹¹C]PK11195 was synthesized by [¹¹C]-N-methylation of desmethyl precursor as previously described in detail¹²¹⁾.

Animals

Male rats weighing 300–400 g and a male rhesus monkey (*Macaca mulatta*) weighing 7.0 kg were used. The animals were maintained and handled in accordance with recommendations by the US National Institutes of Health and our guidelines (National Institute of Radiological Sciences, Chiba, Japan). The studies were approved by the Animal Ethics Committee of the National Institute of Radiological Sciences.

Neural lesion of hippocampus

Rats were anesthetized with pentobarbital (60 mg/kg) and a cannula (Plastic One Inc. USA) was implanted into the dorsal hippocampus (A/P -4.0 mm; L 2.5 mm, D/V 3.5 mm from bregma). Kainic acid (10 nmol in 5 μL of phosphate buffered saline at pH 7.4) was infused into the right dorsal hippocampus for 5 min using a syringe-pump (BAS Instruments, USA). Vehicle was injected into the left hippocampus as control. The rats were allowed to recover for 7 days before *ex vivo* or *in vitro* autoradiography. The uptake of

[¹¹C]DAA1106 was evaluated by the ratio of the normal or lesioned hippocampus to the cerebral cortex. One-way ANOVA following post-hoc analysis with Scheffe's test was used for the evaluation.

***Ex vivo* autoradiography of [¹¹C]DAA1106**

[¹¹C]DAA1106 (26–55 MBq) was injected into rats via tail vein under diethyl ether anesthesia. Thirty min after the injection, rats were sacrificed by decapitation. Brains were immediately removed and frozen in powdered dry ice. The frozen brain was cut into 40 μm thick sagittal or transaxial sections using a cryotome (HM560; Carl Zeiss Co. LTD., Germany). The sections were then dried under warm blowing air and contacted to an imaging plate (Fuji Film Co. LTD, Japan) for 2 hr. The imaging plate data was analyzed by BAS1800 II system (Fuji Film Co. LTD, Japan). Regions of interest were placed on the olfactory bulb, pons/medulla, cerebellum, hippocampus, striatum, thalamus and frontal cortex, and photo-stimulated luminescence (PSL)/mm² values were used for quantification.

***In vitro* autoradiography of [¹¹C]DAA1106**

The frozen rat brain was cut into 20-μm thick sagittal sections with a cryotome (HM560; Carl Zeiss Co. LTD., Germany) at -15°C. The sections were mounted on slide glass (Matsunami Glass Ind., Ltd., Japan) and stored in a deep-freezer (-80°C). The brain sections were pre-incubated in 50 mM Tris-HCl buffer (pH 7.4, room temperature) for 15 min, and then incubated in 50 mM Tris-HCl buffer (pH 7.4, 25°C) with [¹¹C]DAA1106 (74 MBq/L, about 0.5 nM) for 60 min. After the incubation they were rinsed with ice-cold Tris-HCl buffer for 2 min twice, and finally dipped into ice-cold water for 10 sec. The autoradiograms were obtained by similar procedures as for the above-mentioned *ex vivo* autoradiography. Non-specific binding of [¹¹C]DAA1106 was determined by incubation in the presence of 10 μM of DAA1106¹¹⁶⁾.

The ratio of total binding (specific binding plus non-specific binding) relative to the frontal cortex was used as a relative index of the *ex vivo* and *in vitro* bindings, because it was difficult to keep at the same injection dose (mol) of [¹¹C]DAA1106 in every experiment. The regional differences of the 6 brain regions and lesioned hippocampus were

evaluated by one-way ANOVA. Correlation between *ex vivo* and *in vitro* [¹¹C]DAA1106 binding in the same region was evaluated by the coefficient of determination (r^2) by linear correlation.

Monkey PET study

Flumazenil (Anexate[®], Yamanouchi Pharmaceutical Co. Ltd., Japan) and PK11195 (Tocris Cookson Ltd., UK) were purchased. Both DAA1106 and PK11195 were dissolved in propylene glycol with 20% ethanol. Each drug was slowly injected just before tracer injection via the tibial vein for 2 min. [¹¹C]DAA1106 was injected 5 min after drug treatment. Drug treatments were separated by at least 2-week intervals.

All PET scans were performed using SHR-7700 PET described as Chapter 1. The monkey was repeatedly anesthetized with ketamine at 10 mg/kg/hr *i.m.* (Ketalar[®], Sankyo Co. LTD., Japan) every hour throughout the session and immobilized with a head fixation device to ensure accuracy of re-positioning. After transmission scans for attenuation correction using a ⁶⁸Ge-⁶⁸Ga source for 30 min, dynamic emission scan in 3-dimensional acquisition mode was performed for 90 min (1 min × 4 scans, 2 min × 8 scans, 5 min × 8 scans, 10 min × 3 scans). The injected doses of [¹¹C]DAA1106 were 90.6 ± 9.3 MBq (mean ± S.D.).

After *i.v.* administration of [¹¹C]DAA1106, arterial blood was collected at 10, 20, 45 sec, 1, 1.5, 2, 3, 4, 5, 6, 8, 10, 15, 20, 25, 30, 45, 60, 75, 90 min after tracer injection. The radioactivities of whole blood samples (1.0 mL) and plasma samples were measured with a well-type γ -scintillation counter. The plasma samples were centrifuged at 15,000 rpm for 1 min at 4°C. Radioactivity was corrected for decay.

Plasma samples (250 μ L) at 2, 10, 30, 60, 90 min after tracer injection were collected in a test tube containing CH₃CN (500 μ L), stirred for 15 sec, and centrifuged at 15,000 rpm for 1 min for deproteinization. An aliquot of the supernatant (100–500 μ L) was injected into the HPLC system with column CAPCELL PAK C18 ϕ 4.6mm × 250 mm (Shiseido Co. LTD, Tokyo) and a highly sensitive positron detector under the mobile phase of CH₃CN/H₂O (1:1) at a flow rate of 2.0 mL/min. Unchanged [¹¹C]DAA1106 (retention time=10.6 min) to the total radioactivity (corrected for decay) from the HPLC

chromatogram was calculated as $\% = [(\text{radioactive peak area for unchanged } [^{11}\text{C}]\text{DAA1106} / \text{total radioactive peak area}) \times 100]$.

All emission scan images were reconstructed with a 4.0mm Colsher filter, and circular regions of interest of 4-mm diameter were placed on the occipital cortex, frontal cortex and cerebellum using image analysis software with reference to the MR image of monkey brain (in-house software PET Analyzer for Windows[®]). The uptake was expressed as the percent of injected dose per volume (% dose/mL) or the percent of maximum uptake, and plotted against time. PET data from one monkey was analyzed by 3-compartment kinetics model using PMOD[®] (PMOD Technologies LTD, Switzerland), and k_1 , k_2 , k_3/k_4 and distribution volume (DV) were determined. The radioactivity in arterial plasma with metabolite and decay-corrected was used for reference.

RESULTS

First, I evaluated the [^{11}C]DAA1106 binding *ex vivo* or *in vitro* by autoradiography in rats. Fig. 2-5A shows the *ex vivo* and *in vitro* autoradiograms of rat brain with [^{11}C]DAA1106. Background count from seven films was 0.91 ± 0.19 PSL/mm² (mean \pm S.D.). The PSL/mm² levels in the brain were at least 20-fold higher than the background level (data not shown). Significant regional difference was observed both *ex vivo* ($F_{(6,46)}=8.9$, $p<0.01$) and *in vitro* ($F_{(6,41)}=15.7$, $p<0.01$). The highest binding was observed in the olfactory bulb, followed by the pons/medulla and cerebellum, the frontal cortex and hippocampus both *ex vivo* and *in vitro*. The relative binding in the olfactory bulb was significantly higher than in the other 5 brain regions ($P<0.01$). The relative [^{11}C]DAA1106 binding in the cortex *ex vivo* correlated well with that *in vitro* (slope function =0.996, $r^2=0.96$, $p<0.001$; Fig. 2-5B). High uptake was also observed in the choroid plexus area, particularly *ex vivo* (Fig. 2-5A, left panel). In the presence of 10 μM of unlabeled DAA1106 or PK11195, cortical [^{11}C]DAA1106 binding was reduced by 70% compared to control binding (data not shown). This result suggested that specific binding of [^{11}C]DAA1106 occupies 30% of the total binding in the cortex.

Fig. 2-6 shows the increase of hippocampal [^{11}C]DAA1106 binding *ex vivo* and *in vitro* produced by kainic acid. The rats were treated with kainic acid (10 nmol) into the right hippocampus (Fig. 2-6A), and the binding was evaluated at 7 days after the infusion. The ratio to the cortex value of [^{11}C]DAA1106 binding in the lesioned hippocampus was increased 2-fold compared to that in the normal hippocampus of *in vitro* binding [$F_{(1,11)}=52.89$, $p<0.001$] (Fig. 2-6B, right columns). This increment of [^{11}C]DAA1106 binding was similar to that of [^{11}C]PK11195 binding in the ischemic cortex of rat¹²³). The ratio of specific binding of [^{11}C]DAA1106 in the lesioned hippocampus to that in the cortex was 5.4 ± 0.7 *in vitro* (data not shown). A significant increase of [^{11}C]DAA1106 binding by kainic acid was also observed in the *ex vivo* condition [$F_{(1,11)}=8.75$, $p<0.05$] (Fig. 2-6B, left columns). The magnification is well correlated between *ex vivo* and *in vitro* (Fig. 2-5B).

To investigate the detailed brain kinetics of [^{11}C]DAA1106, I carried out PET scan using one rhesus monkey. The time-activity curves of [^{11}C]DAA1106 in the monkey brain,

whole blood and plasma are shown in Fig 2-7. [^{11}C]DAA1106 rapidly went into the brain and remained at almost the same uptake level during the scan time of 90 min in all measured brain regions. Radioactivity in the occipital cortex was slightly higher than that in the frontal cortex and cerebellum. The radioactivity in the occipital cortex was evaluated by 3-compartment model analysis. The calculated parameters were 5.9 for k_1 , 0.9 for k_2 , 69.4 for DV and 10.9 for k_3/k_4 . The plasma half-life of unchanged [^{11}C]DAA1106 was estimated as 13.6 min (data not shown). The main metabolite was considered to be only DAA1123, a precursor of [^{11}C]DAA1106.

Fig. 2-8A shows the summation images of [^{11}C]DAA1106 and [^{11}C]PK11195 in monkey brain. The accumulation of [^{11}C]DAA1106 in the occipital cortex was slightly higher than in other brain structures, while obvious accumulation of [^{11}C]PK11195 was not observed. The time-activity curves of [^{11}C]DAA1106 and [^{11}C]PK11195 in the occipital cortex are shown in Fig. 2-8B. Radioactivity was adjusted to the injected dose (% dose/mL). The initial uptake of [^{11}C]PK11195 decreased rapidly, whereas the initial uptake of [^{11}C]DAA1106 remained at almost the same level for 90 min. The radioactivity of [^{11}C]DAA1106 in the occipital cortex at 30 min after tracer injection was 4-time higher compared to that of [^{11}C]PK11195. To compare the lipophilicity of [^{11}C]PK11195 with [^{11}C]DAA1106, I determined the logD between phosphate buffer (pH7.4) and octanol. The logD for [^{11}C]PK11195 was 2.7, and was 10-fold lower than 3.7 for [^{11}C]DAA1106.

I determined whether the [^{11}C]DAA1106 binding in monkey brain corresponded to specific binding for PBR. Fig. 2-9A shows the effect of pretreatment with DAA1106 (0.5 and 1 mg/kg) or PK11195 (5 and 10 mg/kg) on [^{11}C]DAA1106 binding in the occipital cortex. Each drug was administered 5 min before tracer injection. The uptake of [^{11}C]DAA1106 in the occipital cortex was dose-dependently decreased by DAA1106. PK11195 also inhibited the uptake of [^{11}C]DAA1106, but there was no clear dose dependency between 5 mg/kg and 10 mg/kg. There was a marked increase in the initial uptake of [^{11}C]DAA1106 by both DAA1106 and PK11195 pretreatment. On the other hand, flumazenil (0.1 mg/kg, *i.v.*) did not affect the uptake of [^{11}C]DAA1106. Similar inhibition was obtained in the frontal cortex (Fig. 2-9B). Since treatment with PBR ligand increased the initial uptake of radioactivity of [^{11}C]DAA1106, the time-activity curves were

normalized to the initial peak (Fig. 2-9C and 2-9D). The uptake of [¹¹C]DAA1106 was inhibited by 1 mg/kg of DAA1106 or 10 mg/kg of PK11195 to 20 or 30% of the control uptake, respectively.

The [¹¹C]DAA1106 binding seemed to be irreversible due to the slow elimination from brain. I demonstrated by *in vivo* displacement test whether [¹¹C]DAA1106 binding could behave in a reversible manner. The [¹¹C]DAA1106 binding was displaced by *i.v.* treatment with DAA1106 (1 mg/kg) or PK11195 (5 mg/kg) 30 min after tracer injection (Fig. 2-10).

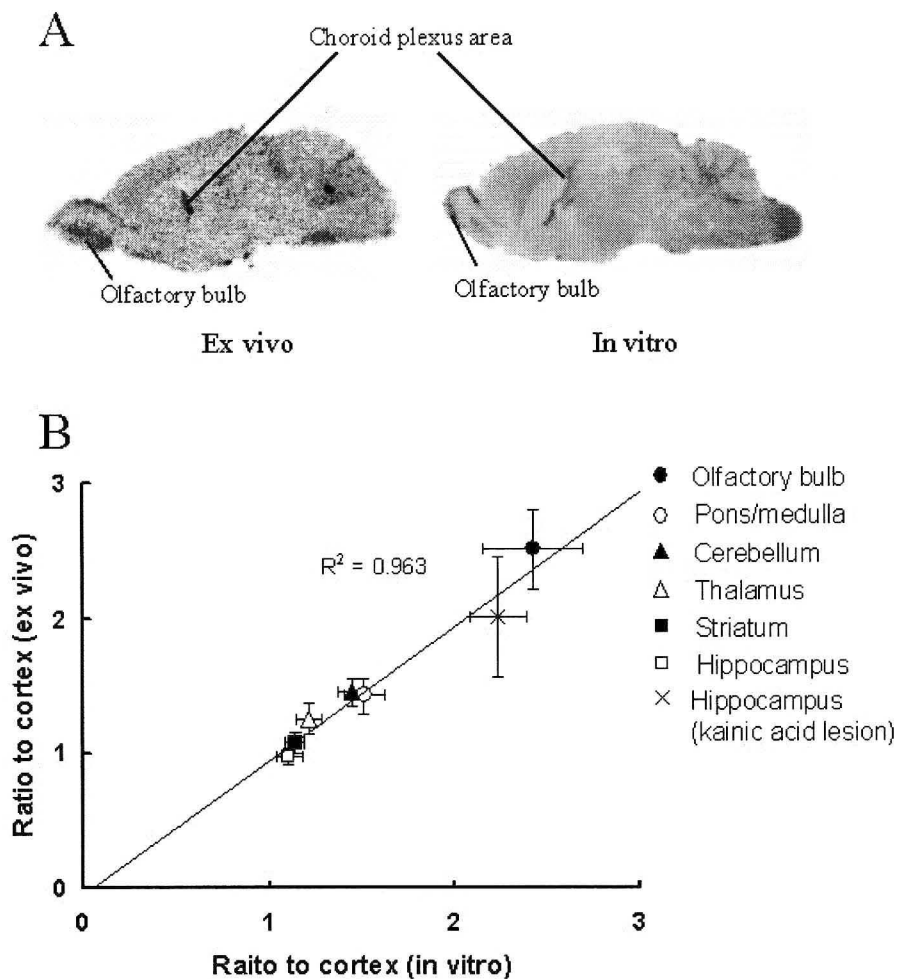


Fig. 2-5

A: Ex vivo (left panel) and in vitro (right panel) autoradiograms of [^{11}C]DAA1106 of the rat brain. **B:** Linear regression between ex vivo and in vitro ratio of PSL/ mm^2 value relative to the frontal cortex in 6 brain regions — olfactory bulb, pons/medulla, cerebellum, thalamus, normal or lesioned hippocampus and striatum. Significant correlation was obtained between *ex vivo* and *in vitro* [^{11}C]DAA1106 binding. Data are presented as mean value of the PSL/ mm^2 ratio to the frontal cortex \pm S.E.M.

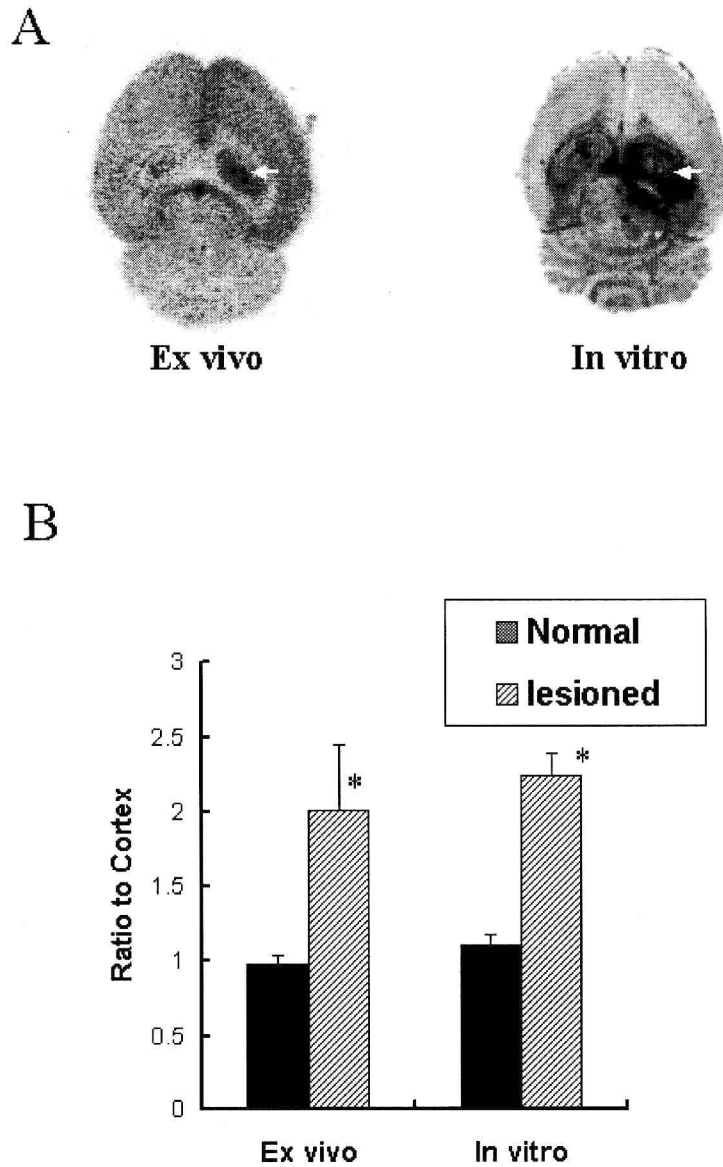


Fig. 2-6

A: *Ex vivo* and *in vitro* autoradiograms of [¹¹C]DAA1106 binding in the unilateral destruction of the dorsal hippocampus produced by kainic acid (10 nmol). The arrow indicates kainic acid-injected side. **B:** The [¹¹C]DAA1106 binding (ratio to cortex) in the normal and lesioned hippocampus *ex vivo* and *in vitro*. Closed and hatched column represents normal and lesioned hippocampus, respectively. The destruction of hippocampus neurons was 2.0-fold higher than in the normal hippocampus in both autoradiograms.

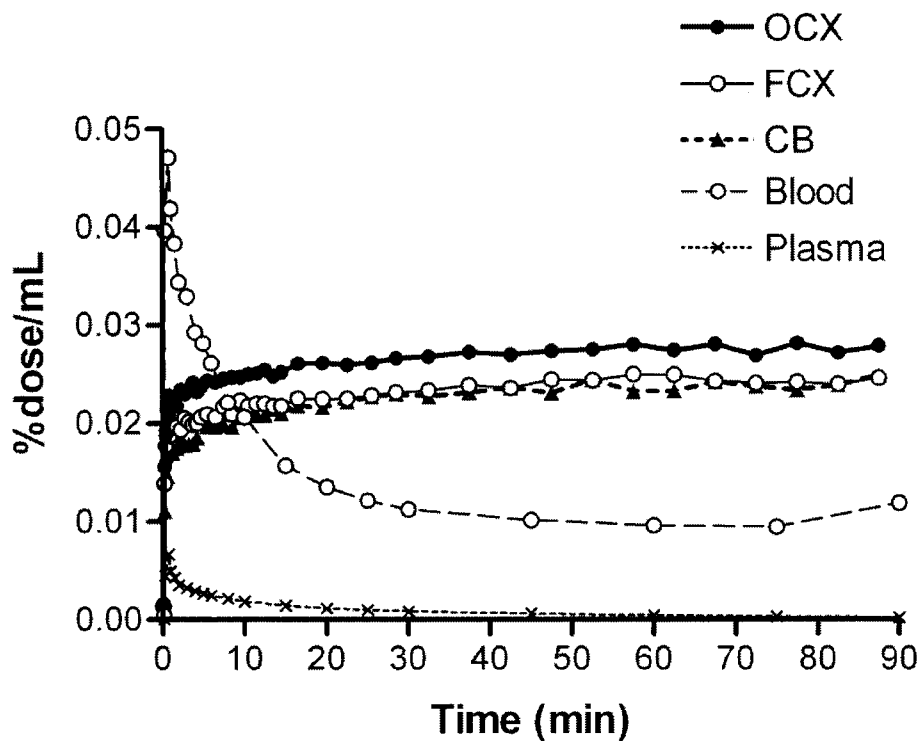


Fig. 2-7

Time activity curve of [^{11}C]DAA1106 of the monkey in the occipital cortex, frontal cortex, cerebellum, whole blood and plasma. Radioactivity in plasma was corrected with unchanged [^{11}C]DAA1106. The half-life of [^{11}C]DAA1106 in plasma was estimated as 13.6 min.

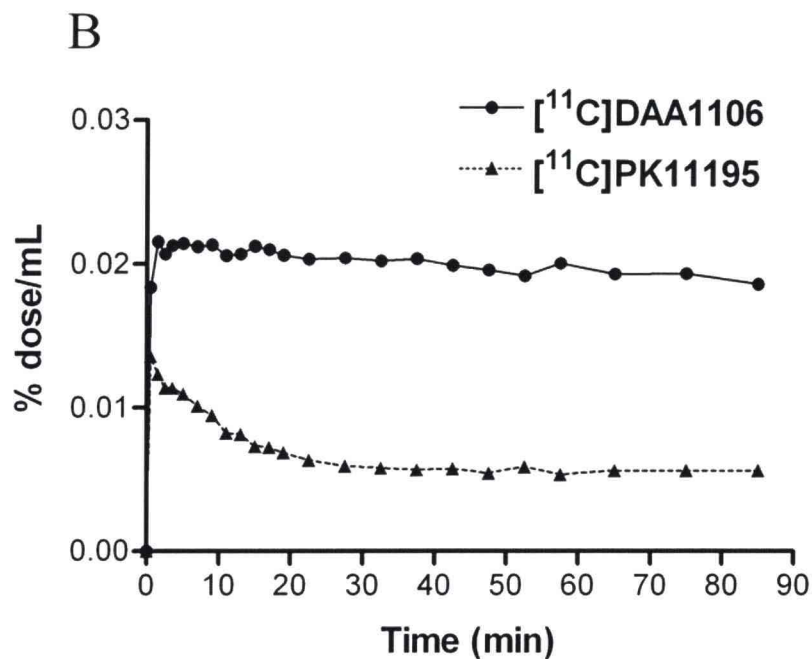
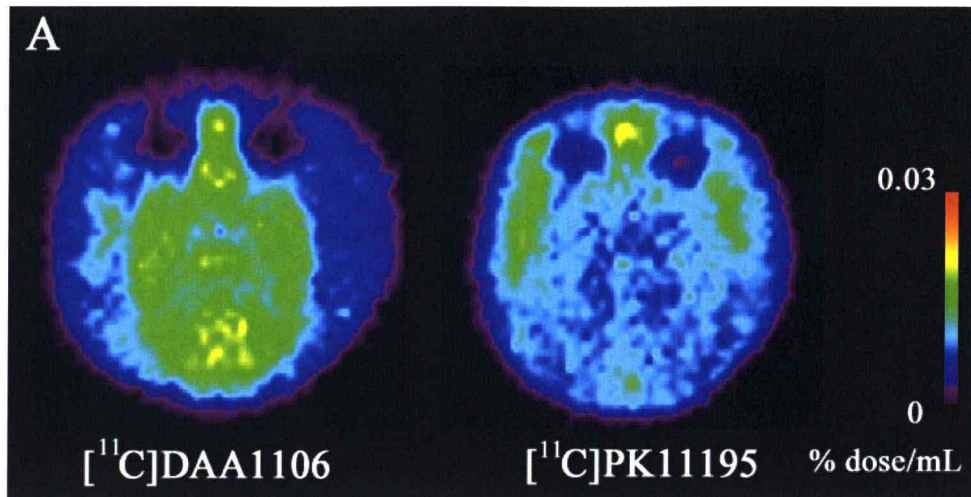


Fig. 2-8

A: Summation images (0-90 min) of $[^{11}\text{C}]\text{DAA1106}$ (left panel) and $[^{11}\text{C}]\text{PK11195}$ (right panel) from the brain of the same rhesus monkey. **B:** Time activity curves of $[^{11}\text{C}]\text{DAA1106}$ and $[^{11}\text{C}]\text{PK11195}$ in the occipital cortex. Data were normalized to the percent of injected dose (%dose) per volume (mL). The radioactivity of $[^{11}\text{C}]\text{DAA1106}$ was 4-times higher than that of $[^{11}\text{C}]\text{PK11195}$ from 30 min after the injection.

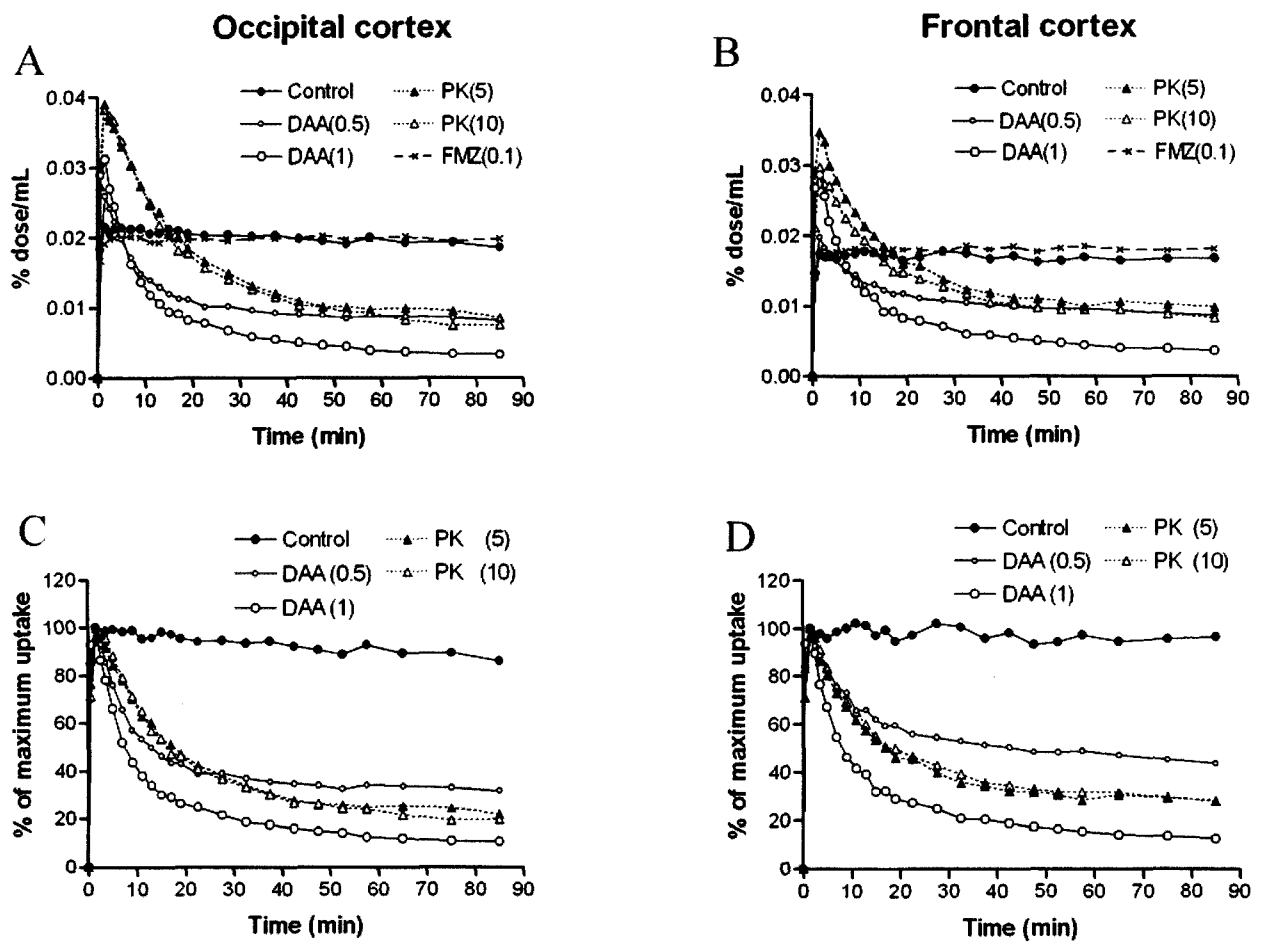


Fig. 2-9

A, B: The effect of drugs with affinity to PBR or to CBR on [^{11}C]DAA1106 binding in the occipital cortex (**A**) and frontal cortex (**B**) of the monkey. The uptake was expressed as the percent of injection dose per volume (% dose/mL). **C, D:** Data in the occipital cortex (**C**) and frontal cortex (**D**) are normalized to the initial maximum uptake of tracer as 100%. The uptake of [^{11}C]DAA1106 was inhibited by 1 mg/kg of DAA1106 and 10 mg/kg of PK11195 to approximate 20 and 35% of the control uptake, respectively.

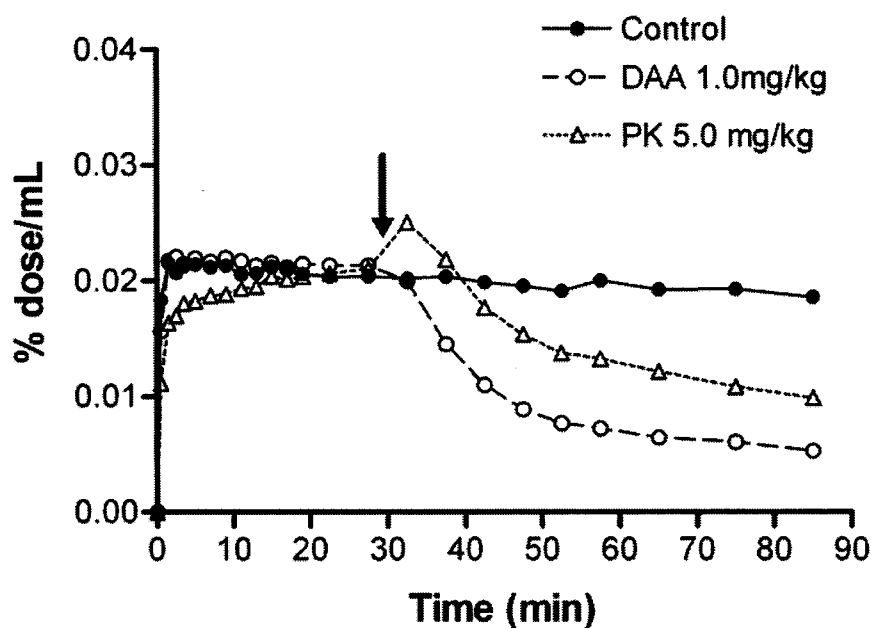


Fig. 2-10

Displacement of [^{11}C]DAA1106 binding by DAA1106 (1 mg/kg) and PK11195 (5 mg/kg) in the occipital cortex of the monkey. Treatment with each drug was carried out 30 min after tracer injection (solid arrow). The uptake was expressed as the percent of injection dose per volume (% dose/mL).

DISCUSSION

The present results showed that [^{11}C]DAA1106 had high specific binding for PBRs in the brain *ex vivo* as well as *in vitro*. The *ex vivo* binding of [^{11}C]DAA1106 correlated well with *in vitro* binding (Fig. 2-5B). The distribution of [^{11}C]DAA1106 in the rat brain was consistent with previous *in vitro* autoradiography studies using [^3H]Ro5-4864^{101,102}) and [^3H]PK11195⁹³). [^{11}C]DAA1106 binding in the rat brain was highest in the olfactory bulb while that in the monkey brain was highest in the occipital cortex. The relatively higher accumulation of [^{11}C]DAA1106 in the occipital cortex was similar to the *in vitro* binding of [^3H]Ro5-4864 and [^3H]PK11195 in the primate brain^{102,124}).

The uptake of [^{11}C]DAA1106 was markedly decreased by pretreatment with 1.0 mg/kg of DAA1106 or 10 mg/kg of PK11195 despite initial increases in uptake. I expected that the decrement of [^{11}C]DAA1106 uptake by 1.0 mg/kg of DAA1106 was about 80% of total radioactivity, corresponding to the specific binding *in vivo*. The increase of initial uptake by pretreatments with DAA1106 and PK11195 can be explained by precluded [^{11}C]DAA1106 from the peripheral organs, since the accumulation of [^{11}C]DAA1106 and [^3H]PK11195 is highest in the mouse lung, and the accumulation of [^3H]PK11195 was completely blocked by unlabeled PBR ligand¹²¹). Similar cases have been reported with [^{11}C]PK11195¹²⁵) and serotonin transporter ligand [^{11}C]cyanoimipramine¹²⁶).

The time-activity curve of [^{11}C]DAA1106 was analyzed by 3-compartment model. The value of k_3/k_4 reflects the slow dissociation from the binding site in the monkey brain. However, [^{11}C]DAA1106 binding was clearly displaced by PBR ligand at 30 min after the tracer injection (Fig. 2-10), and my preliminary human experiment showed a clear decline in the time-activity curve of [^{11}C]DAA1106 in the brain during the PET experiment.

The uptake of [^{11}C]DAA1106 in the monkey brain at 30 min was about 4-times higher than that of [^{11}C]PK11195. The dissociation constant (K_d) of DAA1106 in the rat brain was 10-fold smaller than that of PK 11195¹¹⁹). LogD values were 3.7 for DAA1106 and 2.7 for PK11195, indicating a lipophilicity of DAA1106 is 10-fold higher than that of PK11195. This difference in lipophilicity and affinity may partially explain the higher permeability and slower kinetics of DAA1106 in the brain compared to PK11195. In addition, the

mechanism of the kinetic difference can be explained by the excretion from the brain through P-glycoprotein, an efflux transporter for multiple drugs, since its substrates are expected to show fast kinetics independent of its pharmacological properties¹²⁷). PK11195 was reported to be a potent substrate of P-glycoprotein in tumor cells with multi-drug resistance¹²⁸). Although it is unknown whether DAA1106 is a substrate for P-glycoprotein, DAA1106 may not be excreted by P-glycoprotein due to the slow elimination from the brain.

PK11195 has weaker potency in inhibition to the [¹¹C]DAA1106 binding than DAA1106 itself. The difference in the brain kinetics between DAA1106 and PK11195 suggested an insufficient amount of PK11195 in the brain. Another cause might be the heterogeneity of the ligand-binding domain on PBR. The binding domain for isoquinoline derivatives such as PK11195 was demonstrated to be on isoquinoline binding protein^{129,130}), while the BZ-binding domain is thought to be on both isoquinoline binding protein and voltage-dependent anion channel¹³¹). B_{max} and K_d of DAA1106 binding for recombinant PBR in bacteria were similar to those of PK11195 binding despite the lack of voltage-dependent anion channel¹¹⁹), and PK11195 fully displaced the [³H]DAA1106 binding^{116,119}). Thus, the binding sites for both PK11195 and DAA1106 were located on isoquinoline binding protein. However, a high concentration of PK11195 was required to displace the [³H]DAA1106 binding. This suggested that the binding domain for DAA1106 would contain an extra component that does not interact efficiently with PK11195^{116,119}).

In the present study using kainic acid, the specific binding of [¹¹C]DAA1106 in the dorsal hippocampus was 5-fold higher than in the frontal cortex *in vitro*. Previous reports *in vitro* [³H]PK11195 and [³H]Ro5-4864 binding demonstrated 3-5-fold increases in specific binding by the infusion of kainic acid^{132,133}). The microinjection of kainic acid into the brain was reported to increase the number of glial cells¹³⁴). Microglia and astrocytes were reported to be susceptible to neural destruction by kainic acid¹³⁴⁻¹³⁶). Kuhlmann and Guilarte¹⁰⁰) reported that increased [³H]PK11195 binding induced by trimethyltin corresponded to both activated microglia and proliferated astrocyte. Although activated microglia were observed after 2 days, astrocytosis was observed after 14 days. Since our experiment was evaluated at 7 days after kainic acid injection, the increased PBR binding

might mainly correspond to the activated microglia.

The mechanism of neural injury-increased PBR binding can be explained by some inflammatory reactions. The activated microglia produce neuroinflammation around the damaged regions due to ablation of neural debris. Inflammatory enzymes and mediators such as phospholipase A₂, tumor necrosis factor α 1 and interleukin-1 were reported to increase PBR binding in brain and cell culture¹³⁷⁻¹⁴⁰). Interestingly, reactive oxygen species generated from mitochondria polymerize few molecules of isoquinoline binding protein through a residue of tyrosine¹⁴¹). The polymer of isoquinoline binding protein exhibits 5-fold higher B_{max} of PK11195 binding than the monomer of isoquinoline binding protein¹⁴¹). These results suggest that measuring *in vivo* PBR binding is useful for evaluating the extent and degree of neuroinflammation following the brain injuries.

In conclusion, [¹¹C]DAA1106 showed sufficient signal to allow quantitative analysis. It seems clear that [¹¹C]DAA1106 binding can be used as an index of activated microglia with a higher signal than [¹¹C]PK11195. Furthermore, recent studies have suggested that activated microglia are involved not only in neurodegeneration but also in neurotrophic action and neural plasticity^{45,142}). Thus, the application of [¹¹C]DAA1106 can provide useful information in the diagnosis of neurodegenerative disorders and the mechanisms of glia-neuron interactions.

Chapter 3

Imaging of peripheral benzodiazepine receptor by ^{18}F -labeled DAA1106

INTRODUCTION

In chapter 2, I has demonstrated that the [^{11}C]DAA1106 is useful for imaging of PBR in the brain. However, the short half-life of a ^{11}C labeled ligand (β^+ ; 99.8%, $T_{1/2}=20.4$ min) often limits its usefulness if a dynamic PET experiment has a turnover time longer than 100 min. Since ^{18}F has advantages over ^{11}C , with a longer half-life (110 min vs. 20 min) and lower positron energy (650 KeV vs. 960 KeV³), an ^{18}F -labeled ligand gives higher quality images with a higher spatial resolution in PET measurements. Moreover, ^{18}F is convenient for long-time storage and long-distance transportation to other facilities. To develop ^{18}F -labeled PET ligand, two [^{18}F]fluoroalkyl analogs of DAA1106: [^{18}F]fluoro-methyl-DAA1106 and [^{18}F]fluoro-ethyl-DAA1106 as putative radioligands for PBR were prepared. In this chapter, *in vivo* or *in vitro* properties of [^{18}F]fluoro-methyl-DAA1106 and [^{18}F]fluoro-ethyl-DAA1106 binding were investigated in the rodent and monkey.

Experiment 3

Synthesis, distribution and metabolite of [¹⁸F]fluoro-methyl-DAA1106 and [¹⁸F]fluoro-ethyl-DAA1106

MATERIALS AND METHODS

Radiochemistry

[¹⁸F]Fluoride was produced by the ¹⁸O (p,n) ¹⁸F reaction on 10-20 atom % H₂¹⁸O using 18 MeV protons (14.2 MeV on target) from the cyclotron and separated from [¹⁸O]H₂O using Dowex 1-X8 anion exchange resin in an irradiating room. The [¹⁸F]F⁻ was eluted from the resin with aqueous K₂CO₃ (3.3mg/0.3mL) into a vial containing CH₃CN (1.5 mL)/4,7,13,16,21,24-hexaoxa-1,10-diazabicyclo[8,8,8]hexacosane (Kryptofix 222, 25 mg) and transferred into a reaction vessel in a hot cell. [¹⁸F]-labeled alkylating intermediate as [¹⁸F]FCH₂I and [¹⁸F]BrCH₂CH₂F were prepared by using a newly developed automated system¹⁴³.

Synthesis of [¹⁸F]fluoro-methyl-DAA1106

[¹⁸F]F⁻ from the irradiating room was transported to a Pyrex glass vessel (5 mL) containing 100 μL of *o*-dichlorobenzene (*o*-DCB), and the [¹⁸F]F⁻ was dried to remove H₂O and CH₃CN at 120°C for 15 min. After CH₂I₂ (100 μL) was added to the radioactive mixture by a helium flow (50 mL/min) at 120°C, [¹⁸F]FCH₂I resulted in this vessel was distilled at once under helium for 3 min, and bubbled into another Pyrex glass vessel containing the demethyl precursor DAA1123 (1.5 mg) and NaH (10 μL, 1.5 g/20 mL dimethylformamide) in anhydrous dimethylformamide (300 μL) at -15°C. After maximum radioactivity was bubbled into the solution, the reaction was terminated by adding CH₃CN/H₂O (6/4, 500 μL). The radioactive mixture was applied to a semi-preparative HPLC column. HPLC semi-preparative purification was completed on YMC J'sphere ODS-H80 column (10 mm inside diameter × 250 mm length) using a mobile phase of CH₃CN/H₂O (60/40) at a flow rate of 6.0 mL/min. The t_R for [¹⁸F]fluoro-methyl-DAA1106

was 11.2 min, whereas that for DAA1123 was 6.7 min. The radioactive fraction corresponding to [¹⁸F]fluoro-methyl-DAA1106 was collected in a sterile flask containing polysorbate (80) (75 µL) and ethanol (150 µL), evaporated to dryness under vacuum, re-dissolved in 7 mL of sterile normal saline and passed through a 0.22 µm Millipore filter to obtain the final product. At the end of synthesis, 180-300 MBq of [¹⁸F]fluoro-methyl-DAA1106 was obtained as an *i.v.* injectable solution at a beam current of 10-15 µA and 20-25 min proton bombardment.

Synthesis of [¹⁸F]fluoro-ethyl-DAA1106

After the [¹⁸F]F⁻ was dried, BrCH₂CH₂OTf (8 µL) in *o*-dichlorobenzene (400 µL) was added to the radioactive mixture. The [¹⁸F]FCH₂CH₂Br in this vessel was distilled under a helium flow (90-100 mL/min) at 130°C for 5 min and bubbled into another vessel containing DAA1123 (1.5 mg) and NaH (10 µL, 1.5 g/20 mL dimethylformamide) in anhydrous dimethylformamide (300 µL) at -15°C, and the reaction mixture was heated and kept at 120°C for 10 min. HPLC semi-preparative purification was performed on a YMC J'sphere ODS-H80 column (10 mm inside diameter × 250 mm length) using a mobile phase of CH₃CN/H₂O (55/45) at a flow rate of 6.0 mL/min. The *t_R* for [¹⁸F]fluoro-ethyl-DAA1106 was 14.2 min. At end of synthesis, 570-780 MBq of [¹⁸F]fluoro-ethyl-DAA1106 was obtained as an *i.v.* injectable solution at a beam current of 10-15 µA and 20-25 min proton bombardment.

Radiochemical purity and specific activity determinations

Radiochemical purity was assayed by analytical HPLC (column: CAPCELL PAK C₁₈, 4.6 mm inside diameter × 250 mm length, UV at 254 nm; mobile phase: CH₃CN/H₂O = 6/4). The retention time for [¹⁸F]fluoro-methyl-DAA1106 and [¹⁸F]fluoro-ethyl-DAA1106 was 6.1 min and 6.3 min at a flow rate of 2.0 mL/min. The specific activity of [¹⁸F]fluoro-methyl-DAA1106 and [¹⁸F]fluoro-ethyl-DAA1106 was determined by comparison of the assayed radioactivity to the mass associated with the carrier UV peak at 254 nm.

***In vitro* binding assay**

Method of *in vitro* binding has been described in Chapter 2-2. Data were expressed as percent of control binding (% control). Competition curve was fitted by graphical soft Prism[®], and 50 percent of inhibitory concentration (IC₅₀) and inhibited constant (K_i) were determined.

***Ex vivo* autoradiography of [¹¹C]DAA1106**

Method of *ex vivo* autoradiography is similar to the Chapter 2-2. Regions of interest were placed on the olfactory bulb, cerebellum and frontal cortex, and photo-stimulated luminescence (PSL)/mm² values were used for quantification. To determine whether the accumulation is specific binding, rats were co-injected with non-radioactive DAA1106 (1 mg/kg).

Metabolite assay for plasma and brain tissue

After *i.v.* injection of [¹⁸F]fluoro-methyl-DAA1106 or [¹⁸F]fluoro-ethyl-DAA1106 (5-10 MBq/100 μL) into ddY mice (n=3), these mice were sacrificed by cervical dislocation at 5, 15, 30 or 60 min. Blood (0.7-1.0 mL) and whole brain samples were removed quickly. The blood sample was centrifuged at 15,000 rpm for 1 min at 4°C to separate plasma, which (250 μL) was collected in a test tube containing CH₃CN (500 μL) and a solution of the authentic unlabeled fluoro-methyl-DAA1106 or fluoro-ethyl-DAA1106 (1.1 mg/5.0 mL of CH₃CN, 10 μL). After the tube was vortexed for 15 sec and centrifuged at 15,000 rpm for 2 min for deproteinization, the supernatant was collected. The extraction efficiency of radioactivity into the CH₃CN supernatant ranged from 70% to 92% of the total radioactivity in the plasma. On the other hand, the cerebellum and forebrain including the olfactory bulb were dissected from the mouse brain and homogenized together in an ice-cooled CH₃CN/H₂O (1/1, 1.0 mL) solution. The homogenate was centrifuged at 15,000 rpm for 1 min at 4°C and supernatant was collected. The recovery of radioactivity into the supernatant was 68-87% based on the total radioactivity in the brain homogenate.

An aliquot of the supernatant (100-500 μL) obtained from the plasma or brain

homogenate was injected into the HPLC system for radioactivity, and analyzed under the same conditions described above except that the mobile phase was CH₃CN/H₂O with a ratio of 1/1. The percent ratio of [¹⁸F]ligand (retention time=10.6 min for [¹⁸F]fluoro-methyl-DAA1106 and 11.8 min for [¹⁸F]fluoro-ethyl-DAA1106) to total radioactivity (corrected for decay) on the HPLC chromatogram was calculated as % = peak area for [¹⁸F] ligand /total peak area × 100.

Monkey PET study

All PET scans were performed using SHR-7700 PET camera described as Chapter 1. A dynamic emission scan in the 3D acquisition mode was performed for 180 min (1 min × 5 frames, 2 min × 5 frames, 3 min × 5 frames and 5 min × 30 frames). All emission scan images were reconstructed with a Colsher filter of 4 mm, and circular regions of interest with a 4-mm diameter were placed over the occipital cortex using an image analysis software. A solution of [¹⁸F]fluoro-methyl-DAA1106 and [¹⁸F]fluoro-ethyl-DAA1106 (80-85 MBq) was injected *i.v.* into the monkey, and time-sequential tomographic scanning was performed on a transverse section of the brain for 180 min. In pre-treatment experiments, non-radioactive DAA1106 (1 mg/kg) or PK11195 (5 mg/kg) was injected at 2 min before the [¹⁸F]fluoro-ethyl-DAA1106 injection. The time-activity curves in the occipital cortex were obtained for each scan of the brain.

RESULT

PBR ligands [^{18}F]fluoro-methyl-DAA1106 and [^{18}F]fluoro-ethyl-DAA1106 were prepared by two methods according to Fig. 3-1A and B, respectively. The first method was a two-step reaction sequence which involved the preparation of the radioactive intermediate [^{18}F]FCH₂I or [^{18}F]FCH₂CH₂Br, followed by the alkylation of DAA1123 with [^{18}F]FCH₂I or [^{18}F]FCH₂CH₂Br. The second method was direct nucleophilic replacement of the iodomethyl analog or tosyloxyethyl analog with [^{18}F]F⁻. For the first method, yields of [^{18}F]fluoro-methyl-DAA1106 and [^{18}F]fluoro-ethyl-DAA1106 were resulted in 90% and 82%, respectively. In the final product solutions, the radiochemical purity of [^{18}F]fluoro-methyl-DAA1106 or [^{18}F]fluoro-ethyl-DAA1106 was higher than 98% and the specific activity was 40-65 GBq/ μmol for [^{18}F]fluoro-methyl-DAA1106 and 110-145 GBq/ μmol for [^{18}F]fluoro-ethyl-DAA1106 as determined from the mass measured by HPLC/UV analysis.

Fig. 3-2 shows *ex vivo* autoradiogram of [^{18}F]fluoro-methyl-DAA1106 and [^{18}F]fluoro-ethyl-DAA1106 binding in the brain. Accumulation of both ligands in the olfactory bulb was highest in the brain. Co-injection with non-radioactive DAA1106 (1 mg/kg) exhibited a significant reduction of [^{18}F]fluoro-methyl-DAA1106 or [^{18}F]fluoro-ethyl-DAA1106 concentration in the brain regions when compared with the control groups (Fig. 3-2b, d and Fig. 3-3). Fig. 3-4 shows competition by 4 PBR ligands to [^{11}C]DAA1106 binding in the cerebellum. Each drug dose-dependently inhibited the DAA1106 binding with manner of one-site competition. The *in vitro* binding affinities (K_i) of the four analogs for PBR were determined from competition for the [^{11}C]DAA1106 binding to PBR using quantitative autoradiography of the rat brain sections (Table 1). Among these compounds, the fluoroethyl analog fluoro-ethyl-DAA1106 was the most active toward PBR. The K_i value (0.078 nM) of fluoro-ethyl-DAA1106 was 2 fold higher than that of DAA1106, and 10 fold higher than that of PK11195. On the other hands, the PBR ligands did not display significant inhibitory effects ($K_i > 1 \mu\text{M}$) on [^{11}C]flumazenil binding in the rat brain.

Fig. 3-5 shows typical PET summation images of the monkey brain acquired from 30

to 180 min after [^{18}F]fluoro-methyl-DAA1106 (a) and [^{18}F]fluoro-ethyl-DAA1106 (b) injection (80-85 MBq). The two images displayed a high accumulation of radioactivity in the brain especially in the occipital cortex. However, in comparison with [^{18}F]fluoro-ethyl-DAA1106, a marked accumulation of [^{18}F]fluoro-methyl-DAA1106 was observed in the skull. Fig. 3-6 (circles) shows the time-activity curve of [^{18}F]fluoro-ethyl-DAA1106 in the occipital cortex of monkey brain after *i.v.* injection. At 2 min after injection, a high level of radioactivity was observed in the occipital cortex, which then remained almost same level during PET measurement (180 min). The radioactivity of [^{18}F]fluoro-ethyl-DAA1106 was 1.5 times higher than that of [^{11}C]DAA1106, and 6 times higher than that of [^{11}C]PK11195 at 30 min after injection (see Chapter 2, Fig. 2-8). Pretreatment with non-radioactive DAA1106 (1.0 mg/kg) or PK11195 (5.0 mg/kg) gave a marked reduction of uptake for the image (Fig. 3-5 c and d) and time-activity curve (Fig. 3-4: triangles and squares) of [^{18}F]fluoro-ethyl-DAA1106 as compared to the control experiment which was obtained under the same conditions.

Fig. 3-7 shows the percentages of unchanged [^{18}F]fluoro-methyl-DAA1106 and [^{18}F]fluoro-ethyl-DAA1106 in the plasma and brain homogenate of mice measured by HPLC. After injection into the mouse, the fraction corresponding to the unmetabolized [^{18}F]fluoro-methyl-DAA1106 in the plasma or brain rapidly decreased to 32% or 35% at 5 min, and to 15% or 22% at 30 min (Fig. 3-5). A major radioactive metabolite with high polarity was observed in the HPLC. Using ion exchange chromatography, the metabolite was assigned to [^{18}F]F $^-$. The fraction corresponding to the unchanged [^{18}F]fluoro-ethyl-DAA1106 in the plasma was 64% at 5 min, 29% at 30 min, and 25% of the total radioactivity at 60 min after injection. No [^{18}F]F $^-$ but another radioactive metabolite was observed in the HPLC. As estimated by its retention time (retention time=1.9 min), the metabolite was much more polar than [^{18}F]fluoro-ethyl-DAA1106 (retention time=11.8 min), while only [^{18}F]fluoro-ethyl-DAA1106 was detected in the brain homogenate with no evidence (<5%) of any radioactive metabolites even at 60 min after injection. After its injection into the monkey, [^{18}F]fluoro-ethyl-DAA1106 in plasma decreased to 77% at 5 min, 56% at 30 min and 18% at 90 min. From then, the amount of unchanged [^{18}F]fluoro-ethyl-DAA1106 continued to decrease, while that of a radioactive

metabolite increased to 90% by the end (180 min) of the PET experiment. The radioactive metabolite in the monkey plasma was the same metabolite determined in the mouse plasma.

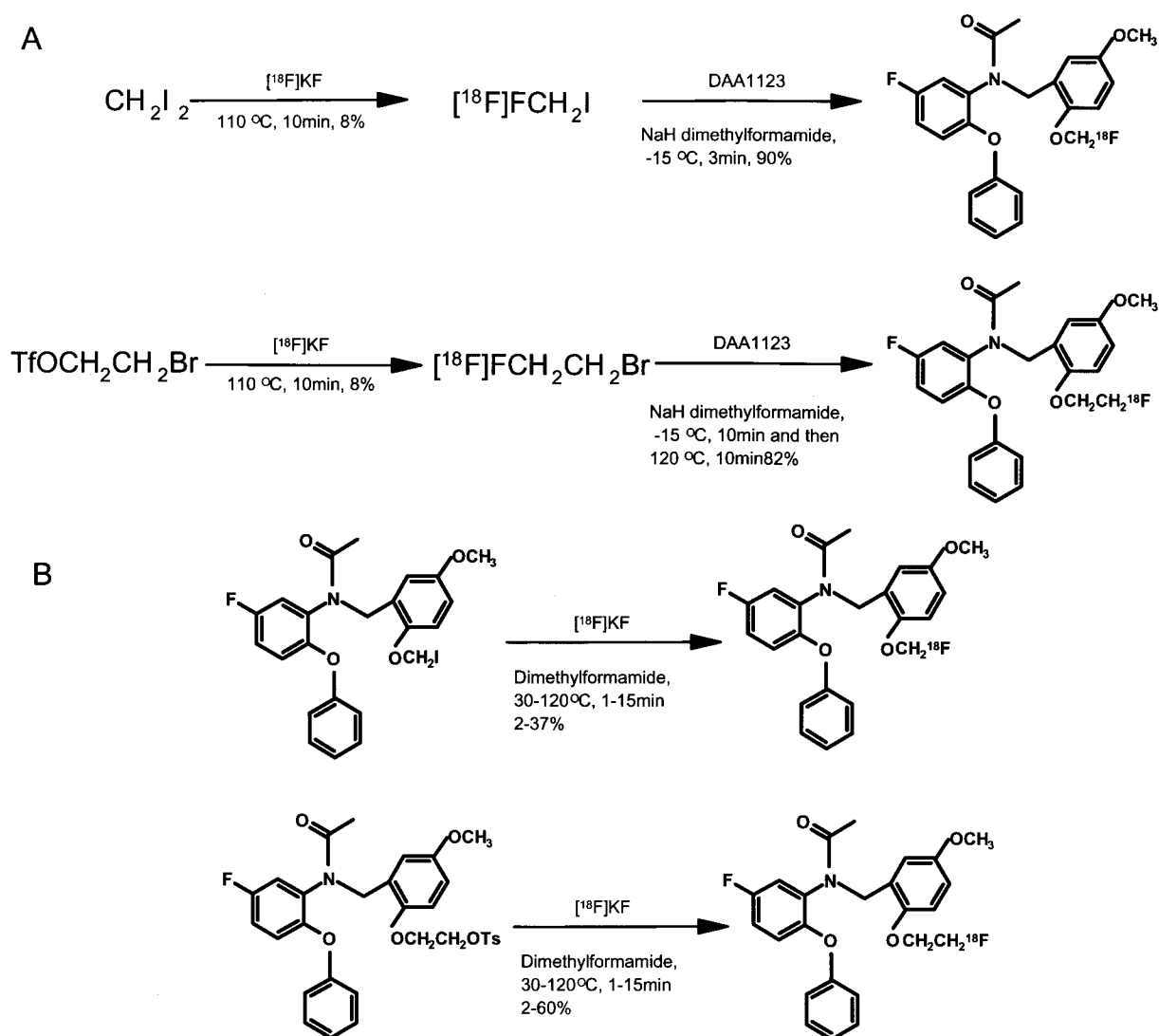


Fig. 3-1

Radiosynthesis of [^{18}F]fluorine-labeled DAA compounds. **A:** Two-step reaction sequence with the preparation of the radioactive intermediate [^{18}F]FCH₂I or [^{18}F]FCH₂CH₂Br, followed by the alkylation of DAA1123 with [^{18}F]FCH₂I or [^{18}F]FCH₂CH₂Br. **B:** Direct nucleophilic replacement of the iodomethyl analog or tosyloxyethyl analog with [^{18}F]F⁻.

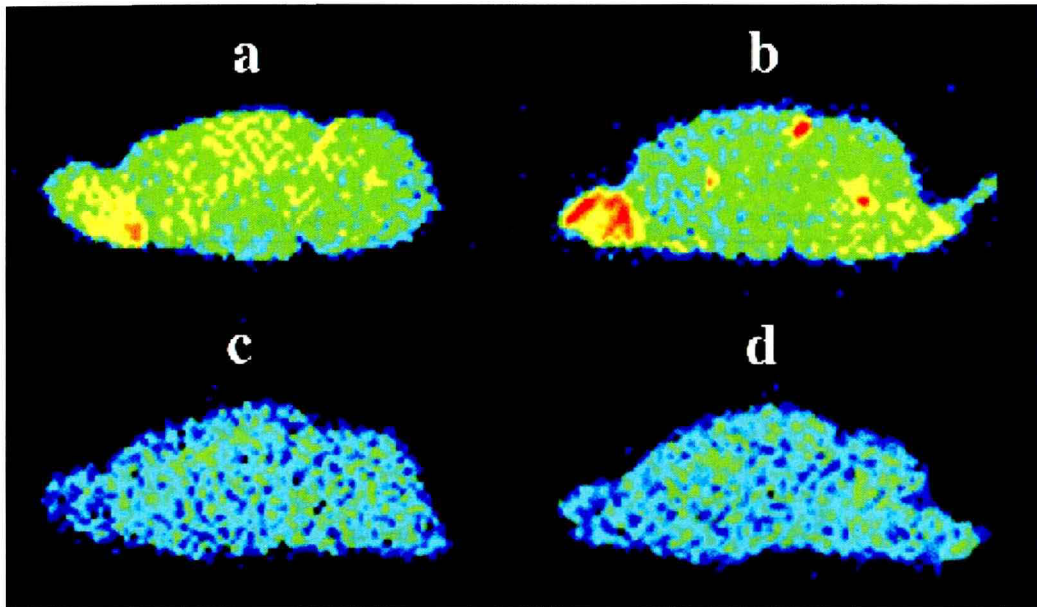


Fig. 3-2

Ex vivo autoradiogram of [^{18}F] fluoro-methyl-DAA1106 and [^{18}F] fluoro-ethyl-DAA1106 in the sagittal sections of rat brains at 30 min postinjection (20 MBq, 0.1 nmol):

(a) [^{18}F] fluoro-methyl-DAA1106; (b) [^{18}F] fluoro-ethyl-DAA1106;

(c) [^{18}F] fluoro-methyl-DAA1106 + DAA1106 (1 mg/kg),

(d) [^{18}F] FEDAA1106 + DAA1106 (1 mg/kg).

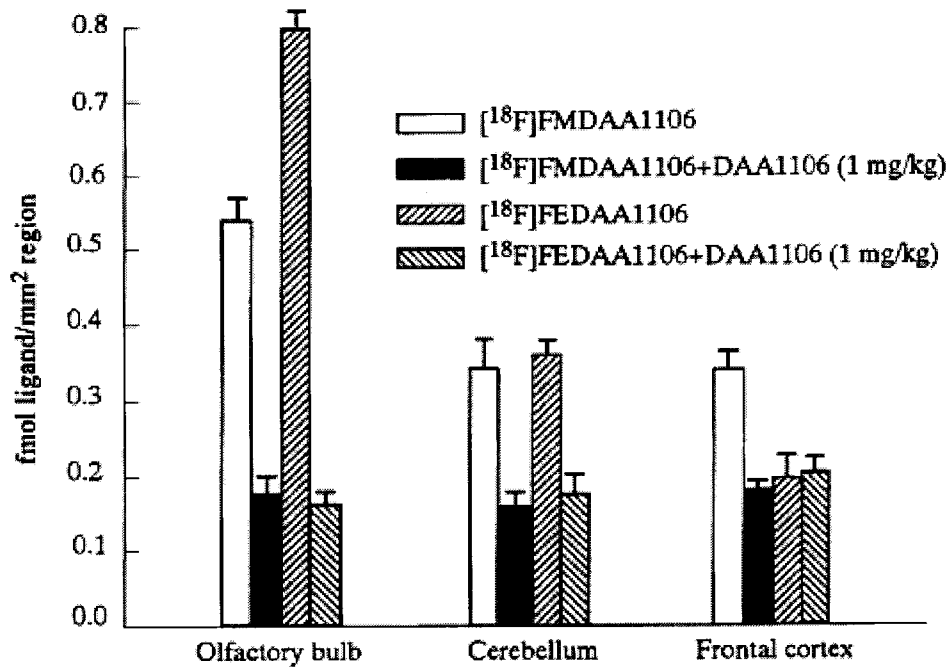


Fig. 3-3

Ex vivo autoradiographic localizations of [¹⁸F]fluoro-methyl-DAA1106 (FMDAA1106) and [¹⁸F]fluoro-ethyl-DAA1106 (FEDAA1106) in the rat brains at 30 min postinjection (20 MBq, 0.1 nmol). Data were expressed as fmol/mm².

Competition of [¹¹C]DAA1106 binding

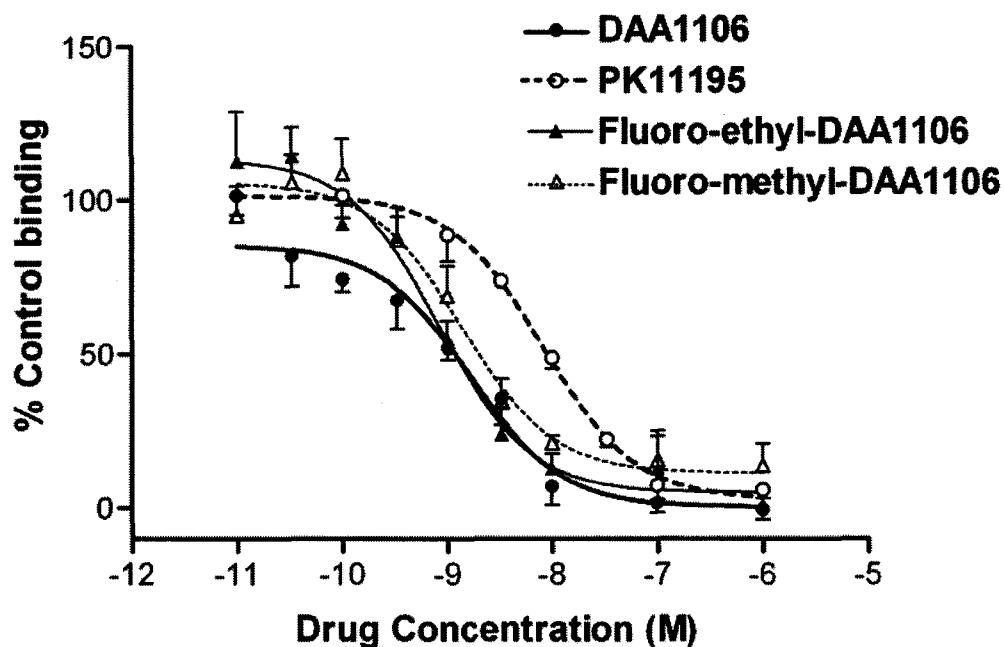
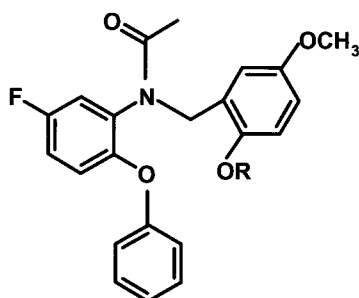


Fig. 3-4

Displacement curve of [¹¹C]DAA1106 binding in the rat cerebellum by 4 PBR ligands, DAA1106, PK11195, fluoro-ethyl-DAA1106 and fluoro-methyl-DAA1106. The data were fitted to one-site competition curve as $y = \text{Bottom} + (\text{Top}-\text{Bottom}) / (1+10^{(x-\text{LogIC}_{50})})$. K_i values were calculated to Table 3-1.

Table 3-1 *In vitro* binding affinity (K_i) of DAA1106 analogs for PBR and CBR and octanol/phosphate buffer (pH7.4) distribution coefficient



Ligand	R	K_i (nM)		LogD*
		[^{11}C]DAA1106 (PBR)	[^{11}C]flumazenil (CBR)	
Fluoro-methyl- DAA1106	FCH ₂	0.17 ± 0.02	>1,000	3.70
Fluoro-ethyl- DAA1106	FCH ₂ CH ₂	0.078 ± 0.01	>1,000	3.81
	I CH ₂	4.8 ± 0.68	>1,000	4.02
	TsOCH ₂ CH ₂	18.1 ± 1.30	>1,000	4.65
DAA1106	CH ₃	0.16 ± 0.02	>1,000	3.65
PK11195	—————	0.83 ± 0.24	>1,000	2.78

*The logD values were determined in the phosphate buffer (pH =7.4)/octanol system using the shaking flask method. All results were presented as mean values (n=3).

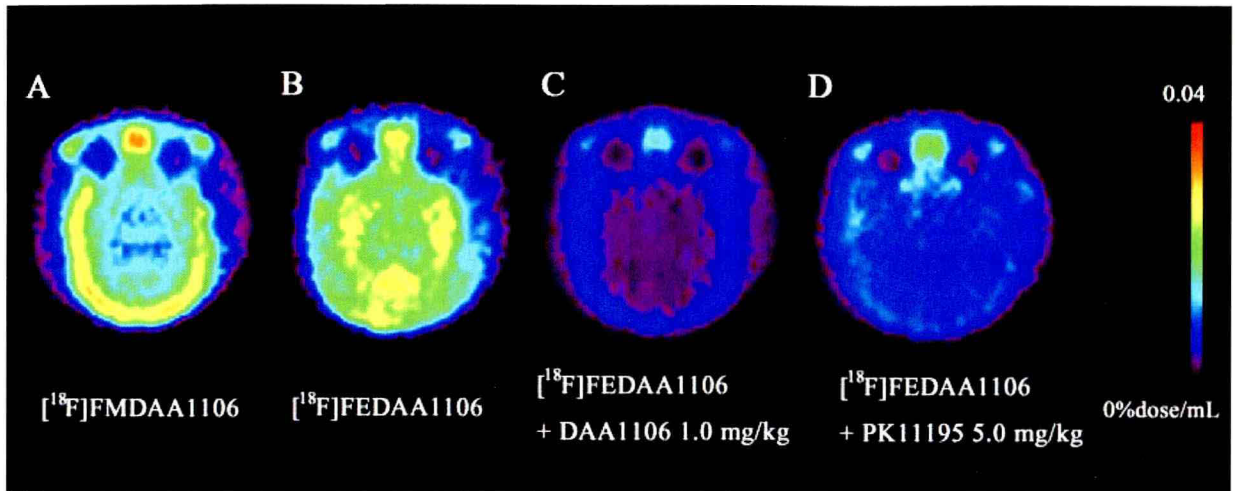


Fig. 3-5

PET summation images of the monkey brain acquired between 30 and 180 min after $[^{18}\text{F}]$ ligand injection. The images were obtained from the same subject. A: $[^{18}\text{F}]$ fluoro-methyl-DAA1106 (FMDAA1106); B: $[^{18}\text{F}]$ fluoro-ethyl-DAA1106 (FEDAA1106); C: $[^{18}\text{F}]\text{FEDAA1106}$ after treatment with DAA1106 (1 mg/kg); D: $[^{18}\text{F}]\text{FEDAA1106}$ after treatment with PK11195 (5 mg/kg).

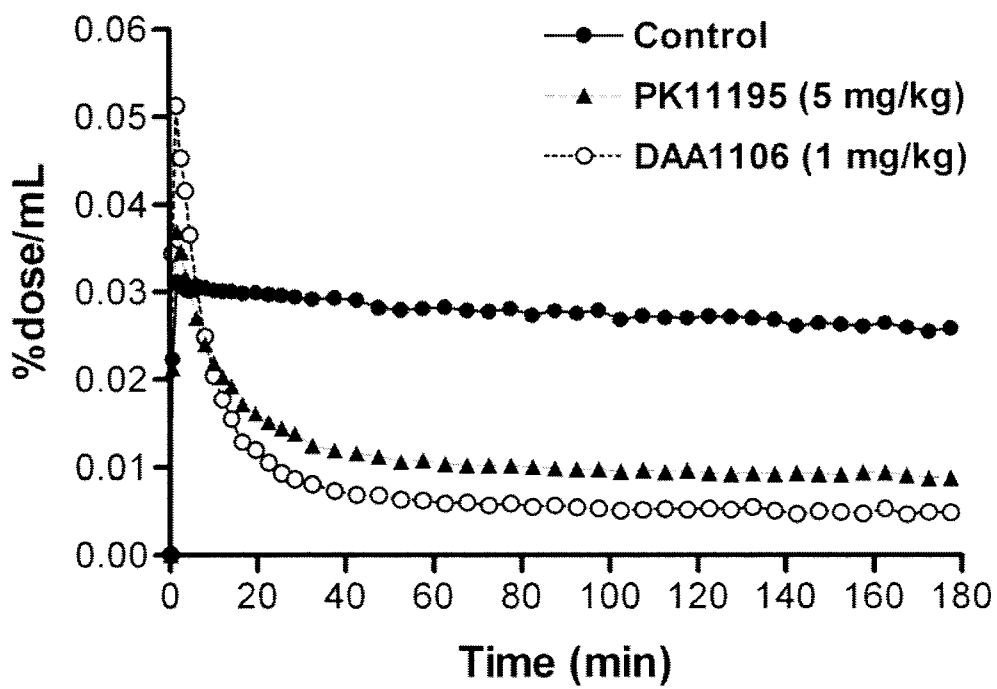


Fig. 3-6

Time-activity curves of [^{18}F]fluoro-ethyl-DAA1106 in the occipital cortex of monkey brain. The radioactivity of the control (circles) was inhibited by pretreatment with DAA1106 1 mg/kg (triangles) and PK11195 5mg/kg (squares).

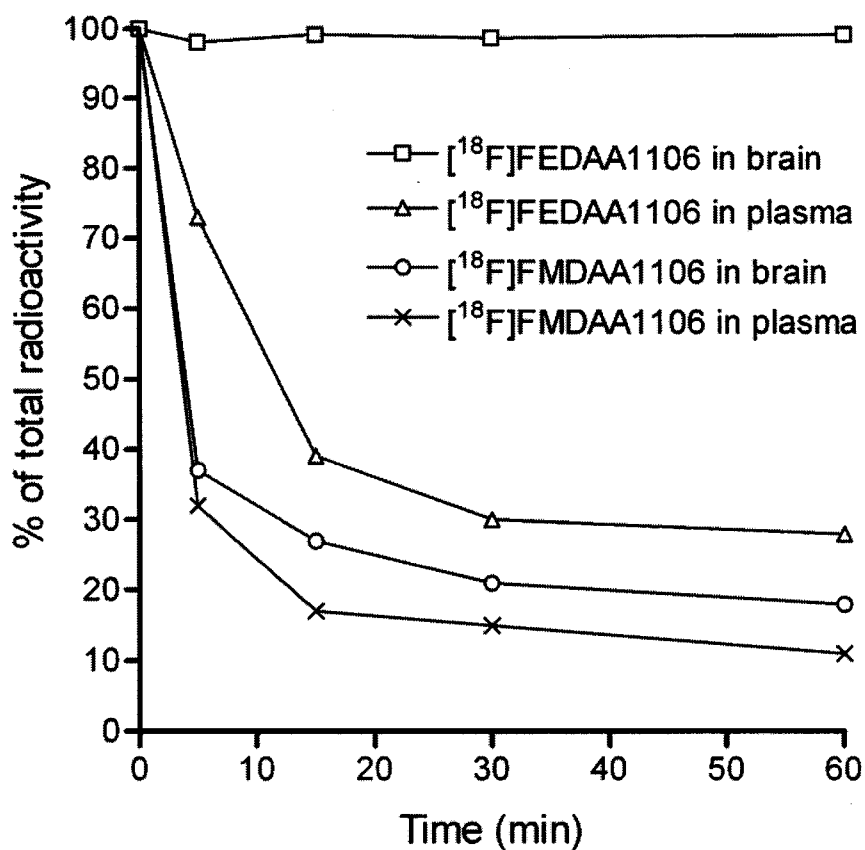


Fig. 3-7

Percent conversion of [^{18}F]fluoro-methyl-DAA1106 or [^{18}F]fluoro-ethyl-DAA1106 to metabolite in the mouse plasma and brain at several time points after *i.v.* injection of tracer (5-10 MBq) into the mouse ($n=3$). The unchanged tracers and metabolites were analyzed by HPLC for CH_3CN extracts from the plasma and brain homogenate prepared as described in the experimental section

DISCUSSION

To develop PET ligands for imaging PBR in the human brain, two analogs for PBR were synthesized and evaluated. The two fluoroalkyl analogs fluoro-methyl-DAA1106 and fluoro-ethyl-DAA1106 had higher or same affinities for PBR than the parent compound DAA1106, and had no potency for CBR. The PET ligands [^{18}F]fluoro-methyl-DAA1106 and [^{18}F]fluoro-ethyl-DAA1106 were respectively synthesized by the alkylation of the desmethyl precursor DAA1123 with [^{18}F]FCH₂I and [^{18}F]FCH₂CH₂Br in reproducible radiochemical yields.

In vitro binding affinities of DAA1106 analogs suggested that substituting *O*-CH₃ group with *O*-CH₂CH₂F group was favorable for augmenting its binding affinity for PBR. The fluoromethyl analog fluoro-methyl-DAA1106 displayed a similar affinity to DAA1106, suggesting that substitution with an *O*-CH₂F group did not obviously affect the affinity. This may be due to the molecular similarity and bioisoteric property of the *O*-CH₂F and *O*-CH₃ groups. The iodomethyl and tosyloxyethyl analog had 30 and 110 times lower affinity than DAA1106, respectively. These results suggested that the relative bulk groups in this series were not favorable for the binding of PBR¹¹⁸⁾. However, although it was moderately potent ($K_i = 4.8$ nM) for PBR, the iodomethyl analog may become a suitable candidate of a SPECT ligand for imaging PBR. Similarly, the binding affinities of DAA1106 analogs for CBR were measured using CBR-selective [^{11}C]flumazenil. As shown in Table 3-1, these DAA analogs did not display inhibitory effects ($K_i > 1$ μM) on [^{11}C]flumazenil binding in the rat brain. The negligible affinities of these analogs for CBR may be due to a difference from the typical BZ structure¹¹⁶⁻¹¹⁸⁾, which resulted in high selectivity for PBR.

The uptake of [^{18}F]fluoro-methyl-DAA1106 and [^{18}F]fluoro-ethyl-DAA1106 in the monkey brain was examined using PET. In the previous *in vitro* study for postmortem human brain, the highest density of PBR was observed in the occipital cortex¹²⁴⁾, so the region of interest in this PET experiment was placed on the occipital cortex. The distribution patterns of [^{18}F]fluoro-methyl-DAA1106 and [^{18}F]fluoro-ethyl-DAA1106 in the monkey brain were consistent with the distribution of PBR. However, compared with

[¹⁸F]fluoro-ethyl-DAA1106, [¹⁸F]fluoro-methyl-DAA1106 exhibited a high accumulation of radioactivity in the skull (Fig. 3-5a). This image is visual evidence that [¹⁸F]fluoro-methyl-DAA1106 was decomposed to [¹⁸F]F⁻ *in vivo* as reflected in the high accumulation of [¹⁸F]fluoro-methyl-DAA1106 in the bone. The accumulation of [¹⁸F]fluoro-methyl-DAA1106 in the skull indicated that it was not a useful PET ligand for brain because of interference to measure of the radioactivity in the brain. Therefore, no further evaluation of [¹⁸F]fluoro-methyl-DAA1106 was carried out using PET in the monkey brain. The uptake of [¹⁸F]fluoro-ethyl-DAA1106 in the monkey brain in the occipital cortex was 1.5 times higher than that of [¹¹C]DAA1106, and 6 times (maximum value) higher than that of [¹¹C]PK11195. Pretreatment with DAA1106 or PK11195 significantly reduced the radioactivity levels of [¹⁸F]fluoro-ethyl-DAA1106 to 20-30% of the control in the brain, suggesting a high specific binding of [¹⁸F]fluoro-ethyl-DAA1106 to PBR in the monkey brain. No radioactive metabolite of [¹⁸F]fluoro-ethyl-DAA1106 was detected in the brain although it was metabolized in the plasma by debenzoylation.

As shown in Fig. 3-6, pretreatment with DAA1106 enhanced the initial maximal uptake of [¹⁸F]fluoro-ethyl-DAA1106. The increase may be derived from [¹⁸F]fluoro-ethyl-DAA1106 dispossessed by mass non-radioactive DAA1106 from lung abundant in PBR. Similar cases have been presented in the PET studies of [¹¹C]PK11195¹²⁵⁾ and [¹¹C]DAA1106 (Fig. 2-8). From 30 min after injection to the end (180 min) of the PET scan, pretreatment with DAA1106 reduced the level of radioactivity to about 20% of the control. This result suggested high specific binding of [¹⁸F]fluoro-ethyl-DAA1106 present in the occipital cortex. Pretreatment with the PBR-selective PK11195 (5 mg/kg) also reduced the radioactivity in the occipital cortex, as shown in the image (Fig. 3-5d) and time-activity curve (Fig. 3-6: squares). The radioactivity was reduced to about 30% of the control from 30 min after injection to the end of the PET scan. The reduction percentage on the uptake of [¹⁸F]fluoro-ethyl-DAA1106 by PK11195 was slightly lower than that by DAA1106, which was probably due to the weaker affinity of PK11195 for PBR and its lower penetration¹¹²⁾ into the brain than that of DAA1106. These findings confirmed that [¹⁸F]fluoro-ethyl-DAA1106 may have high specific binding for PBR in the monkey brain.

In the imaging brain study, the presence of metabolites in the plasma of the subject may

preclude the evaluation of a PET ligand if the metabolites enter the brain and are retained/bound at the target sites. Therefore, metabolite analyses were performed for [^{18}F]fluoro-ethyl-DAA1106 in the plasma and brain of mouse, and the plasma of monkey. For comparison, similar analyses were also performed for [^{18}F]fluoro-methyl-DAA1106. The percentages of unchanged [^{18}F]fluoro-methyl-DAA1106 and [^{18}F]fluoro-ethyl-DAA1106 in the plasma and brain homogenate of mice measured by HPLC. After injection into the mouse, the fraction corresponding to the unmetabolized [^{18}F]fluoro-methyl-DAA1106 in the plasma or brain rapidly decreased to 32% or 35% at 5 min, and to 15% or 22% at 30 min. A major radioactive metabolite with high polarity was observed in the HPLC. Using ion exchange chromatography, the metabolite was assigned to [^{18}F]F $^-$. Since [^{18}F]F $^-$ is probably impermeable into the brain, [^{18}F]fluoro-methyl-DAA1106 may be metabolized in the plasma and brain, respectively (Fig. 3-8).

After [^{18}F]fluoro-ethyl-DAA1106 injection into the mouse, the percent of unchanged [^{18}F]fluoro-ethyl-DAA1106 in the plasma continued to decrease during the entire experiment. The metabolite analysis was also performed using monkey plasma. As reported previously, debenzilation of DAA1106 and [^{11}C]DAA1106 was a main route of metabolism¹¹⁶). Since the fluoroethyl analog [^{18}F]fluoro-ethyl-DAA1106 had molecular similarity to and the bioisoteric property of [^{11}C]DAA1106, it may be metabolized with a similar profile to [^{11}C]DAA1106 (Fig. 3-8). A radioactive metabolite with a benzyl moiety and non-radioactive metabolite (*N*-(5-fluoro-2-phenoxyphenyl)acetamide may be the putative metabolite of [^{18}F]fluoro-ethyl-DAA1106. The debenzylated compound had no affinity for PBR and CBR ($\text{IC}_{50} > 10 \mu\text{M}$)¹¹⁶). Therefore, the presence of the non-radioactive metabolite could not interfere with the specific binding of [^{18}F]fluoro-ethyl-DAA1106 to PBR in the brain, even if it passed the BBB and entered the brain. Since no radioactive metabolites including [^{18}F]fluoro-ethyl-DAA1106 were detected in the mouse brain homogenates, the chemical structure of [^{18}F]F-labeled benzyl was not further identified. These findings could reveal that although [^{18}F]fluoro-ethyl-DAA1106 was extensively metabolized in the plasma, all of the specific binding determined in the monkey brain may be due to this ligand itself, and not influenced by its radioactive or non-radioactive metabolite.

In conclusion, [^{18}F]fluoro-ethyl-DAA1106 was high permeability and stable in the brain, while [^{18}F]fluoro-methyl-DAA1106 was catabolized to [^{18}F]fluorine which accumulated in bone. It was suggested that [^{18}F]fluoro-ethyl-DAA1106 but not [^{18}F]fluoro-methyl-DAA1106 is promise PET tracer for PBR in the brain. Imaging of glia with [^{18}F]fluoro-ethyl-DAA1106 may be useful for diagnosis of various diseases, such as Alzheimer's disease, multiple sclerosis and stroke.

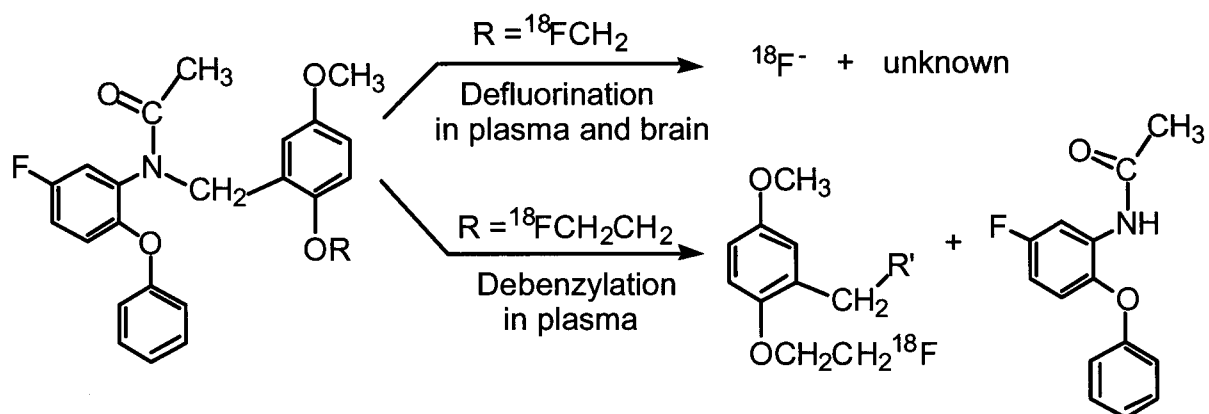


Fig. 3-8

Metabolic pathway of [${}^{18}\text{F}$]fluorine-labeled DAA1106 analogs fluoro-methyl-DAA1106 and fluoro-ethyl-DAA1106.

General Conclusion

Based on the above findings, the following can be concluded:

Chapter 1:

[¹¹C]Ro15-4513 was highly accumulated in the anterior cingulate cortex, insular cortex, and lower temporal cortex in the monkey brain. The high-affinity binding was insensitive to zolpidem, which has affinity for α_1 , α_2 , and α_3 subunits of the GABA_A receptor. These results suggest that these *in vivo* bindings of [¹¹C]Ro15-4513 can be interpreted as a relatively high accumulation in the fronto-temporal limbic regions and represents its binding to the α_5 subunit of the GABA_A/BZ receptor. The α_5 subunit has been reported to involve in alcoholism, benzodiazepine-induced amnesia and tolerance to benzodiazepine. I consider that the [¹¹C]Ro15-4513 PET gives information about underlying mechanism of α_5 subunit of the GABA_A/BZ receptor on those symptoms.

Chapter 2:

A high uptake of [¹¹C]DAA1106 was observed in the olfactory bulb followed by the pons/medulla and cerebellum by performing an *in vivo* autoradiography of the rat brain. This correlates with the PK11195 binding *in vitro*. The DAA1106 binding was increased in kainic acid-induced neural lesions. The accumulation of [¹¹C]DAA1106 was four-times higher compared to the binding of [¹¹C]PK11195 in the monkey occipital cortex. The accumulation was inhibited by pretreatment with PBR. These results indicate that [¹¹C]DAA1106 may be a good ligand for *in vivo* imaging of PBR.

Chapter 3:

The two fluoroalkyl analogs, fluoro-methyl-DAA1106 and fluoro-ethyl-DAA1106, had higher or same affinities for PBR as compared to that of their parent compound, DAA1106, and had no affinity for CBR. The uptake of [¹⁸F]fluoro-ethyl-DAA1106 in the occipital cortex of the monkey brain was 1.5-times higher than that of [¹¹C]DAA1106, and six-times (maximum value) higher than that of [¹¹C]PK11195. A significant amount of

radioactivity was detected in the skull when [^{18}F]fluoro-methyl-DAA1106 was used for PET images of the monkey brain. This indicates that [^{18}F]fluoro-methyl-DAA1106 was not useful as a PET ligand because of its remarkable defluorination *in vivo*. These results suggest that [^{18}F]fluoro-ethyl-DAA1106 is a potential PET ligand for imaging of PBR in brain.

Previous reports have demonstrated that the density of PBR binding increases in the human brain with Alzheimer's disease. I expect that the [^{11}C]DAA1106 or [^{18}F]fluoro-ethyl-DAA1106 PET become more objective and early diagnostics on Alzheimer's disease.

List of publications

This thesis based on the following original publications:

1. Maeda J, Suhara T, Kawabe K, Okauchi T, Obayashi S, Hojo J, Suzuki K: Visualization of $\alpha 5$ subunit of GABA_A/benzodiazepine receptor by [¹¹C]Ro15-4513 using positron emission tomography. *Synapse* 47, 200-208 (2003): Chapter 1
2. Zhang MR, Kida T, Noguchi J, Furutsuka K, Maeda J, Suhara T, Suzuki K. [¹¹C]DAA1106: radiosynthesis and in vivo binding to peripheral benzodiazepine receptors in mouse brain. *Nucl Med Biol* 30, 513-519 (2003): Chapter 2
3. Maeda J, Suhara T, Zhang MR, Okauchi T, Yasuno F, Ikoma Y, Inaji M, Nagai Y, Takano A, Obayashi S, Suzuki K. Novel peripheral benzodiazepine receptor ligand [¹¹C]DAA1106 for PET: An imaging tool for glial cells in the brain. *Synapse* 52, 283-291 (2004): Chapter 2
4. Zhang MR, Maeda J, Furutsuka K, Yoshida Y, Ogawa M, Suhara T, Suzuki K. [¹⁸F]FMDAA1106 and [¹⁸F]FEDAA1106: two positron-emitter labeled ligands for peripheral benzodiazepine receptor (PBR). *Bioorg Med Chem Lett.* 13, 201-204 (2003): Chapter 3
5. Zhang MR, Maeda J, Ogawa M, Noguchi J, Ito T, Yoshida Y, Okauchi T, Obayashi S, Suhara T, Suzuki K. Development of a new radioligand, N-(5-Fluoro-2-phenoxyphenyl)-N-(2-[¹⁸F]fluoroethyl-5-methoxybenzyl)acetamide, for PET Imaging of peripheral benzodiazepine receptor in primate brain. *J Med Chem.* 47, 2228-2235 (2004): Chapter 3

Acknowledgements

I will never complete this work without the help of the following people/organizations:

First, I would like to express my gratitude and appreciation to Professor Tsutomu Suzuki (Department of Toxicology, Hoshi University), Dr. Tetsuya Suhara (Brain Imaging Project, National Institute of Radiological Sciences) and Associate Professor Minoru Narita (Department of Toxicology, Hoshi University) for their helpful guidance in my work and preparing this dissertation.

Further, I wish to Dr. Shigeru Obayashi, Mr. Takashi Okauchi, Dr. Kouichi Kawabe, Mr. Motoki Inaji, Mr. Yuji Nagai, Dr. Fumihiko Yasuno, Dr. Yoko Ikoma and Dr. Akihiro Takano (Brain Imaging Project, National Institute of Radiological Sciences) for helpful advice and assistance in my research. I gratefully acknowledge Dr. Kazutoshi Suzuki, Dr. Ming-Rong Zhang, Ms. Junko Hojo and the other members of the Radiopharmaceutical and Radiopharmacological Section (Department of Medical Imaging, National Institutes of Radiological Sciences) for the production of radioisotopes.

Also, I am grateful to Dr. Shigeru Okuyama and Dr. Atsuro Nakazato (Taisho Pharmaceutical Co. LTD, Japan) for providing us with the samples (DAA1106 and DAA1123) and for useful suggestions.

Finally I wish to thank for staffs concerned with my study in Brain Imaging Project, National Institute of Radiological Sciences, Department of Toxicology and Department of Pharmacology, Hoshi University.

References

- 1) Zanzonico, P., Positron emission tomography: a review of basic principles, scanner design and performance, and current systems, *Semin. Nucl. Med.*, **34**, 87-111 (2004).
- 2) Alavi, A., Kung, J.W., Zhuang, H., Implications of PET based molecular imaging on the current and future practice of medicine, *Semin. Nucl. Med.*, **34**, 56-69 (2004).
- 3) Wolf, A.P., Fowler, J.S., Positron emitter-labeled radiotracers-chemical consideration. *Positron Emission Tomography*, Alan R. Liss, Inc., New York, pp63-80 (1985).
- 4) Fowler, J.S., Ding, Y.S., Volkow, N.D., Radiotracers for positron emission tomography imaging, *Semin. Nucl. Med.*, **33**, 14-27 (2003).
- 5) Nakamoto, Y., Clinical application of FDG-PET for cancer diagnosis. *Nippon Igaku Hoshasen Gakkai Zasshi*, **63**, 285-293 (2003).
- 6) Anderson, C.D., The apparent existence of easily deflectable positives, *Science*, **76**, 238-239 (1932).
- 7) Joliot, F., Curie, I., Artificial production of a new kind of radio-element, *Nature*, **133**, 201-203 (1934).
- 8) Anderson, C.D., The positive electron. *Phys. Rev.*, **43**, 491-494 (1933).
- 9) Lawrence, E.O., Livingston, M.S., The production of high speed light ions without the use of high voltages, *Phys Rev*, **40**, 19-35 (1932).
- 10) Lawrence, E.O., Livingston, M.S., White M.G., The disintegration of lithium by swiftly-moving protons, *Phys Rev*, **42**, 150-151 (1932).
- 11) Lawrence, E.O., The medical cyclotron of the William H. Crocker Radiation Laboratory, *Science*, **90**, 407-408 (1939).
- 12) Wrenn, W.H., Good, M.I., Handler, P. H., The use of positron-emitting radioisotopes for the localization of brain tumors, *Science*, **113**, 525-527 (1951).
- 13) Sweet, W.H., The use of nuclear disintegration in the diagnosis and treatment of brain tumor, *N. Engl. J Med.*, **245**, 875-878 (1951).

- 14) Ter-Pogossian, M.M., Positron emission tomography instrumentation, Positron Emission Tomography, Alan R. Liss, Inc., New York, pp43-61 (1985).
- 15) Ter-Pogossian, M.M., Phelps, M.E., Hoffman, E.J., Mullani, N.A., A positron-emission transaxial tomograph for nuclear imaging (PETT), Radiology, **114**, 89-98 (1975).
- 16) Kilbourn, M.R., Nguyen, T.B., Snyder, S.E., Koppe, R.A., One for all or one for each? Matching radiotracers and regional brain pharmacokinetics, Quantitative Functional Brain Imaging with Positron Emission Tomography, Academic Press, San Diego, pp261-266 (1998).
- 17) Wagner, H.N., Jr., Burns, H.D., Dannals, R.F., Wong, D.F., Langstrom, B., Duelfer, T., Frost, J.J., Ravert, H.T., Links, J.M., Rosenbloom, S.B., Lukas, S.E., Kramer, A.V., Kuhar, M.J., Imaging dopamine receptors in the human brain by positron tomography, Science, **221**, 1264-1266 (1983).
- 18) Farde, L., Ehrin, E., Eriksson, L., Greitz, T., Hall, H., Hedstrom, C.G., Litton, J.E., Sedvall, G., Substituted benzamides as ligands for visualization of dopamine receptor binding in the human brain by positron emission tomography. Quantitative analysis of D₂ dopamine receptor binding in the living human brain by PET, Proc. Natl. Acad. Sci. U.S.A., **82**, 3863-3867 (1985).
- 19) Farde, L., Hall, H., Ehrin, E., Sedvall, G., Quantitative analysis of D₂ dopamine receptor binding in the living human brain by PET, Science, **231**, 258-261 (1986).
- 20) Terasaki, T., Hosoya, K., The blood-brain barrier efflux transporters as a detoxifying system for the brain, Adv. Drug Deliv. Rev. **36**, 195-209 (1999).
- 21) Dishino, D.D., Welch, M.J., Kilbourn, M.R., Raichle, M.E., Relationship between lipophilicity and brain extraction of C-11-labeled radiopharmaceuticals, J. Nucl. Med., **24**, 1030-1038 (1983).
- 22) Elfving, B., Bjornholm, B., Ebert, B., Knudsen, G.M., Binding characteristics of selective serotonin reuptake inhibitors with relation to emission tomography studies, Synapse, **41**, 203-211 (2001).
- 23) Waterhouse, R.N., Determination of lipophilicity and its use as a predictor of blood-brain barrier penetration of molecular imaging agents, Mol. Imaging Biol., **5**,

- 376-389 (2003).
- 24) Osman, S., Lundkvist, C., Pike, V.W., Halldin, C., McCarron, J.A., Swahn, C.G., Ginovart, N., Luthra, S.K., Bench, C.J., Grasby, P.M., Wikstrom, H., Barf, T., Cliffe, I.A., Fletcher, A., Farde, L., Characterization of the radioactive metabolites of the 5-HT_{1A} receptor radioligand, [O-methyl-¹¹C]WAY-100635, in monkey and human plasma by HPLC: comparison of the behaviour of an identified radioactive metabolite with parent radioligand in monkey using PET, *Nucl. Med. Biol.*, **23**, 627-634 (1996).
 - 25) Osman, S., Lundkvist, C., Pike, V.W., Halldin, C., McCarron, J.A., Swahn, C.G., Farde, L., Ginovart, N., Luthra, S.K., Gunn, R.N., Bench, C.J., Sargent, P.A., Grasby, P.M., Characterisation of the appearance of radioactive metabolites in monkey and human plasma from the 5-HT_{1A} receptor radioligand, [carbonyl-¹¹C]WAY-100635-explanation of high signal contrast in PET and an aid to biomathematical modeling, *Nucl. Med. Biol*, **25**, 215-223 (1998).
 - 26) Mehta, A.K., Ticku, M.K., An update on GABA_A receptors, *Brain Res. Brain Res. Rev.* **29**, 196-217 (1999).
 - 27) Langer, S.Z. Arbilla, S., Limitations of the benzodiazepine receptor nomenclature: a proposal for a pharmacological classification as omega receptor subtypes, *Fundam. Clin. Pharmacol.*, **2**, 159-170 (1988).
 - 28) Drugan, R.C., Holmes, P.V., Central and peripheral benzodiazepine receptors: involvement in an organism's response to physical and psychological stress, *Neurosci. Biobehav. Rev.*, **15**, 277-298 (1991).
 - 29) Luddens, H., Korpi, E.R., Seeburg, P.H., GABA_A/benzodiazepine receptor heterogeneity: neurophysiological implications, *Neuropharmacology*, **34**, 245-254 (1995).
 - 30) Smith, G.B., Olsen. R.W., Functional domains of GABA_A receptors, *Trends Pharmacol. Sci.*, **16**, 162-168 (1995).
 - 31) Barnard, E.A., Skolnick, P., Olsen, R.W., Mohler, H., Sieghart, W., Biggio, G., Braestrup, C., Bateson, A.N., Langer, S.Z., International Union of Pharmacology. XV. Subtypes of gamma-aminobutyric acid_A receptors: classification on the basis

- of subunit structure and receptor function, *Pharmacol. Rev.*, **50**, 291-313 (1998).
- 32) Comar, D., Maziere, M., Godot, J.M., Berger, G., Soussaline, F., Menini, C., Arfel, G., Naquet, R., Visualisation of ¹¹C-flunitrazepam displacement in the brain of the live baboon, *Nature*, **280**, 329-331 (1979).
- 33) Hantraye, P., Kajjima, M., Prenant, C., Guibert, B., Sastre, J., Crouzel, M., Naquet, R., Comar, D., Maziere, M., Central type benzodiazepine binding sites: a positron emission tomography study in the baboon's brain, *Neurosci. Lett.*, **48**, 115-120 (1984).
- 34) Savic, I., Widen, L., Stone-Elander, S., Feasibility of reversing benzodiazepine tolerance with flumazenil, *Lancet*, **337**, 133-137, (1991).
- 35) Henry, T.R., Frey, K.A., Sackellares, J.C., Gilman, S., Koeppe, R.A., Brunberg, J.A., Ross, D.A., Berent, S., Young, A.B., Kuhl, D.E., In vivo cerebral metabolism and central benzodiazepine-receptor binding in temporal lobe epilepsy, *Neurology*, **43**, 1998-2006 (1993).
- 36) Holthoff, V.A., Koeppe, R.A., Frey, K.A., Penney, J.B., Markel, D.S., Kuhl, D.E., Young, A.B., Positron emission tomography measures of benzodiazepine receptors in Huntington's disease, *Ann. Neurol.*, **34**, 76-81 (1993).
- 37) Homanics, G.E., Ferguson, C., Quinlan, J.J., Daggett, J., Snyder, K., Lagenaur, C., Mi, Z.P., Wang, X.H., Grayson, D.R., Firestone, L.L., Gene knockout of the $\alpha 6$ subunit of the γ -aminobutyric acid type A receptor, lack of effect on responses to ethanol, pentobarbital, and general anesthetics, *Mol. Pharmacol.*, **51**, 588-596 (1997).
- 38) McKernan, R.M., Rosahl, T.W., Reynolds, D.S., Sur, C., Wafford, K.A., Atack, J.R., Farrar, S., Myers, J., Cook, G., Ferris, P., Garrett, L., Bristow, L., Marshall, G., Macaulay, A., Brown, N., Howell, O., Moore, K.W., Carling, R.W., Street, L.J., Castro, J.L., Ragan, C.I., Dawson, G.R., Whiting, P.J., Sedative but not anxiolytic properties of benzodiazepines are mediated by the GABA_A receptor $\alpha 1$ subtype, *Nat Neurosci*, **3**, 587-592 (2000).
- 39) Low, K., Crestani, F., Keist, R., Benke, D., Brunig, I., Benson, J.A., Fritschy, J.M., Rulicke, T., Bluethmann, H., Mohler, H., Rudolph U., Molecular and neuronal

- substrate for the selective attenuation of anxiety, *Science* **290**, 131-134 (2000).
- 40) Rudolph, U., Crestani, F., Mohler, H., GABA_A receptor subtypes: dissecting their pharmacological functions. *Trends. Pharmacol. Sci.*, **22**, 188-194 (2001).
 - 41) Tobler, I., Kopp, C., Deboer, T., Rudolph, U., Diazepam-induced changes in sleep: role of the $\alpha 1$ GABA_A receptor subtype, *Proc. Natl. Acad. Sci. U.S.A.*, **98**, 6464-6469 (2001).
 - 42) Luddens, H., Seeburg, P.H., Korpi, E.R., Impact of β and γ variants on ligand-binding properties of gamma-aminobutyric acid type A receptors, *Mol. Pharmacol.*, **45**, 810-814 (1994).
 - 43) Braestrup, C., Squires, R.F., Specific benzodiazepine receptors in rat brain characterized by high-affinity ³H-diazepam binding, *Proc. Natl. Acad. Sci. U.S.A.*, **74**, 3805-3809 (1977).
 - 44) Anholt, R.R., De Souza, E.B., Oster-Granite, M.L., Snyder, S.H., Peripheral-type benzodiazepine receptors: autoradiographic localization in whole-body sections of neonatal rats, *J. Pharmacol. Exp. Ther.*, **233**, 517-526 (1985).
 - 45) Banati, R.B., Visualising microglial activation in vivo, *Glia*, **40**, 206-217 (2002).
 - 46) Bergstrom, M., Mosskin, M., Ericson, K., Ehrin, E., Thorell, J.O., von Holst, H., Noren, G., Persson, A., Halldin, C., Stone-Elander, S., Peripheral benzodiazepine binding sites in human gliomas evaluated with positron emission tomography. *Acta. Radiol. Suppl.*, **369**, 409-411 (1986).
 - 47) Junck, L., Olson, J.M., Ciliax, B.J., Koeppe, R.A., Watkins, G.L., Jewett, D.M., McKeever, P.E., Wieland, D.M., Kilbourn, M.R., Starosta-Rubinstein, S., PET imaging of human gliomas with ligands for the peripheral benzodiazepine binding site. *Ann. Neurol.*, **26**, 752-758 (1989).
 - 48) Sigel, E., Buhr, A., The benzodiazepine binding site of GABA_A receptors, *Trends Pharmacol. Sci.* **18**, 425-429 (1997).
 - 49) Shinotoh, H., Yamasaki, T., Inoue, O., Itoh, T., Suzuki, K., Hashimoto, K., Tateno, Y., Ikehira, H., Visualization of specific binding sites of benzodiazepine in human brain, *J. Nucl. Med.*, **27**, 1593-1599 (1986).
 - 50) Pappata, S., Samson, Y., Chavoix, C., Prenant, C., Maziere, M., Baron. J.C.,

- Regional specific binding of [^{11}C]RO 15 1788 to central type benzodiazepine receptors in human brain: quantitative evaluation by PET, *J. Cereb. Blood Flow Metab.*, **8**, 304-313 (1988).
- 51) Abadie, P. Baron, J.C., Bisserbe, J.C., Boulenger, J.P., Rioux, P., Traverso, J.M., Barre, L., Petit-Tabou, M.C., Zarifian, E., Central benzodiazepine receptors in human brain: estimation of regional B_{max} and K_D values with positron emission tomography, *Eur. J. Pharmacol.* **213**, 107-115 (1992).
- 52) Inoue, O., Suhara, T., Itoh, T., Kobayashi, K., Suzuki, K., Tateno, Y., In vivo binding of [^{11}C]Ro15-4513 in human brain measured with PET, *Neurosci. Lett.* **145**, 133-136 (1992).
- 53) Suhara, T., Inoue, O., Kobayashi, K., Suzuki, K., Itoh, T., Tateno, Y., No age-related changes in human benzodiazepine receptor binding measured by PET with [^{11}C]Ro 15-4513, *Neurosci. Lett.*, **159**, 207-210 (1993).
- 54) Foged, C., Halldin, C., Loc'h, C., Maziere, B., Pauli, S., Maziere, M., Hansen, H.C., Suhara, T., Swahn, C.G., Karlsson, P., Farde, L., Bromine-76 and carbon-11 labelled NNC 13-8199, metabolically stable benzodiazepine receptor agonists as radioligands for positron emission tomography., *Eur. J. Nucl. Med.*, **24**, 1261-1267 (1997).
- 55) Millet, P., Graf, C., Buck, A., Walder, B., Westera, G., Broggin, C., Arigoni, M., Slosman, D., Bouras, C., Ibanez, V., Similarity and robustness of PET and SPECT binding parameters for benzodiazepine receptors, *J. Cereb. Blood Flow Metab.*, **20**, 1587-1603 (2000).
- 56) Inoue, O., Hosoi, R., Kobayashi, K., Itoh, T., Gee, A., Suzuki, K., Different sensitivities to competitive inhibition of benzodiazepine receptor binding of ^{11}C -iomazenil and ^{11}C -flumazenil in rhesus monkey brain. *Ann. Nucl. Med.*, **15**, 137-139 (2001).
- 57) Brouillet, E., Chavoix, C., Khalili-Varasteh, M., Bottlaender, M., Hantraye, P., Yorke, J.C., Maziere, M., Quantitative evaluation of benzodiazepine receptors in live *Papio papio* baboons using positron emission tomography. *Mol. Pharmacol.* **38**, 445-450 (1990).

- 58) Onoe, H., Tsukada, H., Nishiyama, S., Nakanishi, S., Inoue, O., Langstrom, B., Watanabe, Y., A subclass of GABA_A/benzodiazepine receptor exclusively localized in the limbic system, *Neuroreport*, **8**, 117-122 (1996).
- 59) Nakano, T., Satoh, T., Mori, K., Inoue, O., Imaging of the super high affinity binding sites for [³H]Ro15-4513 in rat hippocampus: comparison between in vitro and in vivo binding, *Neurosci Lett*, **250**, 161-164 (1998).
- 60) Wisden, W., Laurie, D.J., Monyer, H., Seeburg, P.H., The distribution of 13 GABA_A receptor subunit mRNAs in the rat brain. I. Telencephalon, diencephalon, mesencephalon, *J. Neurosci.*, **12**, 1040-1062 (1992).
- 61) Pirker, S., Schwarzer, C., Wieselthaler, A., Sieghart, W., Sperk, G., GABA_A receptors: immunocytochemical distribution of 13 subunits in the adult rat brain, *Neuroscience*, **101**, 815-850 (2000).
- 62) Hadingham, K.L., Wingrove, P., Le Bourdelles, B., Palmer, K.J., Ragan, C.I., Whiting, P.J., Cloning of cDNA sequences encoding human α 2 and α 3 γ -aminobutyric acid_A receptor subunits and characterization of the benzodiazepine pharmacology of recombinant α 1-, α 2-, α 3-, and α 5-containing human γ -aminobutyric acid_A receptors, *Mol. Pharmacol.* **43**, 970-975 (1993).
- 63) Wieland, H.A., Luddens, H., Four amino acid exchanges convert a diazepam-insensitive, inverse agonist-preferring GABA_A receptor into a diazepam-preferring GABA_A receptor, *J. Med. Chem.*, **37**, 4576-4580 (1994).
- 64) Suzuki, K., Inoue, O., Hashimoto, K., Yamasaki, T., Kuchiki, M., Tamate, K., Computer-controlled large scale production of high specific activity [¹¹C]RO 15-1788 for PET studies of benzodiazepine receptors, *Int. J. Appl. Radiat. Isot.*, **36**, 971-976 (1985).
- 65) Noguchi, J., Suzuki, K., Automated synthesis of the ultra high specific activity of [¹¹C]Ro15-4513 and its application in an extremely low concentration region to an ARG study, *Nucl. Med. Biol.*, **30**, 335-343 (2003).
- 66) Obayashi, S., Suhara, T., Kawabe, K., Okauchi, T., Maeda, J., Akine, Y., Onoe, H., Iriki, A., Functional brain mapping of monkey tool use, *Neuroimage*, **14**, 853-861 (2001).

- 67) Okauchi, T., Suhara, T., Maeda, J., Kawabe, K., Obayashi, S., Suzuki, K., Effect of endogenous dopamine on endogenous dopamine on extrastriated [¹¹C]FLB 457 binding measured by PET, *Synapse*, **41**, 87-95 (2001).
- 68) Watanabe, M., Okada, H., Shimizu, K., Omura, T., Yoshikawa, E., Kosugi, T., Mori, S., Yamashita, T., A high resolution animal PET scanner using compact PS-PMT detectors, *IEEE Trans. Nucl. Sci.*, **44**, 1277-1282 (1997).
- 69) Maeda, J., Suhara, T., Ogawa, M., Okauchi, T., Kawabe, K., Zhang, M.R., Semba, J., Suzuki, K., In vivo binding properties of [carbonyl-¹¹C]WAY-100635: effect of endogenous serotonin, *Synapse*, **40**, 122-129 (2001).
- 70) Farde, L., Eriksson, L., Blomquist, G., Halldin, C., Kinetic analysis of central [¹¹C]raclopride binding to D₂-dopamine receptors studied by PET-a comparison to the equilibrium analysis, *J. Cereb. Blood Flow Metab.*, **9**, 696-708 (1989).
- 71) Suhara, T., Sudo, Y., Okauchi, T., Maeda, J., Kawabe, K., Suzuki, K., Okubo, Y., Nakashima, Y., Ito, H., Tanada, S., Halldin, C., Farde, L., Extrastriatal dopamine D₂ receptor density and affinity in the human brain measured by ³D PET, *Int. J. Neuropsychopharmacol.*, **2**, 73-82 (1999).
- 72) Dennis, T., Dubois, A., Benavides, J., Scatton, B., Distribution of central ω_1 (benzodiazepine₁) and ω_2 (benzodiazepine₂) receptor subtypes in the monkey and human brain. An autoradiographic study with [³H]flunitrazepam and the ω_1 selective ligand [³H]zolpidem, *J. Pharmacol. Exp. Ther.*, **247**, 309-322 (1988).
- 73) Luddens, H., Pritchett, D.B., Kohler, M., Killisch, I., Keinanen, K., Monyer, H., Sprengel, R., Seeburg, P.H., Cerebellar GABA_A receptor selective for a behavioural alcohol antagonist, *Nature*, **346**, 648-651 (1990).
- 74) Korpi, E.R., Kleingoor, C., Kettenmann, H., Seeburg, P.H., Benzodiazepine-induced motor impairment linked to point mutation in cerebellar GABA_A receptor, *Nature*, **361**, 356-359 (1993).
- 75) Yang, W., Drewe, J.A., Lan, N.C., Cloning and characterization of the human GABA_A receptor $\alpha 4$ subunit: identification of a unique diazepam-insensitive binding site, *Eur. J. Pharmacol.*, **291**, 319-325 (1995).
- 76) Pritchett, D.B., Seeburg, P.H., γ -aminobutyric acid_A receptor $\alpha 5$ -subunit creates

- novel type II benzodiazepine receptor pharmacology, *J. Neurochem.*, **54**, 1802-1804 (1990).
- 77) Schmid, L., Bottlaender, M., Fuseau, C., Fournier, D., Brouillet, E., Maziere, M., Zolpidem displays heterogeneity in its binding to the nonhuman primate benzodiazepine receptor in vivo, *J. Neurochem.*, **65**, 1880-1886 (1995).
- 78) Halldin, C., Farde, L., Litton, J.E., Hall, H., Sedvall, G., [¹¹C]Ro 15-4513, a ligand for visualization of benzodiazepine receptor binding. Preparation, autoradiography and positron emission tomography, *Psychopharmacology*, **108**, 16-22 (1992).
- 79) Mehta, A.K., Shank, R.P., Characterization of a benzodiazepine receptor site with exceptionally high affinity for Ro 15-4513 in the rat CNS, *Brain. Res.*, **704**, 289-297 (1995).
- 80) Laruelle, M., Imaging synaptic neurotransmission with in vivo binding competition techniques: a critical review. *J. Cereb. Blood Flow Metab.*, **20**, 423-451 (2000).
- 81) Bottlaender, M., Brouillet, E., Varastet, M., Le Breton, C., Schmid, L., Fuseau, C., Sitbon, R., Crouzel, C., Maziere, M., In vivo high intrinsic efficacy of triazolam: a positron emission tomography study in nonhuman primates, *J. Neurochem.*, **62**, 1102-1111 (1994).
- 82) Fritschy, J.M., Benke, D., Johnson, D.K., Mohler, H., Rudolph, U., GABA_A-receptor α -subunit is an essential prerequisite for receptor formation in vivo, *Neuroscience*, **81**, 1043-1053 (1997).
- 83) Jechlinger, M., Pelz, R., Tretter, V., Klausberger, T., Sieghart, W., Subunit composition and quantitative importance of hetero-oligomeric receptors: GABA_A receptors containing $\alpha 6$ subunits, *J. Neurosci.*, **18**, 2449-2457 (1998).
- 84) Hevers, W., Korpi, E.R., Luddens, H., Assembly of functional $\alpha 6\beta 3\gamma 2\delta$ GABA_A receptors in vitro, *Neuroreport* **11**, 4103-4106 (2000).
- 85) Mihalek, R.M., Banerjee, P.K., Korpi, E.R., Quinlan, J.J., Firestone, L.L., Mi, Z.P., Lagenaur, C., Tretter, V., Sieghart, W., Anagnostaras, S.G., Sage, J.R., Fanselow, M.S., Guidotti, A., Spigelman, I., Li, Z., DeLorey, T.M., Olsen, R.W. Homanics,

- G.E. Attenuated sensitivity to neuroactive steroids in γ -aminobutyrate type A receptor δ subunit knockout mice, *Proc. Natl. Acad. Sci. U.S.A.*, **96**, 12905-12910 (1999).
- 86) Suhara, T., Yasuno, F., Sudo, Y., Yamamoto, M., Inoue, M., Okubo, Y., Suzuki, K., Dopamine D₂ receptors in the insular cortex and the personality trait of novelty seeking, *Neuroimage*, **13**, 891-895 (2001).
- 87) Suhara, T., Okubo, Y., Yasuno, F., Sudo, Y., Inoue, M., Ichimiya, T., Nakashima, Y., Nakayama, K., Tanada, S., Suzuki, K., Halldin, C., Farde, L., Decreased dopamine D₂ receptor binding in the anterior cingulate cortex in schizophrenia, *Arch. Gen. Psychiatry*, **59**, 25-30 (2002).
- 88) Squires, R.F., Braestrup, C., Benzodiazepine receptors in rat brain, *Nature*, **266**, 723-734 (1977).
- 89) Anholt, R.R., Pedersen, P.L., De Souza, E.B., Snyder, S.H., The peripheral-type benzodiazepine receptor. Localization to the mitochondrial outer membrane, *J. Biol. Chem.*, **261**, 576-583 (1986).
- 90) Antkiewicz-Michaluk, L., Guidotti, A., Krueger, K.E., Molecular characterization and mitochondrial density of a recognition site for peripheral-type benzodiazepine ligands, *Mol. Pharmacol.*, **34**, 272-278 (1988).
- 91) Gavish, M., Bachman, I., Shoukrun, R., Katz, Y., Veenman, L., Weisinger, G., Weizman, A., Enigma of the peripheral benzodiazepine receptor, *Pharmacol. Rev.*, **51**, 629-650 (1999).
- 92) Schoemaker, H., Bliss, M., Yamamura, H.I., Specific high-affinity saturable binding of [³H] Ro5-4864 to benzodiazepine binding sites in the rat cerebral cortex. *Eur. J. Pharmacol.*, **71**, 173-175 (1981).
- 93) Benavides, J., Quarteronet, D., Imbault, F., Malgouris, C., Uzan, A., Renault, C., Dubroeuq, M.C., Gueremy, C., Le Fur, G., Labelling of "peripheral-type" benzodiazepine binding sites in the rat brain by using [³H]PK 11195, an isoquinoline carboxamide derivative: kinetic studies and autoradiographic localization, *J. Neurochem.*, **41**, 1744-1750 (1983).
- 94) Le Fur, G., Perrier, M.L., Vaucher, N., Imbault, F., Flamier, A., Benavides, J. Uzan,

- A., Renault, C., Dubroeuq, M.C., Gueremy, C., Peripheral benzodiazepine binding sites: effect of PK 11195, 1-(2-chlorophenyl)-N-methyl-N-(1-methylpropyl)-3-isoquinolinecarboxamide, I. In vitro studies., *Life Sci.*, **32**, 1839-1847 (1983).
- 95) Schoemaker, H., Boles, R.G., Horst, W.D., Yamamura, H.I., Specific high-affinity binding sites for [³H]Ro 5-4864 in rat brain and kidney, *J. Pharmacol. Exp. Ther.*, **225**, 61-69 (1983).
- 96) Jayakumar, A.R., Panickar, K.S., Norenberg, M.D., Effects on free radical generation by ligands of the peripheral benzodiazepine receptor in cultured neural cells, *J. Neurochem.*, **83**, 1226-1234 (2002).
- 97) Myers, R., Manjil, L.G., Cullen, B.M., Price, G.W., Frackowiak, R.S., Cremer, J.E., Macrophage and astrocyte populations in relation to [³H]PK 11195 binding in rat cerebral cortex following a local ischaemic lesion, *J. Cereb. Blood Flow Metab.*, **11**, 314-322 (1991).
- 98) Stephenson, D.T., Schober, D.A., Smalstig, E.B., Mincy, R.E., Gehlert, D.R., Clemens, J.A., Peripheral benzodiazepine receptors are colocalized with activated microglia following transient global forebrain ischemia in the rat, *J. Neurosci.*, **15**, 5263-5274 (1995).
- 99) Banati, R.B., Myers, R., Kreutzberg, G.W., PK ('peripheral benzodiazepine')-binding sites in the CNS indicate early and discrete brain lesions: microautoradiographic detection of [³H]PK11195 binding to activated microglia, *J. Neurocytol.*, **26**, 77-82 (1997).
- 100) Kuhlmann, A.C., Guilarte, T.R., Cellular and subcellular localization of peripheral benzodiazepine receptors after trimethyltin neurotoxicity, *J. Neurochem.*, **74**, 1694-1704 (2000).
- 101) Anholt, R.R., Murphy, K.M., Mack, G.E. Snyder, S.H., Peripheral-type benzodiazepine receptors in the central nervous system: localization to olfactory nerves, *J. Neurosci.*, **4**, 593-603 (1984).
- 102) Cymerman, U., Pazos, A., Palacios, J.M., Evidence for species differences in 'peripheral' benzodiazepine receptors: an autoradiographic study, *Neurosci. Lett.*

- 66, 153-158 (1986).
- 103) Caggiano, A.O., Brunjes, P.C., Microglia and the developing olfactory bulb, *Neuroscience*, **52**, 717-724 (1993).
- 104) Antkiewicz-Michaluk, L., Mukhin, A.G., Guidotti, A., Krueger, K.E., Purification and characterization of a protein associated with peripheral-type benzodiazepine binding sites, *J. Biol. Chem.* **263**, 17317-17321 (1988).
- 105) Sprengel, R., Werner, P., Seeburg, P.H., Mukhin, A.G., Santi, M.R., Grayson, D.R., Guidotti, A., Krueger, K.E., Molecular cloning and expression of cDNA encoding a peripheral-type benzodiazepine receptor, *J. Biol. Chem.*, **264**, 20415-20421 (1989).
- 106) Parola, A.L., Stump, D.G., Pepperl, D.J., Krueger, K.E., Regan, J.W., Laird, H.E. 2nd, Cloning and expression of a pharmacologically unique bovine peripheral-type benzodiazepine receptor isoquinoline binding protein, *J. Biol. Chem.*, **266**, 14082-14087 (1991).
- 107) McEnery, M.W., Snowman, A.M., Trifiletti, R.R., Snyder, S.H., Isolation of the mitochondrial benzodiazepine receptor: association with the voltage-dependent anion channel and the adenine nucleotide carrier, *Proc. Natl. Acad. Sci. U.S.A.*, **89**, 3170-3174 (1992).
- 108) Casellas, P., Galiegue, S., Basile, A.S., Peripheral benzodiazepine receptors and mitochondrial function, *Neurochem. Int.*, **40**, 475-486 (2002).
- 109) Li, H., Yao, Z., Degenhardt, B., Teper, G., Papadopoulos, V., Cholesterol binding at the cholesterol recognition/ interaction amino acid consensus (CRAC) of the peripheral-type benzodiazepine receptor and inhibition of steroidogenesis by an HIV TAT-CRAC peptide, *Proc. Natl. Acad. Sci. U.S.A.*, **98**, 1267-1272 (2001).
- 110) Banati, R.B., Newcombe, J., Gunn, R.N., Cagnin, A., Turkheimer, F., Heppner, F., Price, G., Wegner, F., Giovannoni, G., Miller, D.H., Perkin, G.D., Smith, T., Hewson, A.K., Bydder, G., Kreutzberg, G.W., Jones, T., Cuzner, M.L., Myers, R., The peripheral benzodiazepine binding site in the brain in multiple sclerosis: quantitative in vivo imaging of microglia as a measure of disease activity, *Brain* **123**, 2321-2337 (2000).

- 111) Cagnin, A., Brooks, D.J., Kennedy, A.M., Gunn, R.N., Myers, R., Turkheimer, F.E., Jones, T., Banati, R.B., In-vivo measurement of activated microglia in dementia, *Lancet*, **358**, 461-467 (2001).
- 112) Debruyne, J.C., Van Laere, K.J., Versijpt, J., De Vos, F., Eng, J.K., Strijckmans, K., Santens, P., Achten, E., Slegers, G., Korf, J., Dierckx, R.A., De Reuck, J.L., Semiquantification of the peripheral-type benzodiazepine ligand [¹¹C]PK11195 in normal human brain and application in multiple sclerosis patients, *Acta. Neurol. Belg.* **102**, 127-135 (2002).
- 113) Pappata, S., Levasseur, M., Gunn, R.N., Myers, R., Crouzel, C., Syrota, A., Jones, T., Kreutzberg, G.W., Banati, R.B., Thalamic microglial activation in ischemic stroke detected in vivo by PET and [¹¹C]PK1195, *Neurology*, **55**, 1052-1054 (2000).
- 114) Goerres, G.W., Revesz, T., Duncan, J., Banati, R.B., Imaging cerebral vasculitis in refractory epilepsy using [¹¹C](R)-PK11195 positron emission tomography, *A.J.R. Am. J. Roentgenol.*, **176**, 1016-1018 (2001).
- 115) Banati, R.B., Brain plasticity and microglia: is transsynaptic glial activation in the thalamus after limb denervation linked to cortical plasticity and central sensitisation?, *J. Physiol. Paris*, **96**, 289-299 (2002).
- 116) Chaki, S., Funakoshi, T., Yoshikawa, R., Okuyama, S., Okubo, T., Nakazato, A., Nagamine, M., Tomisawa, K., Binding characteristics of [³H]DAA1106, a novel and selective ligand for peripheral benzodiazepine receptors, *Eur. J. Pharmacol.* **371**, 197-204 (1999).
- 117) Okuyama, S., Chaki, S., Yoshikawa, R., Ogawa, S., Suzuki, Y., Okubo, T., Nakazato, A., Nagamine, M., Tomisawa, K., Neuropharmacological profile of peripheral benzodiazepine receptor agonists, DAA1097 and DAA1106, *Life Sci.*, **64**, 1455-1464 (1999).
- 118) Okubo, T., Yoshikawa, R., Chaki, S., Okuyama, S., Nakazato, A., Design, synthesis and structure-affinity relationships of aryloxyanilide derivatives as novel peripheral benzodiazepine receptor ligands, *Bioorg. Med. Chem.*, **12**, 423-438 (2004).

- 119) Culty, M., Silver, P., Nakazato, A., Gazouli, M., Li, H., Muramatsu, M., Okuyama, S., Papadopoulos, V., Peripheral benzodiazepine receptor binding properties and effects on steroid synthesis of two new phenoxyphenyl-acetamide derivatives, DAA1097 and DAA1106. *Drug Dev. Res.*, **52**, 475-484 (2002).
- 120) Takei, M., Kida, T., Suzuki, K., Sensitive measurement of positron emitters eluted from HPLC, *Appl. Radiat. Isot.*, **55**, 229-234 (2001).
- 121) Hashimoto, K., Inoue, O., Suzuki, K., Yamasaki, T., Kojima, M., Synthesis and evaluation of ^{11}C -PK 11195 for in vivo study of peripheral-type benzodiazepine receptors using positron emission tomography, *Ann. Nucl. Med.* **3**, 63-71 (1989).
- 122) Zhang, M.R., Tsuchiyama, A., Haradahira, T., Furutsuka, K., Yoshida, Y., Kida, T., Noguchi, J., Irie, T., Suzuki, K., Synthesis and preliminary evaluation of [^{18}F]FETP4A, a promising PET tracer for mapping acetylcholinesterase in vivo, *Nucl. Med. Biol.*, **29**, 463-468 (2002).
- 123) Cremer, J.E., Hume, S.P., Cullen, B.M., Myers, R., Manjil, L.G., Turton, D.R., Luthra, S.K., Bateman, D.M., Pike, V.W., The distribution of radioactivity in brains of rats given [N-methyl- ^{11}C]PK 11195 in vivo after induction of a cortical ischaemic lesion, *Int. J. Rad. Appl. Instrum. B*, **19**, 159-166 (1992).
- 124) Rao, V.L. Butterworth, R.F., Characterization of binding sites for the ω_3 receptor ligands [^3H]PK11195 and [^3H]RO5-4864 in human brain, *Eur. J. Pharmacol.*, **340**, 89-99 (1997).
- 125) Petit-Taboue, M.C., Baron, J.C., Barre, L., Travers, J.M., Speckel, D., Camsonne, R., MacKenzie, E.T., Brain kinetics and specific binding of [^{11}C]PK 11195 to ω_3 sites in baboons: positron emission tomography study. *Eur. J. Pharmacol.*, **200**, 347-351 (1991).
- 126) Suhara, T., Sudo, Y., Yoshida, K., Okubo, Y., Fukuda, H., Obata, T., Yoshikawa, K., Suzuki, K., Sasaki, Y., Lung as reservoir for antidepressants in pharmacokinetic drug interactions, *Lancet*, **351**, 332-335 (1998).
- 127) Passchier, J., van Waarde, A., Doze, P., Elsinga, P.H., Vaalburg, W., Influence of P-glycoprotein on brain uptake of [^{18}F]MPPF in rats, *Eur. J. Pharmacol.*, **407**, 273-280 (2000).

- 128) Jakubikova, J., Duraj, J., Hunakova, L., Chorvath, B., Sedlak, J., PK11195, an isoquinoline carboxamide ligand of the mitochondrial benzodiazepine receptor, increased drug uptake and facilitated drug-induced apoptosis in human multidrug-resistant leukemia cells in vitro, *Neoplasma*, **49**, 231-236 (2002).
- 129) Doble, A., Ferris, O., Burgevin, M.C., Menager, J., Uzan, A., Dubroeuq, M.C., Renault, C., Gueremy, C., Le Fur, G., Photoaffinity labeling of peripheral-type benzodiazepine-binding sites, *Mol Pharmacol* **31**, 42-49 (1987).
- 130) Riond, J., Leplatois, P., Laurent, P., Le Fur, G., Caput, D., Loison, G., Ferrara, P., Expression and pharmacological characterization of the human peripheral-type benzodiazepine receptor in yeast, *Eur. J. Pharmacol.*, **208**, 307-312 (1991).
- 131) Garnier, M., Dimchev, A.B., Boujrad, N., Price, J.M., Musto, N.A., Papadopoulos V., In vitro reconstitution of a functional peripheral-type benzodiazepine receptor from mouse Leydig tumor cells, *Mol. Pharmacol.*, **45**, 201-211 (1994).
- 132) Benavides, J., Fage, D., Carter, C., Scatton, B., Peripheral type benzodiazepine binding sites are a sensitive indirect index of neuronal damage, *Brain Res.*, **421**, 167-172 (1987).
- 133) Dubois, A., Benavides, J., Peny, B., Duverger, D., Fage, D., Gotti, B., MacKenzie, E.T., Scatton, B., Imaging of primary and remote ischaemic and excitotoxic brain lesions. An autoradiographic study of peripheral type benzodiazepine binding sites in the rat and cat, *Brain Res.* **445**, 77-90 (1988).
- 134) Marty, S., Dusart, I., Peschanski, M., Glial changes following an excitotoxic lesion in the CNS-I. Microglia/macrophages., *Neuroscience*, **45**, 529-539 (1991).
- 135) Murabe, Y., Ibata, Y., Sano Y., Morphological studies on neuroglia. III. Macrophage response and "microgliocytosis" in kainic acid-induced lesions, *Cell Tissue Res.*, **218**, 75-86 (1981).
- 136) Dusart, I., Marty, S., Peschanski, M., Glial changes following an excitotoxic lesion in the CNS-II. Astrocytes, *Neuroscience*, **45**, 541-549 (1991).
- 137) Havoundjian, H., Cohen, R.M., Paul, S.M. Skolnick, P., Differential sensitivity of "central" and "peripheral" type benzodiazepine receptors to phospholipase A₂, *J. Neurochem.*, **46**, 804-811 (1986).

- 138) Bourdiol, F., Toulmond, S., Serrano, A., Benavides, J., Scatton, B., Increase in ω 3 (peripheral type benzodiazepine) binding sites in the rat cortex and striatum after local injection of interleukin-1, tumour necrosis factor- α and lipopolysaccharide, *Brain Res.*, **543**, 194-200 (1991).
- 139) Oh, Y.J., Francis, J.W., Markelonis, G.J. Oh, T.H., Interleukin-1- β and tumor necrosis factor- α increase peripheral-type benzodiazepine binding sites in cultured polygonal astrocytes, *J. Neurochem.*, **58**, 2131-2138 (1992).
- 140) Rey, C., Mauduit, C., Naureils, O., Benahmed, M., Louisot, P., Gasnier, F., Up-regulation of mitochondrial peripheral benzodiazepine receptor expression by tumor necrosis factor α in testicular leydig cells. Possible involvement in cell survival, *Biochem. Pharmacol.*, **60**, 1639-1646 (2000).
- 141) Delavoie, F., Li, H., Hardwick, M., Robert, J.C., Giatzakis, C., Peranzi, G., Yao, Z.X., Maccario, J., Lacapere, J.J., Papadopoulos, V., In vivo and in vitro peripheral-type benzodiazepine receptor polymerization: functional significance in drug ligand and cholesterol binding, *Biochemistry*, **42**, 4506-4519 (2003).
- 142) Streit, W.J., Microglia as neuroprotective, immunocompetent cells of the CNS, *Glia*, **40**, 133-139 (2002).